

THE PRODUCTION AND DISPERSION OF DISSOLVED METHANE
IN SOUTHEASTERN BERING SEA

by

Joel D. Cline, Kimberly Kelly-Hansen,
and Charles N. Katz

Pacific Marine Environmental Laboratory
National Oceanic and Atmospheric Administration

Final Report
Outer Continental Shelf Environmental Assessment Program
Research Unit 153

1982

309

TABLE OF CONTENTS

	List of Figures	313
	List of Tables	317
1.	INTRODUCTION	319
	1.1 Purpose of Study	319
	1.2 Objectives	319
	1.3 Relevance to OCSEAP ..*	320
2.	BACKGROUND	322
	2.1 Chemical Tracers	322
	2.2 Southeastern Bering Sea ..* ..*	323
	2.3 North Aleutian Shelf ..*	325
	2.4 St. George Basin	326
3.	METHODOLOGY	327
	3.1 Sample Collection	327
	3.2 Preconcentration	327
	3.3 Gas Chromatography	327
4.	RESULTS	329
	4.1 St. George Basin	329
	4.2 North Aleutian Shelf	340
5.	TRANSPORT MODELS	358
	5.1 Horizontal Trajectory Model	358
	5.2 Vertical Flux Model	363
6.	DISCUSSION	366
	6.1 North Aleutian Shelf	366
	6.1.1 August 1980	369
	6.1.2 February 1981	376
	6.1.3 May 1981 ..*	378
	6.1.4 Port Moller Tidal Flux	383
	6.1.5 North Aleutian Shelf Summary	385

6.2	St. George Basin	387
6.2.1	August 1980	391
6.2.2	February 1981	393
6.2.3	May 1981	393
6.2.4	Summary of St. George Basin Studies	396
6.2.5	Oil Spill Scenario, St. George Basin	398
6.2.6	Horizontal Transport of Methane	406
6.2.7	Vertical Transport of Methane	409
7.	CONCLUSIONS	413
7.1	North Aleutian Shelf Studies	413
7.2	St. George Basin Studies	414
8.	REFERENCES	415

LIST OF FIGURES

Figure

1. Study regions and regional setting in the southeastern Bering Sea.
2. Stations occupied in St. George Basin in (a) August 1980, (b) February 1981, and (c) May 1981. Station prefixes are Unimak Pass (UP), St. George Basin (SG), North Aleutian Shelf (NA) and PROBES line (PL).
3. The vertical distributions of (a) salt, (b) temperature, (c) density, and (d) dissolved methane along the PROBES line in August 1980. See Fig. (2a) for the station positions.
4. The vertical distributions of (a) salt, (b) temperature, (c) density, and (d) dissolved methane along the PROBES line in February 1981. See Fig. (2b) for the station positions.
5. The vertical distributions of (a) salt, (b) temperature, (c) density, and (d) dissolved methane along the PROBES line in May 1981. See Fig. (2c) for the station positions.
6. The near-bottom distribution of dissolved methane in (a) August 1980, (b) February 1981, and (c) May 1981. Concentrations were averaged over the lower 20 m of the water column.
7. The vertical distribution of (a) density and (b) methane at Station PL6. Measurements were made on 29 August and 3 September 1980. Small but significant inversions in the density profile are the result of lateral mixing and the formation of salt fingering (Coachman and Charnell, 1979).
8. The vertical distribution of (a) dissolved methane and (b) density (σ_t) at Station SG 70. Measurements were made May 19, 23 and June 1, 1981, and show the temporal variability in circulation across St. George Basin.
- 9a. The location of stations occupied in August 1980 along the NAS.
- 9b. The location of stations occupied in February 1981 along the NAS.
- 9c. The location of stations occupied in May 1981 along the NAS.
10. The seasonal distribution of salinity and temperature along the NAS. The coastal zone was defined to include all waters whose depth was less than 40 m.
11. The seasonal distribution of salinity and temperature along the southern boundary of the middle shelf. The middle shelf was operationally defined to include all stations at which the depth of water exceeded 41 m.

12. The seasonal distribution of salinity, temperature, and density (σ_t) at Station 27 in the coastal zone. Note the well-mixed water column.
13. The seasonal distribution of salinity, temperature, and density (σ_t) at Station 23 in the middle **shelf**. Note the isothermal, **isohaline** conditions in February 1981.
14. The average longitudinal distribution of salinity along the NAS coastal zone. Only stations at which the depth of water was less than 40 m were included in the analysis. The dashed arrows indicate the range of values about the mean. Note the large variations at the entrance to Port **Moller**.
15. The distribution of methane at the surface along the NAS in (a) August 1980, (b) February 1981, and (c) May 1981. Concentrations are in **nL/L (STP)**.
16. The vertical distributions of methane along sections IV and V east of Port **Moller** (see Fig. 9a). Measurements were made in August 1980.
17. The location of 24-hour time series stations at the entrance to Port **Moller**. Stations PM1, PM2, PM3 were occupied in August 1980; Station PM3 in February 1981; and Stations 39A, 38B, and **39C** in May 1981.
18. The time-averaged distribution of methane across the entrance to Port **Moller** in (a) August 1980, (b) February 1981, and (c) May 1981. In those cases where more than one measurement was made, the vertical lines indicate the range of **values** about the mean.
19. The diel variation in temperature, salinity, and methane at Station PM3. Measurements were made on 5-6 February 1981. Note that low salinity, methane-enriched water is found at the entrance to Port **Moller** during ebb tide.
20. A schematic diagram of the NAS region. The significant transport terms include **longshore** advection vC' , and the flux divergence KyC'' . The well mixed coastal zone is approximately 20 m deep and 32 km wide. Not shown in the diagram is the air-sea exchange of methane, which is proportional to the concentration of methane.
21. The average distribution of dissolved methane across the entrance to Port **Moller**. Observations were conducted in August 1980. The mean and range of values (n observations) are shown by the closed triangles and dashed arrows. The concentration of methane **shoreward** of Station PM13 was assumed constant. A background of 0.45 $\mu\text{L/L}$ was subtracted to give the concentration of excess methane from Port **Moller**.
22. The depth-averaged distribution of (a) dissolved methane and (b) salinity and Port **Moller** in August 1980. A "background concentration of 0.45 $\mu\text{L/L}$ was subtracted from the" observed field, leaving a residual concentration of 0.03 $\mu\text{L/L}$ north of the inner front. The inner front is located near the dashed line (approximately 45 m).

23. Model ~~simulation~~ of the distribution of methane for $u = 3.8$ cm/s and $k = 5.0 \times 10^{-7}$ /s. This is the best fit to the observations shown in Fig. 22a. Concentrations are in $\mu\text{L/L}$. The position of the 45 m isobath is indicated by the dashed line.
24. Model simulations ~~of~~ the distribution of methane for (a) $u = 2.5$ cm/s, $k = 2.5 \times 10^{-7}$ /s and (b) $u = 5.0$ cm/s and $k = 7.5 \times 10^{-7}$ /s in August 1980. Concentrations are expressed in $\mu\text{L/L}$. The position of the 45 m isobath is indicated by the dashed line.
25. Model ~~simulation~~ of the distribution of methane for $u = 7.5$ cm/s and $k = 5.0 \times 10^{-7}$ /s in August 1980. Concentrations are in $\mu\text{L/L}$. The position of the 45 m isobath is indicated by the dashed line.
26. The depth-averaged distribution of (a) dissolved methane and (b) salinity in February 1981. A background concentration of 0.11 $\mu\text{L/L}$ has been subtracted from the concentration field, leaving a mean residual of 0.014 $\mu\text{L/L}$. The inner front is located near the 45 m isobath and is indicated by the dashed line.
27. Model simulations of ~~the~~ distributions of methane for (a) $u = 3.0$ cm/s, and $k = 4.3 \times 10^{-7}$ /s, and (b) $u = 7.0$ cm/s and $k = 1.2 \times 10^{-7}$ /s in February 1981. Both distributions are reasonably good fits to the observed distributions. Concentrations are in $\mu\text{L/L}$. The position of the inner front is indicated by the dashed line.
28. The depth-averaged distribution of dissolved methane in May 1981. A background concentration of 0.1 $\mu\text{L/L}$ has been subtracted from the concentration field, leaving a mean residual of 0.013 $\mu\text{L/L}$. The inner front is located near the 45 m isobath and is indicated by the dashed line.
29. Model simulations of the distribution of dissolved methane for (a) $u = 2.0$ cm/s and $k = 2.4 \times 10^{-7}$ /s and (b) $u = 3.0$ cm/s and $k = 4.8 \times 10^{-7}$ /s in May 1981. Both distributions are reasonably good fits to the observed distribution. Concentrations are in $\mu\text{L/L}$. The position of the inner front is near the 45 m isobath and is indicated by the dashed line.
30. Distributions of (a) clay content and (b) total carbon in the surface sediments of St. George Basin. The locus of the high carbon concentrations is approximately $56^{\circ}\text{N } 167^{\circ}\text{W}$, which is the location of Stations SG5, SG29, SG24, and SG70 (see Fig. 2). This figure was taken from the report by Gardner et al., 1978.
31. The average excess concentration of methane in the benthic boundary layer across the center of the plume. Data were collected in (a) August 1980, (b) February 1981, and (c) May 1981. Concentrations are expressed $\mu\text{L/L}$.
32. (a) The average near-bottom concentration of dissolved methane in St. George Basin in August 1980. The axes show the position of the model grid. (b) The model simulation of the methane distribution using the source function shown in Fig. (31a). The best fit was obtained for $u = 2.0$ cm/s and $k = 8.6 \times 10^{-8}$ /s.

33. (a) The average near-bottom concentration of dissolved methane in St. George Basin in February 1981. The axes show the position of the model grid. (b) The model simulation of the methane distribution using the source function shown in Fig. (31b). The best fit was obtained for $u = 2.0$ cm/s and $k = 5.6 \times 10^{-8}$ /s.
34. (a) The average near-bottom concentration of dissolved methane in St. George Basin in May 1981. The axes show the position of the model grid. (b) The model simulation of the methane distribution using the source function shown in Fig. (31c). The best fit was obtained for $u = 2.0$ cm/s and $k = 9.2 \times 10^{-8}$ /s.
35. The development of a plume of 'dissolved' oil resulting from an instantaneous release of 6.7×10^8 g (50,000 bbls) confined to a 40 m, vertical-lens of water. The centerline distribution shows the temporal history of the spill locus for a mean current speed of 2.5 cm/s. Reference concentrations of 0.1 and 1.0 ppm 'dissolved' oil also are indicated.
36. The development of a plume of 'dissolved' oil resulting from an instantaneous release of 6.7×10^8 g (50,000 bbls) confined to a 40 m, vertical-lens of water. The centerline distribution shows the temporal history of the spill locus for a mean current speed of 5.0 cm/s. Reference concentrations of 0.1 and 1.0 ppm 'dissolved' oil also are indicated.
37. The development of a plume of 'dissolved' oil resulting from an instantaneous release of 6.7×10^8 g (50,000 bbls) confined to a 40 m, vertical-lens of water. The centerline distribution shows the temporal history of the spill locus for a mean current speed of 10 cm/s. Reference concentrations of 0.1 and 1.0 ppm 'dissolved' oil also are indicated.
38. The vertical distribution of methane in the water column and surficial sediments at (a) Station SG67 and (b) SG70. These data were collected in May-June 1981. Note the scale change in concentrations between the water and the pore fluids.
39. The relationship between salinity and methane at Station PL-6 in August 1980. The linear relationship suggests conservative mixing between the surface and bottom waters.
40. The relationship between the apparent vertical eddy diffusivity, K_z , and the Brunt-Vaaisaala Frequency, N^2 , at Station PL6 in August 1980. The theoretical relationship for shear-induced turbulence is -0.5, which is shown by the dashed lines.

LIST OF TABLES

Table

1. A summary of parameters used to estimate the air-sea exchange rate (**R**) of methane along the NAS coastal zone. The model is

$$R = - \frac{D}{h \cdot \Delta z} (C) - k_a / s (C)$$

2. A comparison of the tidal transport of methane (T_t) from Port Moller with the transport of methane at the tidal boundary (T_m). The mean tidal velocity is \bar{v} and the mean coastal current is \bar{u} .
3. A summary of the mean velocities along the coastal zone of the North Aleutian Shelf as determined from the distributions of dissolved methane. The air-sea exchange and biological rate constant (combined) was varied by $\pm 50\%$.

1. INTRODUCTION

1.1. Purpose of Study

The purpose of this study was to use dissolved methane as a tracer of mean circulation and to define vertical and horizontal mixing scales in local regions of the southeastern Bering Sea. The subregions selected for study included St. George Basin, a fault basin located on the outer **shelf** of Bristol Bay, and the North Aleutian Shelf. Both regions were identified as potential off-shore leasing sites for gas and oil production.

Based on previous investigations in Bristol Bay (Cline, 1976, 1977), it was known that localized sources of methane occurred in both areas. By carefully examining the seasonal distributions of methane and by quantifying the extent and magnitude of these sources, **it** might be possible to delineate horizontal and vertical mixing scales as well as confirming the mean current field.

Methane is a common component of petroleum and is also produced by microorganisms. The origin of methane in petroleum is via thermal cracking of larger organic molecules, whereas methane derived biologically is from the exothermic reduction of carbon dioxide by specialized anaerobic bacteria (Claypool and Kaplan, 1974). In either case, methane is a dissolved gas observed at moderate concentrations in the shelf waters of the Bering Sea and becomes a natural chemical tracer of the movement of the dissolved fractions of crude oil, whether they arise from a tanker spill, pipeline rupture, or well blowouts.

1.2. Objectives

The principal goal of this research was *to* use dissolved methane as a quantitative tracer of circulation processes and mixing dynamics in selected areas of **the** southeastern Bering Sea. This report deals with two **site-specific** areas, the North Aleutian Shelf (**NAS**) and St. George Basin (**SGB**).

Specifically, the objectives were:

1. To quantify the **longshore** mean current and cross-shelf dispersion coefficients along the NAS using the tidal **flux** of methane from the Port **Moller** estuary as a chemical tracer.
2. To estimate near-bottom current trajectories and lateral dispersion coefficients in St. George Basin, using the bottom source of methane as a chemical tracer. .
3. To estimate the depth dependent vertical eddy diffusivity in St. George Basin using a one-dimensional vertical flux model.
4. To analyze the distributions of methane in terms of a **two-**dimensional diffusion-advection model for the purpose of confirming mean current velocities and estimating the magnitude of horizontal and vertical mixing processes.

1.3. Relevance to OCSEAP

The persistence of oil in Bristol Bay depends on physical, chemical and biological processes that act in concert to disperse and degrade petroleum. These processes, each with their characteristic time scales (i.e., half-life), must be considered together in order to determine a characteristic time (or space) scale for the persistence of oil or some fraction thereof. Circulation and mixing processes are characterized by relatively short time scales and thus represent a first-order process. Given that the volume of spilled oil is likely to be small compared to the volume of water in the region, it is anticipated that harmful impacts due to petroleum development will **be** limited to small areas, probably less **than 500 km²**.

Utilization of methane as a chemical tracer of circulation and dispersion allows mesoscale mixing processes to be more clearly defined. In

particular, these studies permit quantitative predictions of water mass trajectories, dispersion characteristics and water mass residence times, all of which are required to quantify the potential impact of oil on living resources.

2. BACKGROUND

2.1. Chemical Tracers

The natural occurrence of dissolved methane is normally due to the metabolic activities of specialized marine bacteria that either selectively reduce molecular CO_2 or ferment simple fatty acids into CO_2 and methane (Claypool, 1974). Regardless of which mechanism prevails in nature, the net result is that a small portion of the **annually** fixed carbon is reduced to methane. Methanogenesis is normally considered an anaerobic process, usually occurring within oxygen-deficient environments (Reeburgh and Heggie, 1977).

Once methane is released to the water column, usually by diffusion, or in some cases, by bubble injection, the water parcel is chemically marked. The resulting distribution of methane is a function of the input rate, the velocity field, eddy diffusion, air-sea exchange, and biological oxidation. Each of these processes will be discussed below, but suffice it to say that under certain limiting conditions, methane may behave as a conservative property so long as the spatial scales are not too great. This condition presumes that biological oxidation and air-sea exchange are insignificant over the time scale of interest. If air-sea exchange and biological oxidation of CH_4 to CO_2 are relatively small effects, then the distribution of methane is largely governed by the magnitude of the source term and the mixing characteristics of the system.

Baseline studies conducted in 1975 and 1976 indicated that anomalously high concentrations of methane were present in St. George Basin and along the North Aleutian Shelf near the Port **Moller** estuary. Whereas both sources appeared to be localized, a detailed observational program was initiated to assess the seasonal distributions and derive independent estimates of mixing

parameters based on model interpretation of the distributions. These **dis-tributions** were similar in scale (actually larger) to proposed oil spill scenarios; thus methane served as a **natural** analog tracer of oil impacts associated with petroleum development.

We now proceed to discuss the geography, hydrology and oceanography of the two regions as necessary introductory information to the discussion to follow.

2.2. Southeastern Bering Sea

The area and volume of the southeastern Bering Sea, computed out to the 200 m isobath, is 419,000 km² and 30,000 km³, respectively, which calculates a mean depth of approximately 70 m. Freshwater input occurs primarily from the Kuskokwim and **Kvichak** Rivers, located on the northern and eastern sides of the region (Fig. 1), which results in a **2‰** salinity difference between the offshore waters and the near-shore areas (Schumacher et al., 1979).

Bristol Bay is characterized by a series of frontal features, primarily located at distinct bathymetric depths (Kinder and Schumacher, 1981a). These fronts occur roughly at the 200 m (shelf break front), 100 m (middle shelf) and 50 m (**inner front**) **isobaths** (see Fig. 4-1; Kinder and Schumacher, 1981a). Mean circulation landward of the middle front is presumed weak (≤ 2 cm S-l) and hydrographic structures are largely determined by buoyancy input, wind stirring and tidal mixing (Kinder and Schumacher, 1981a; see their report for details). There appears to be a weak **cyclonic** circulation around the perimeter of Bristol Bay, largely confined to the coastal zone ($z \leq 50$ m).

The region is partially ice covered in winter, usually beginning in protected bays in November and building to a maximum in March. The **spring** melting results in considerable freshwater added to **the** surface (Schumacher

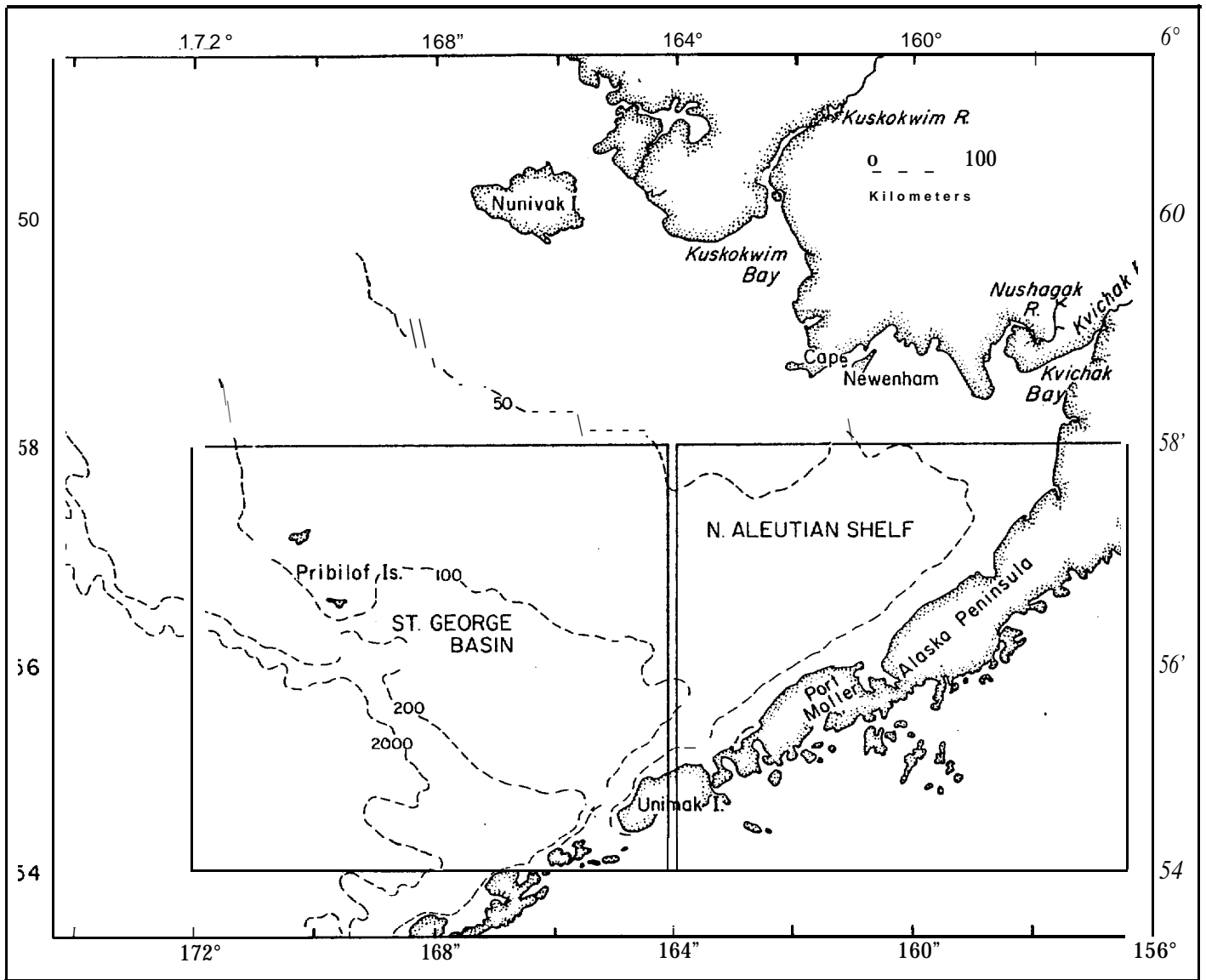


Figure 1. Study regions and regional setting in the southeastern Bering Sea.

et al., 1979). Maximum areal ice coverage is approximately 60%; thickness is usually less than 1 m. Details on hydrography and climate of the region can be found in reports by Kinder and Schumacher, 1981a; Kinder and Schumacher, 1981b; Coachman and Charnell, 1979; Overland, 1981; and references contained therein.

2.3. North Aleutian Shelf (NAS)

The NAS region encompasses the near shore areas from **Unimak** Island on the west to **the Kvichak** River on the east (Fig. 1). This region is characterized by a vertically well mixed coastal zone ($z \leq 50$), which is hydrographically separated from the seasonally stratified regime located seaward. Stratification is most intense in the summer and nearly vanishes during winter. The breakdown of vertical stratification in the coastal zone is reportedly due to wind and tidal mixing (Kinder and Schumacher, 1981a).

There appears to be no major source of freshwater along the **NAS**, except the Kvichak River at the eastern extremity. There are undoubtedly numerous diffuse sources, including the possibility of submarine aquifers originating in the mountains of the Alaska Peninsula. Mean velocities are estimated at no more than $3\text{-}5 \text{ cm s}^{-1}$ to the east (Schumacher et al., 1979), with a strong seasonal variability in direction and magnitude (Personal communication, J. Schumacher).

The principal embayment along the NAS is Port **Moller**, which has two arms, each approximately 38 km in length, with mean depths ranging from 5 m to 15 m. The western arm, **Herendeen** Bay, is the deeper of the two with depths to 100 m in a small inner basin. Tidal currents within the Port **Moller-Herendeen** Bay complex are relatively strong, reaching maximum ebb and flood velocities of approximately 150 cm s^{-1} (Department of Commerce, 1980).

Measurements made in September-October of 1975 and again in July of 1976 (Cline, 1981), revealed that the Port **Moller** estuary was a significant

source of dissolved methane to the surface waters, which could be traced to the northeast for distances of 200 km. The source of methane within Port Moller was not specifically known at that time, but was believed to arise from **methanogenesis** in **anoxic** marine muds or possibly from the discharge of **cannery** wastes at Port Moller.

2.4. St. George Basin

St. George Basin is an offshore fault basin located near the shelf break (Fig. 1). The axis of the basin is northwest-southeast, running roughly from **Unimak** Pass to the **Pribilof** Islands. The basin proper is largely contained between the 100-200 m **isobaths**.

The basin waters are separated from the inner shelf by the middle front at about 100 m and from the Bering Sea water located seaward of the 200 m **isobath** (Kinder and Schumacher, 1981a; see their Fig. 4-1). Dynamic topographies are largely oriented parallel to the **isobaths** and reflect weak mean currents toward the northwest (Coachman and **Charnell**, 1979). Although seasonal variations do exist, surface and near-bottom mean currents are usually $< 5 \text{ cm s}^{-1}$ (Coachman and **Charnell**, 1979; Kinder and Schumacher, 1981a).

The waters overlying SGB appear to be seasonally stratified with a strong erosion and deepening of the **pycnocline** in winter. Because the Alaska Stream-Bering Sea water penetrates the **shelf** seasonally (Kinder and Schumacher, 1981a), it is expected that the basin water is modified seasonally by cross-shelf **advection** and diffusion.

3. METHODOLOGY

3.1. Sample Collection

Water samples were collected using standard 5 L Niskin[®] bottles mounted on a General Oceanics Rosette. Once on deck, water was transferred to clean 1 L glass-stoppered bottles such that air bubbles were not trapped. The samples were stored in the dark at approximately 5°C until analyzed, which was usually within two hours.

3.2. Preconcentration

The analysis of methane was accomplished using a procedure adopted from that originally proposed by Swinnerton and Linnenbom (1967). A detailed discussion of the methods used for analyzing methane and other LMW hydrocarbons can be found in Katz (1980). Briefly, the method is as follows: Dissolved methane was removed from approximately 250 mL of seawater by helium stripping. Gases removed from solution were passed through Drierite[®], Ascarite[®] and Tenax G.C.[®] traps to remove water vapor, carbon dioxide and heavier hydrocarbons. Methane was concentrated on an activated alumina trap at -196°C. After quantitative removal from solution, (-5 minutes at a helium flow rate of 100 mL min⁻¹) the trap was warmed to 100°C and the methane was backflushed directly into a gas chromatography.

3.3. Gas Chromatography

Detection of methane was carried out on a Hewlett-Packard 5710A gas chromatography equipped with dual flame ionization detectors. In order to insure separation of methane from the air gases (N₂ and O₂), chromatography was accomplished with an activated-alumina, 60-80 mesh, column (1.8 m x 0.48 cm). Chromatography was completed in less than two minutes at a carrier flow rate of 50 mL min⁻¹ and the oven held isothermally at 100°C. Quantita-

tion was accomplished by comparing the samples with methane standards of known concentration. The precision of the analysis is $\pm 5\%$ at one standard deviation. **Intercalibration** with NBS showed our analysis to be accurate to 5%.

4. RESULTS

4.1. St. George Basin

Based on measurements made in 1975 and 1976 (Cline, 1980), large accumulations of methane were discovered in the near bottom waters of St. George Basin. The methane plume indicated a northwest current trajectory in agreement with observations (Kinder and Schumacher, 1981), although the nature of the source of CH_4 was poorly defined. In an attempt to clarify the mean circulation and lateral mixing characteristics of the basin, and in particular the near-bottom waters, we examined the distribution of methane seasonally and attempted to determine its source. From these measurements, together with the usual hydrographic parameters (e.g., $S^{\text{‰}}$, $T^{\circ}\text{C}$), we explored methane as a natural tracer of dissolved and emulsified oil that might be released during exploration and production activities.

The station grids occupied during the seasonal visits are shown in Figures (2a-2c). Station prefixes are: UP (Unimak Pass), SG (St. George Basin), and PL (Probes Line). The last of these was a line of stations occupied frequently by the PROBES Program and thus was included in our complement of stations for purposes of continuity, since there was significant overlap in the objectives of the two programs.

In August of 1980, not all of the stations were occupied in St. George Basin due to a priority allocation of time to the North Aleutian Shelf work. More complete coverage was accomplished in February and May of 1981, although in every case, insufficient time was available to trace the methane plume to the northwest beyond the Pribilofs.

In order to summarize the seasonal hydrography of the region, we present the distribution of properties along the PROBES Line. Hydrographic conditions

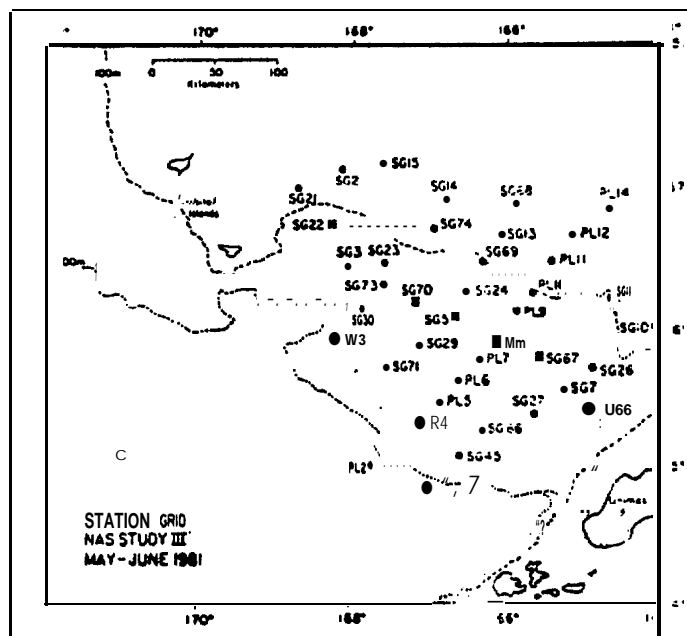
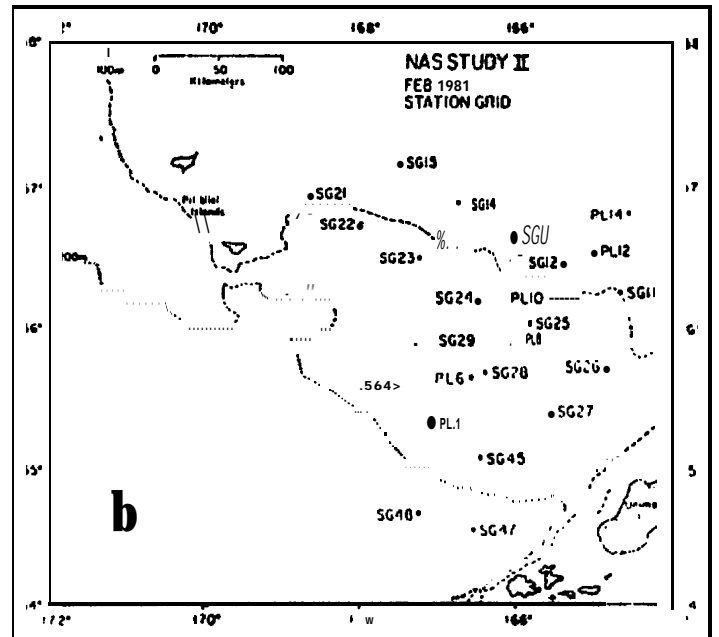
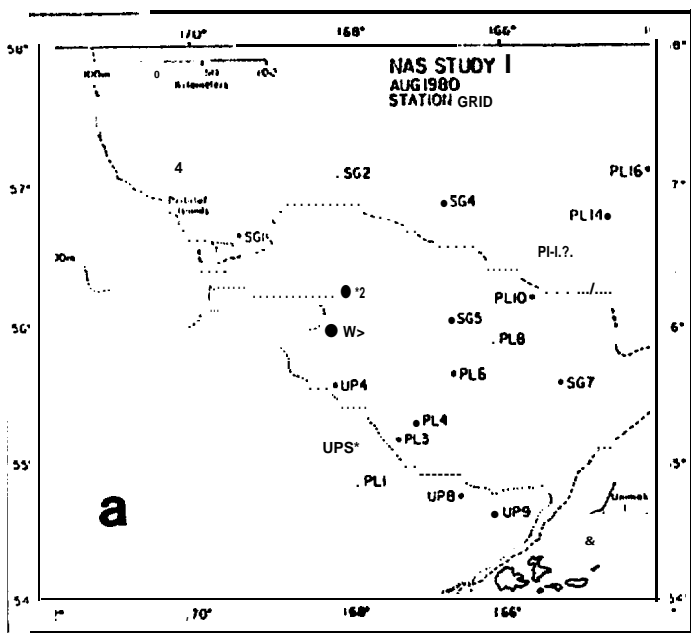


Figure 2. Stations occupied in St. George Basin (a) August 1980, (b) February 1981, and (c) May 1981. Station prefixes are **Unimak Pass** (UP), **St. George Basin** (SG), **North Aleutian Shelf** (NA) and **PROBES line** (PL).

for August 1980 are shown in Figures (3a-3d), including dissolved methane which reveals strong vertical and lateral gradients along the section. The highest concentrations observed were in the near-bottom waters of St. George Basin (near **PL-6**) and a smaller maximum near **PL-14**. Inshore of **PL-14** little vertical structure in the distribution of CH_4 was observed with concentrations between 400-500 nL/L (STP). The **lowest** concentration of methane was found in the offshore surface waters, where concentrations approached 280 nL/L. If the water column were in equilibrium with the atmosphere, the concentration of methane would range between 50-70 nL/L, depending mostly on the water temperature (Yamamoto et al., 1976). Thus, methane is seen to be highly supersaturated, even in the surface layers, with enrichment factors of at least five. The source of methane is most probably biological, although it remains difficult to pinpoint the exact source that contributes to the general background levels. Near-bottom and **benthic** microbial activity as well as **zooplankton** excretion seem the most likely sources (Scranton and Brewer, 1977).

Salinity and temperature distributions for August are shown in Figures (3b,c). The **haline** structure revealed characteristic surface outflow of low salinity water, principally from the **Kvichak** and **Kuskokwim** Rivers and the intrusion of high salinity, cold water onto the shelf from the west or southwest. Inshore of **PL-20**, water properties were uniform with depth, showing the effects of strong vertical turbulence generated by winds and tides (Kinder and Schumacher, 1981a). Within St. George Basin and **particularly** the middle shelf region ($100 \text{ m} < z < 50 \text{ m}$), the lateral gradient in **salt** was suggestive of diffusive salt exchange (Coachman et al., 1981) rather than vigorous advective processes. In fact, Kinder and Schumacher, (1981b) have shown that the mean currents are everywhere less than 5 cm/s throughout the year. The strongest vertical stratification observed along

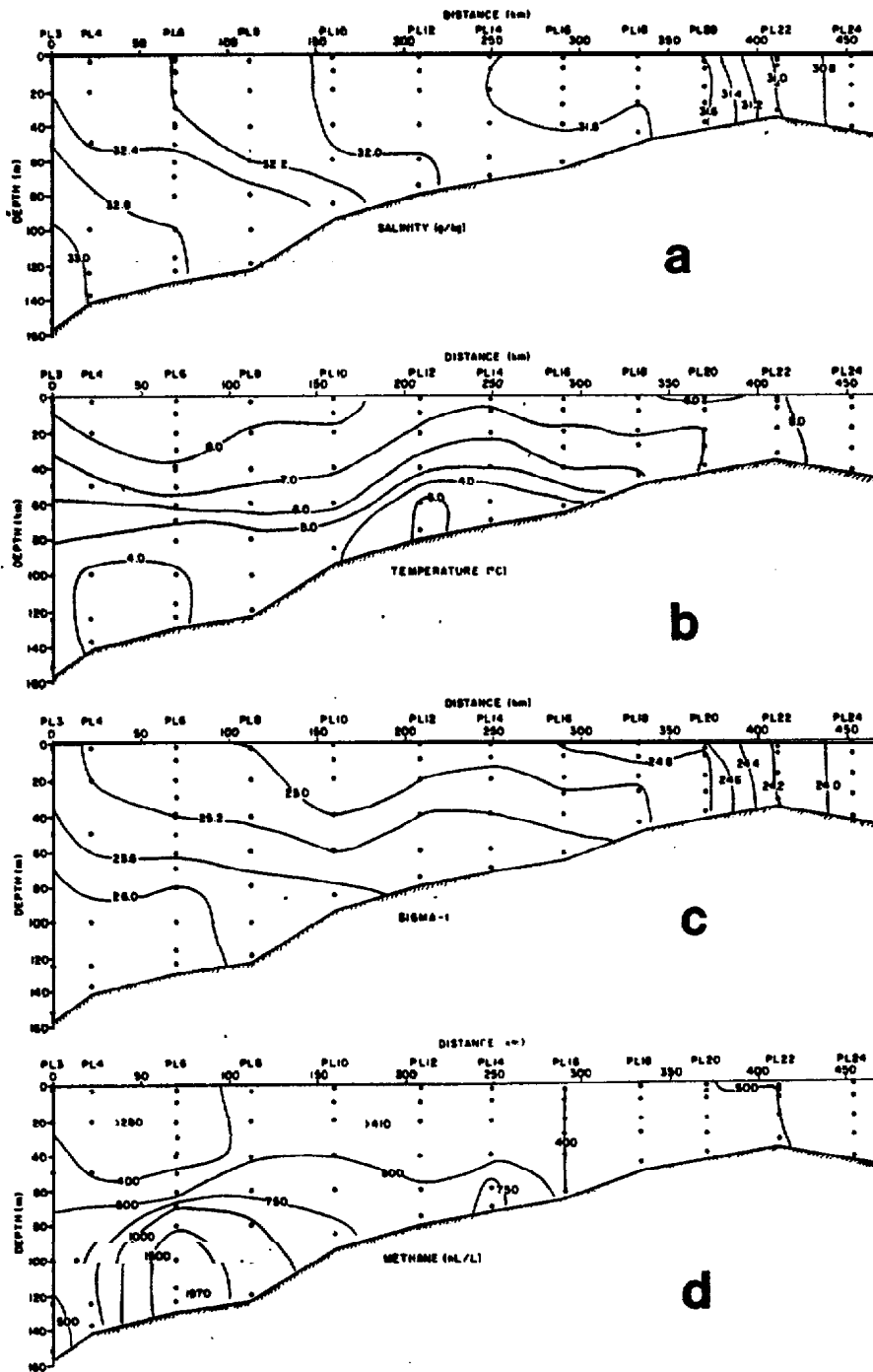


Figure 3. The vertical distributions of (a) salt, (b) temperature, (c) density, and (d) dissolved methane along the PROBES line in August 1980. See Fig. (2a) for the station positions.

the section was near PL-6 (Fig. 3d), which coincides with the maximum thermal and methane gradients. Later on in the discussion, we will elaborate on the significance of this seasonal stratification as it relates to the fate of oil released in this environment.

Figures (4a-4d) show conditions for February 1981. Concentrations of methane were significantly lower than those observed in August, both at the surface and at depth (Fig. 4d). The maximum concentration of methane was near PL-6/PL-8 as observed previously, but was reduced to approximately 25% of the August value. Concentrations in the surface layers remained high at 200 nL/L or about a factor of 3 above saturation (Yamamoto et al., 1976). A reduction in biological activity, and a decrease in vertical stability (Fig. 4c) acted in concert to reduce the near-bottom concentration of dissolved methane. Near-bottom circulation also may have increased during the winter period.

Salinity and temperature distributions are shown in Figures (4a) and (4b). Salinity varied from 31.70‰ in the surface layers at PL-10 to slightly more than 32.75‰ in the near-bottom water at PL-4. Not unlike the situation observed in August 1980, the change in salinity was about 1‰. In contrast however, was the small vertical temperature gradient observed in February. Over St. George Basin, the vertical temperature variation was about 1.2°C in February and 4°C in August, which led to a decrease in the vertical stability (Fig. 4c). The effects of winter cooling was evident in the eastern portion of the section where temperatures had decreased to less than 2.7°C. At this time of the year, the warmest temperatures were found near the bottom of St. George Basin.

The distribution of properties in May-June of 1981 are shown in Figures (5a-5d). Near-bottom concentrations of methane are similar to that observed in February 1981 and again are located near the center of St. George Basin

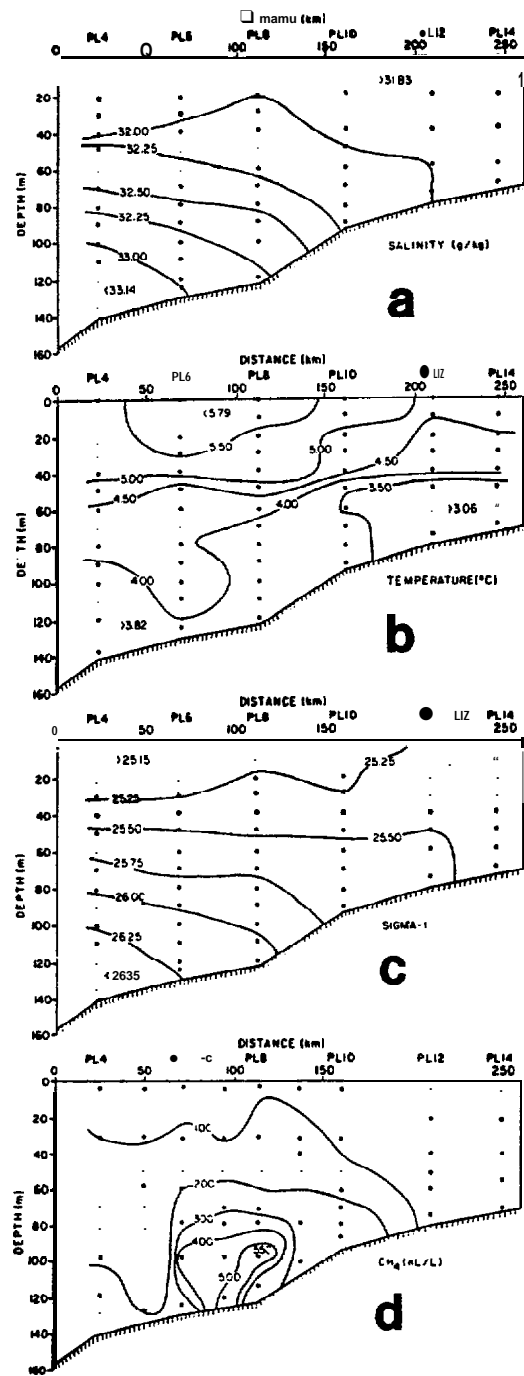


Figure 4. The vertical distributions of (a) salt, (b) temperature, (c) density, and (d) dissolved methane along the PROBES line in February 1981. See Fig. (2b) for the station positions.

(PL-6 to PL-8). In contrast to the previous measurements, surface concentrations were now less than 100 nL/L and suggest a gradual net degassing of the upper water column from February through May. Surface waters over St. George Basin were both **isohaline** and isothermal (Figs. 5a and 5b). The highest salinity was observed in the bottom waters of St. George Basin, about 33°/00, with the surface layers uniform at about 32°/00. Temperature varied from 4°C in the bottom waters to nearly 6°C in the surface layers. Once again, the coldest waters were found over the middle shelf region (PL-10 to PL-14). Thermal stratification was developing due to increased solar insolation, which caused an increase in stability and dissolved methane below the **pycnocline** (Fig. 5c). Of particular note is that although primary production had been increasing since late April or early May, the concentration of dissolved methane was no higher than was observed in February, presumably a time of minimum production. There appears to be a significant lag between the **annual** fixation of carbon and the maximum concentration of methane. Based on these sparse measurements, the lag appears to be at **least** 3 or 4 months (see Figs. 3a and 5a).

The distribution of dissolved methane within 5 m of the bottom is shown in Figures (6a-6c). In general, the near-bottom plume is **bathymetrically** contained within St. George Basin and reveals an ellipsoidal distribution to the north-northwest. The maximum concentration was always found near station SG5 (see Fig. 2c) and was seasonally variable. As noted earlier, the maximum observed concentration of methane was 2500 nL/L in August, followed by a minimum of 1000 nL/L in February and May. The orientation of the plume is determined by the **local** mixing characteristics and the mean velocity field.

Several obvious conclusions can be drawn about circulation by examining the distribution of methane. The plume appears elongated in the northwest-

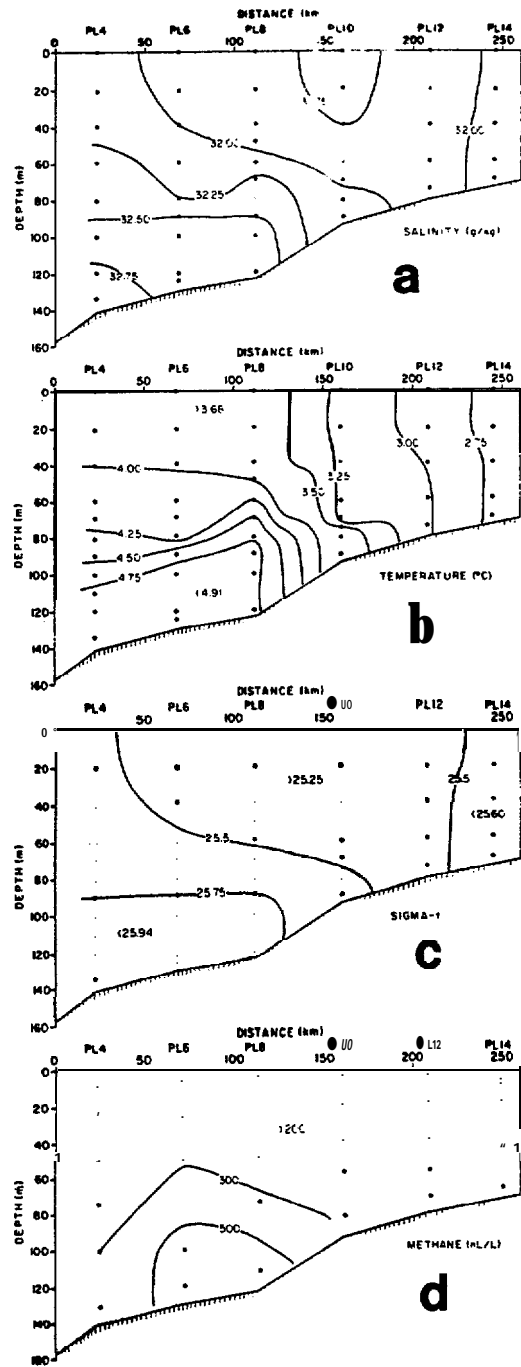


Figure 5. The vertical distributions of (a) salt, (b) temperature, (c) density, and (d) dissolved methane along the PROBES line in May-1981. See Fig. (2c) for the station positions.

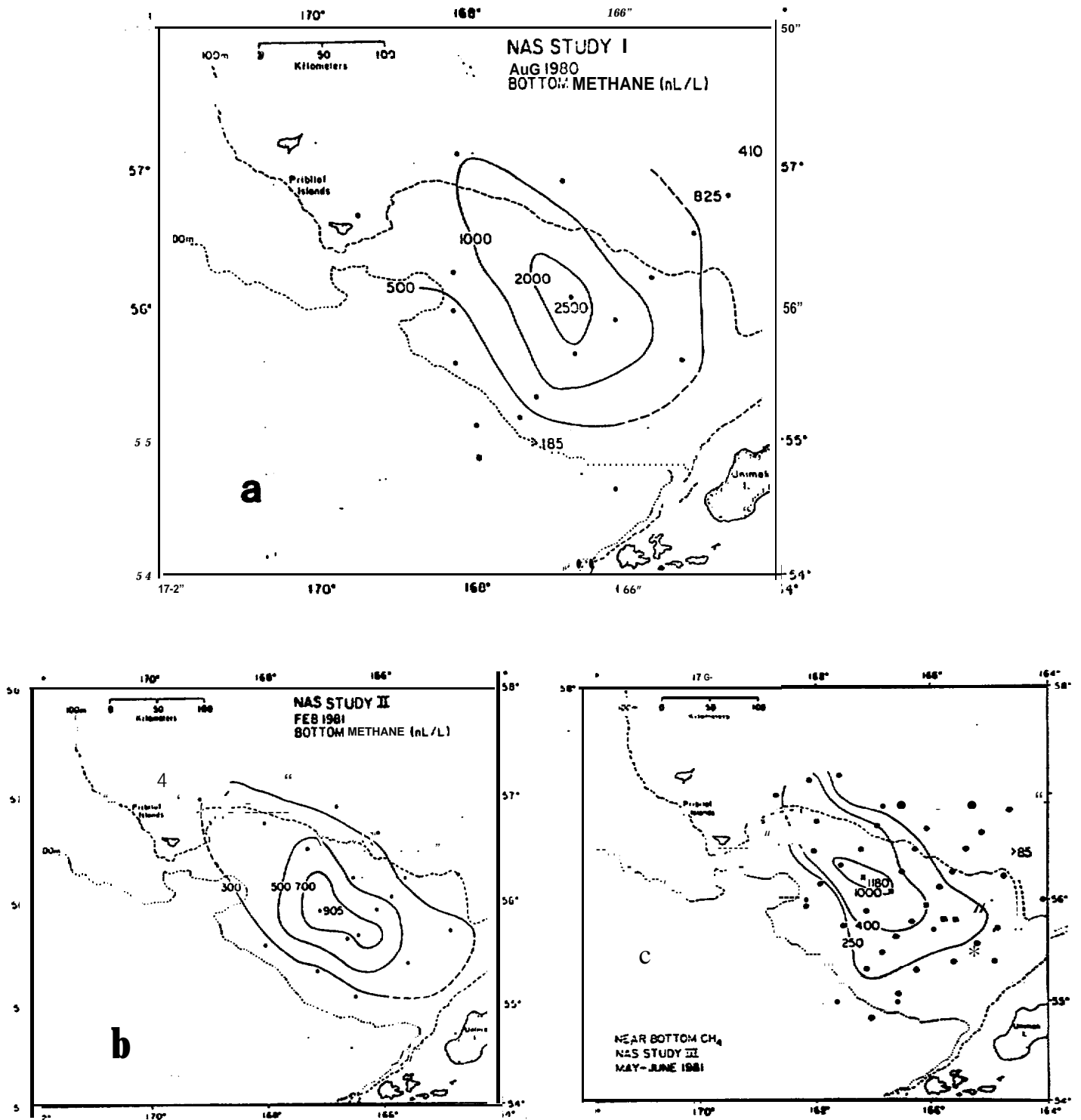


Figure 6. The near-bottom distribution of dissolved methane in (a) August 1980, (b) February 1981, and (c) May 1981. Concentrations were averaged over the lower 20 m of the water column.

southeast dissection in general agreement with the mean velocity field (Kinder and Schumacher, 1981b). The apparent source, located near SG5, coincides with the locus of fine-grained, organic rich sediments (Gardner et al., 1978). Organic carbon concentrations within the region of the plume range from 0.5 to about 1%. The zone of maximum organic carbon roughly coincides with the area circumscribed by the 2000 nL/L isopleth in Figure (6a). Beyond that region, organic carbon decreases and presumably so would the flux of CH₄ to the overlying waters. The absence of a strong trajectory to the northwest suggests that circulation is weak and that the currents are variable.

The distributions of methane shown in Figure (6) are entirely restricted to the near-bottom waters and show no surface outcropping. Even in February 1981 a weak pycnocline over the basin was sufficiently strong so as to inhibit vertical exchange. The vertical distribution of density (σ_t) and methane at station PL-6 in August is shown in Figures (7a,b). This station was occupied twice during a six-day period with little significant change in either the distribution of methane or density. The pycnocline was located between 60 and 80 m with an observed stability of 0.05 m⁻¹. Methane, shown in Figure (7a), showed a sharp gradient in the same region, suggesting that the vertical flux of CH₄ is strongly controlled by stability.

The time dependent nature of the bottom boundary layer is reflected in Figure (8). This station (SG-70) was occupied three times over a 13 day period in May 1981 and revealed the effects of subsurface water replacement on the distribution of methane. The lowest density water was observed on May 23 and it contained the highest concentration of methane. By June 1, however, water of increased density had penetrated the shelf ($Au_t = 0.11$), reducing the concentration of methane from 1200 nL/L to 800 nL/L. It appears that episodic intrusions of water onto the shelf occur with regularity that results in a compression or erosion of the methane plume. Our original

hypothesis was that methane would diffuse off the shelf as had been noted earlier in the Gulf of Alaska (Cline et al, 1978). However, none of our observations to date shows significant dispersion of CH_4 off the shelf, suggesting that any dissolved contaminant introduced into the bottom waters of St. George Basin would be similarly confined to the outer shelf region.

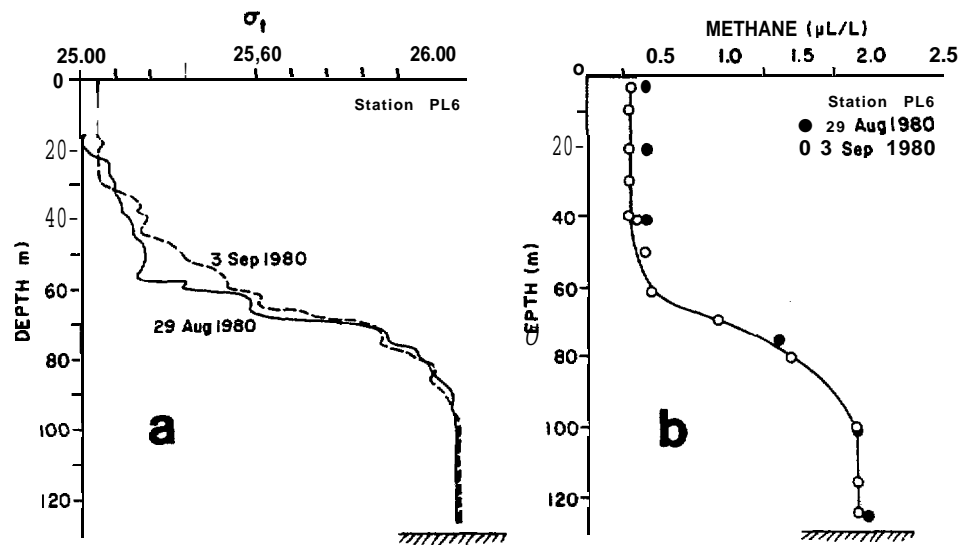


Figure 7 The vertical distribution of (a) density and (b) methane at Station PL6. Measurements were made on 29 August and 3 September 1980. Small but significant inversions in the density profile are the result of lateral mixing and the formation of salt fingering (Coachman and Charnell, 1979).

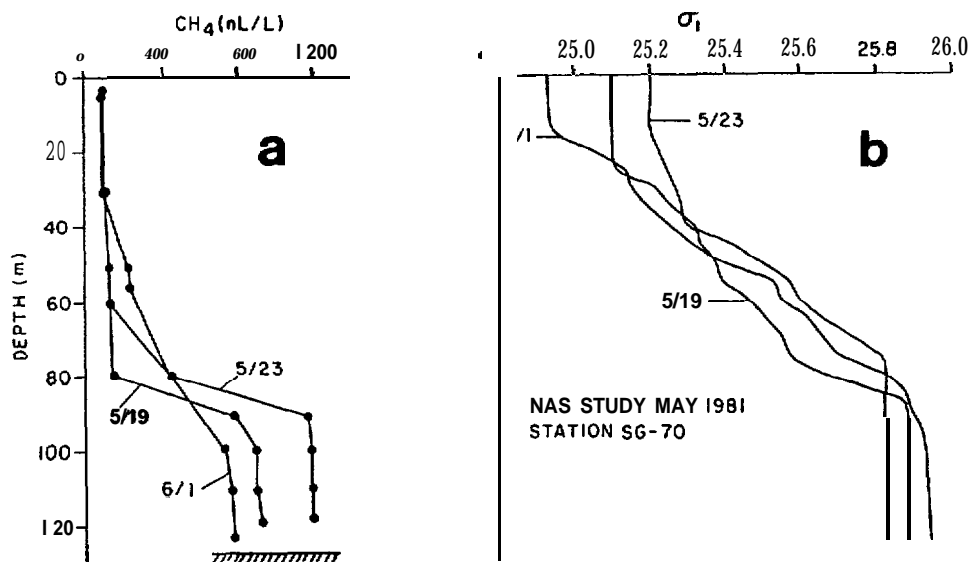


Figure 8. The vertical distribution of (a) dissolved methane and (b) density (σ_t) at Station SG70. Measurements were made May 19, 23, and June 1, 1981, and show the temporal variability in circulation across St. George Basin.

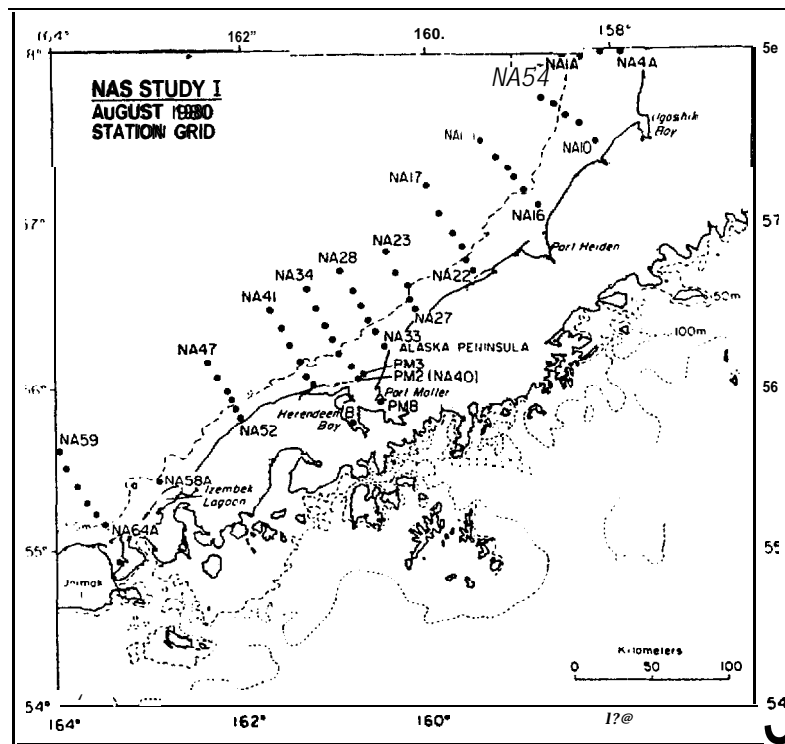


Figure 9a. The location of stations occupied in August 1980 along the NAS.

4.2 North Aleutian Shelf

The North Aleutian Shelf (NAS) extends from Unimak Pass on the west to the Kvichak River on the east (see Fig. 1). Two hydrographic regimes are described in this section, the coastal zone characterized by water depths less than 50 m and the middle shelf representing the slightly deeper offshore water. The coastal zone is usually well mixed due to the dissipation of wind and tidal energy, whereas the middle shelf is seasonally stratified (Schumacher et al., 1979). Because of these hydrographic differences, a frontal-type structure near the 50 m isobath is observed, which may influence the trajectory and dispersion of spilled oil.

The NAS region was surveyed three times to describe its seasonal characteristics. The station locations for each cruise are shown in Figures (9a-9c). The grid pattern was altered slightly during each cruise

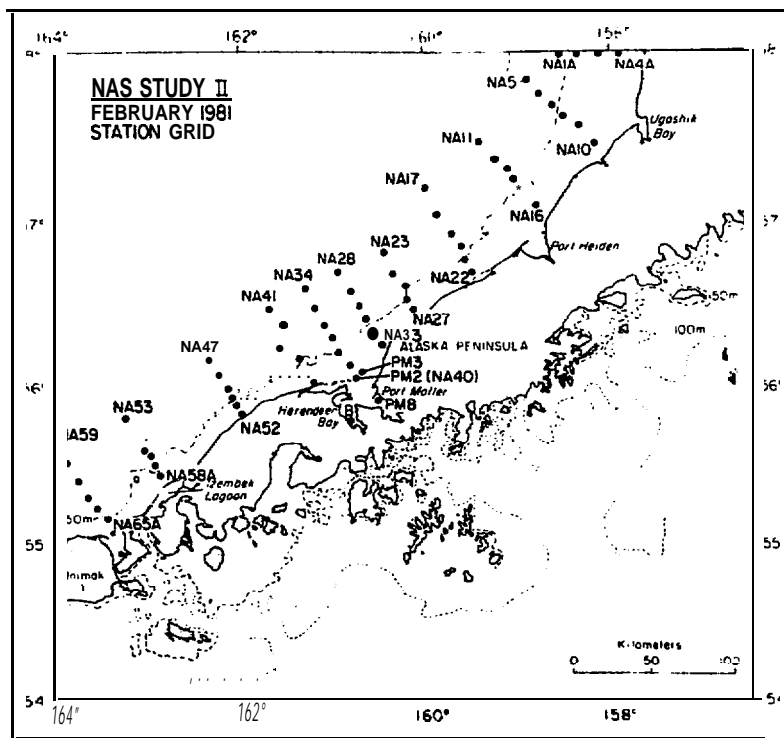


Figure 9b. The location of stations occupied in February 1981 along the NAS.

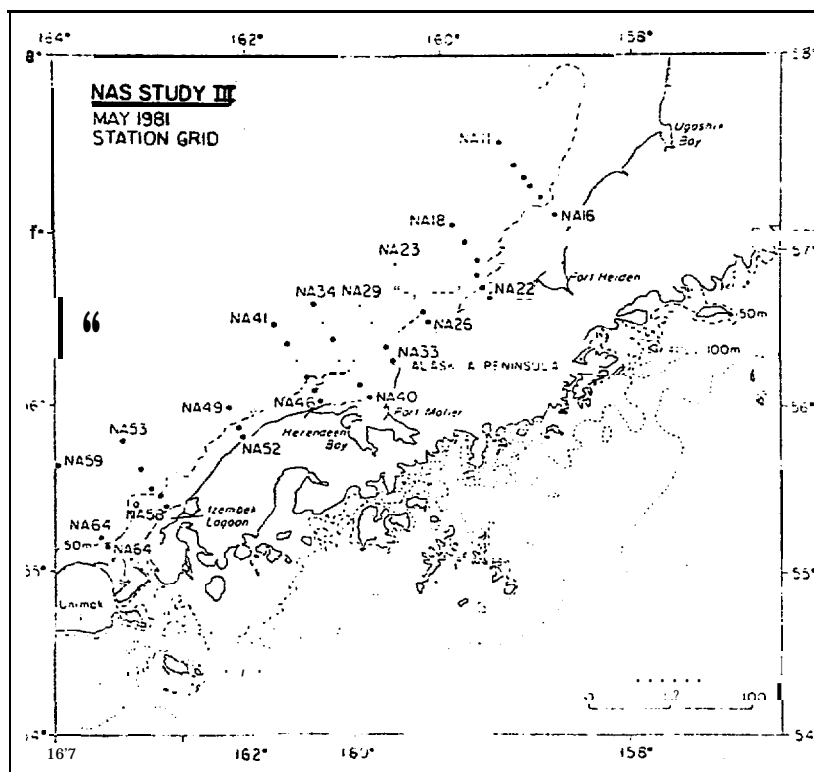


Figure 9c. The location of stations occupied in May 1981 along the NAS.

to account for seasonal hydrography and weather conditions. The methane tracer study emphasized the area adjacent to Port Moller (source) and the downstream region, which extends northeastward to approximately Port Heiden.

In order to summarize the hydrographic conditions for the coastal zone and the middle shelf region, the seasonal T-S relationships for each sub-region are discussed. These relationships are shown in Figures (10) and (11) for the survey periods of August 1980, February 1981, and May 1981.

August, a period of relatively high runoff to the coastal region, is characterized by a strong east-west salinity gradient (Fig. 10). The dominant source of freshwater is the Kvichak River, located at the eastern extremity of the region. There are numerous small sources of freshwater along the NAS, the major source being Port Moller. Diffuse sources of freshwater along the coast lead to relatively low salinities ($S-30^{\circ}/00$) and warm temperatures ($\cong 12^{\circ}\text{C}$). Over most of the coastal regime, however, salinities and temperatures range from $30-32^{\circ}/00$ and $8-11^{\circ}\text{C}$, values typical of summer conditions.

In February, temperatures had decreased to near zero, while salinities remained in the range of $30-32^{\circ}/00$ (Fig. 10). While it is likely that freshwater runoff had diminished significantly because of subzero temperatures, the salinities remained nearly constant. The reason for this lies in the mechanisms by which salt is transported across the shelf. One possible explanation is that a decrease in freshwater input results in a reduction in estuarine transport of salt, particularly within the cyclonic circulation of the coastal zone (Kinder and Schumacher, 1981b).

Water temperatures along the coast in May were intermediate between those observed in August of 1980 and February 1981 (Fig. 10). Temperatures had increased to $5-8^{\circ}\text{C}$, while salinities remained in the typical range $30-31^{\circ}/00$. The mean salinity decreased slightly compared to the previous winter, presumably in response to renewed input of freshwater.

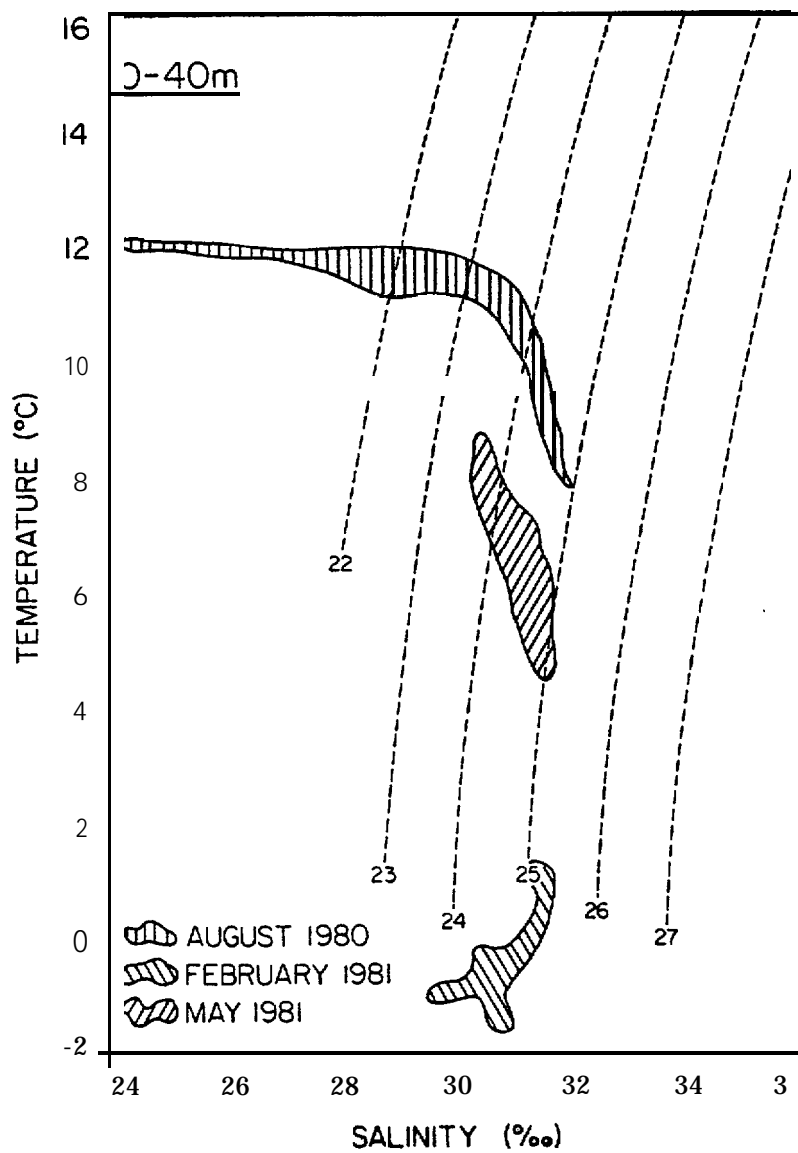


Figure 10. The seasonal distribution of salinity and temperature along the NAS. The coastal zone was defined to include all waters whose depth was less than 40 m.

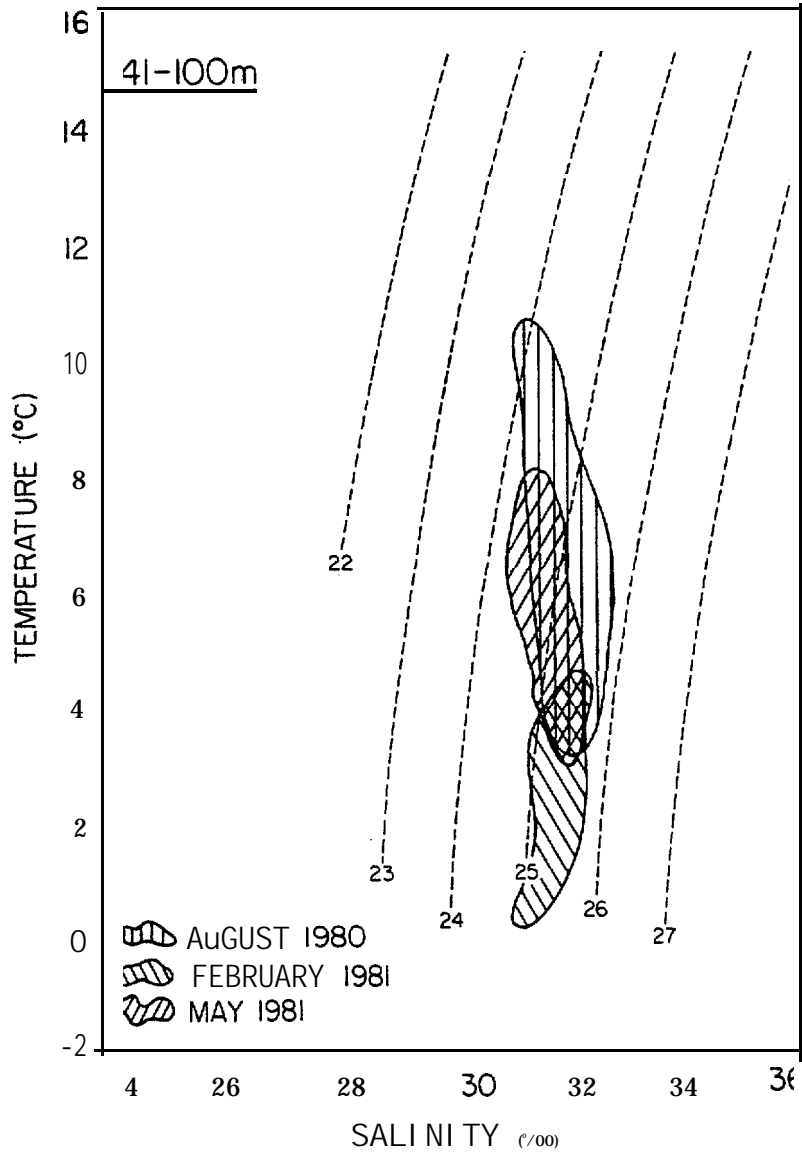


Figure 11. The seasonal distribution of salinity and temperature along the southern boundary of the middle shelf. The middle shelf was operationally defined to include all stations at which the depth of water exceeded 41 m.

The density field, regardless of season, was largely controlled by salinity. The density range (σ_t) was 23 to 25, and largely reflected the longshore distribution of salt.

The seasonal T-S relationships for the southern sector of the middle shelf are shown in Figure 11. In August, the water was nearly **isohaline** at 31-32‰. Temperature ranged from 3°C to 10°C, the colder waters originating during the previous winter. As noted in the coastal zone, warmer water was associated with lower salinities. On the average, however, salinities were higher in this region compared to the coastal zone (compare Figs. 10 and 11). Temperatures as high as 11°C and salinities as low as 29‰ were observed at the eastern extremity of Bristol Bay.

In February, colder water temperatures prevailed (0 to 4°C), but salinities remained constant at 31-32‰ (Fig. 11). Little horizontal or vertical stratification existed; hence, the T-S trajectory was parallel to the **isopycnals**. Densities were uniformly 25 to 25.5 σ_t units, slightly higher than the range of 24 to 25.5 observed in August, 1980.

By May, solar insolation had increased temperatures to 8°C, but salinities remained nearly constant at 31-32‰. Stratification had increased as indicated by the intersection of the **isopycnal** and T-S surfaces. The temperature range over the region was 2 to 8°C, the colder water being a relict feature from the previous winter (Kinder and Schumacher, 1981b).

Examples of the seasonal changes in water column stratification are shown for each **hydrographic** regime in Figures (12a-12c) and (13a-13c). Station 27 and 23 are representative stations in the coastal zone and in the southern sector of the middle shelf respectively. Station 27, which was occupied on each of the three cruises, was located approximately 5 km offshore in 25 m of water. The vertical distribution of properties indicates that the water column normally was well mixed, although some stratification was

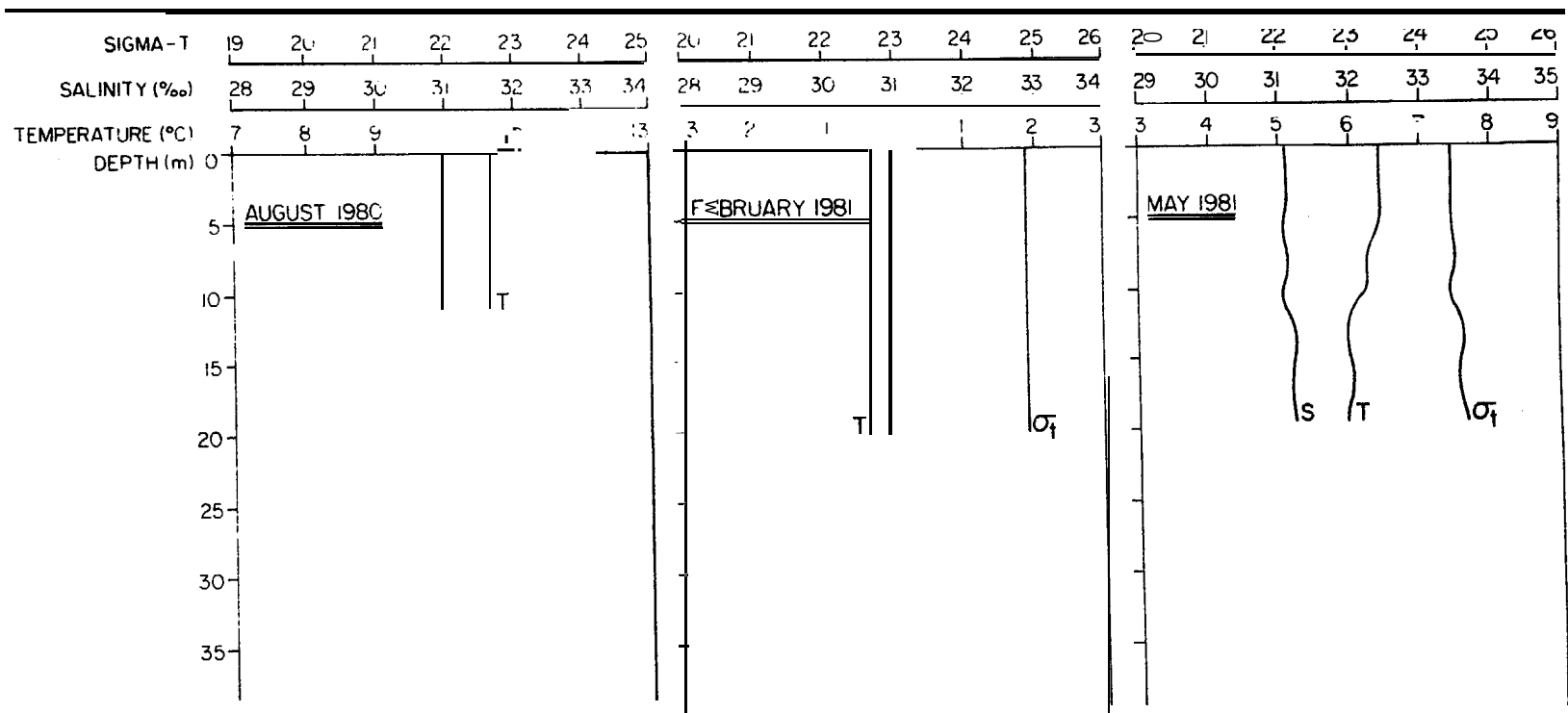


Figure 12. The seasonal distribution of salinity, temperature, and density (σ_t) at Station 27 in the coastal zone. Note the well-mixed water column.

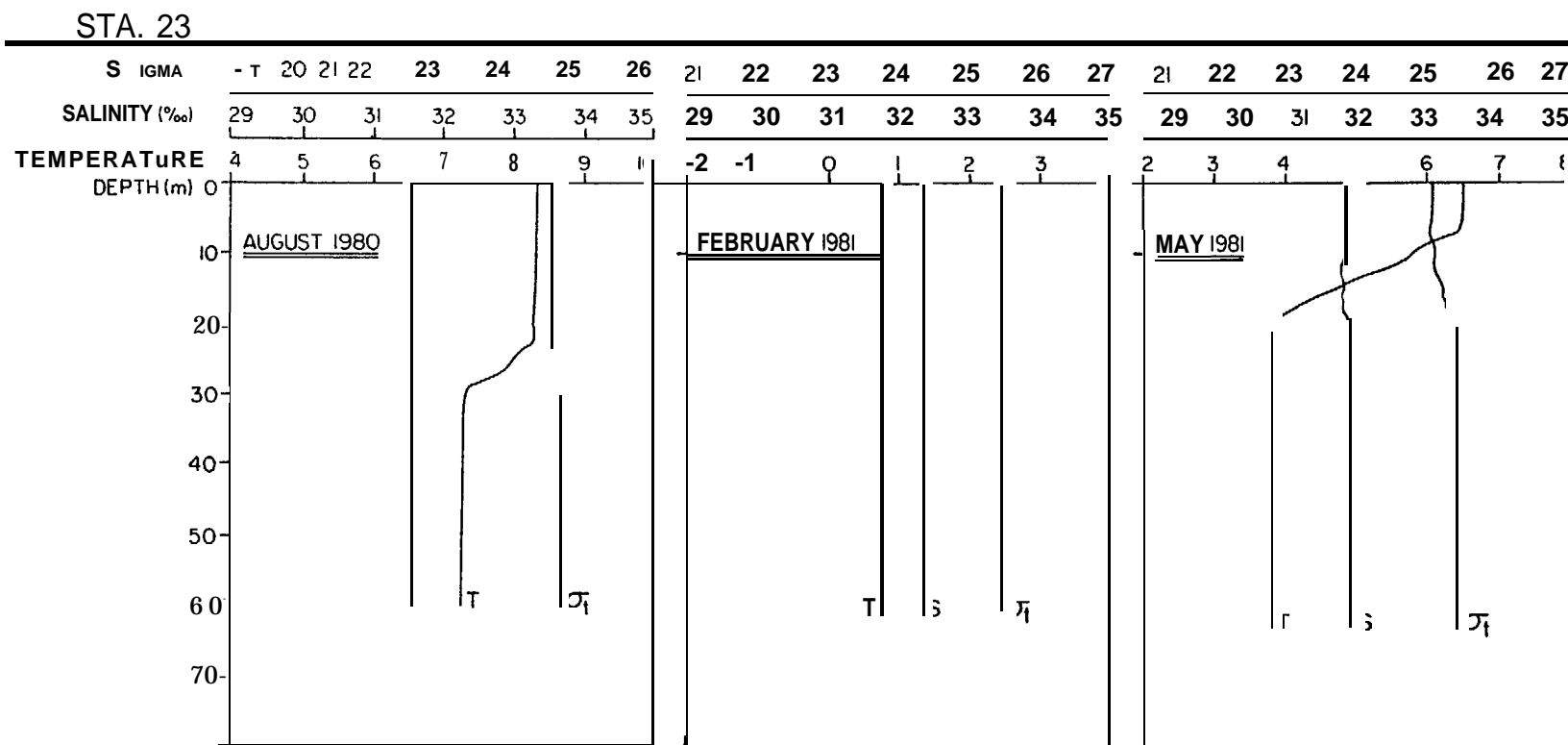


Figure 13. The seasonal distribution of salinity, temperature, and density (σ_t) at Station 23 in the middle shelf. Note the isothermal, **isohaline** conditions in February 1981.

observed in May 1981 (Fig. 12c). This may have been a transient feature, however. As noted above, the salinity remained remarkably constant at 31‰, while the temperature varied from 10°C in August 1980 to less than zero in February 1981.

In contrast to the well-mixed conditions in the coastal zone, the middle shelf region is characterized by weak seasonal stratification (Figures 13a-13c). Station 23, located about 50 km offshore (Figure 9) and at a depth of 68 m, is an example of middle-shelf conditions near the inner front. Salinity was at a minimum in August, increasing to nearly 32‰ in May. With the exception of February, in which the water column was totally unstratified, a weak **thermocline** was present in the upper 30 m of the water column. Because salinity was largely invariant, seasonal warming of the surface layers led to weak stratification, which was strongest in May. Under the influence of solar insolation and wind mixing, the **thermocline** deepens during the summer, but the gradient actually decreases due to the concomitant warming of the bottom waters. The net effect was to decrease the density gradient slightly. Because of large **interannual** variations in sea surface temperatures and the amount of ice formed locally, bottom water temperatures may vary **widely** from year to year (Niebauer, 1981).

There appear to be numerous diffuse sources of freshwater along the **NAS**. In Figure 14 are shown the mean salinities for the coastal zone ($z \leq 40$ m) as a function of distance from **Unimak** Pass. Salinity data from all stations located in less than 40 m of water were averaged horizontally and vertically for each of the three cruises.

In general, the salinity decreases from west to east along the shelf. The most dramatic decrease occurred in August in which salinities decreased from approximately 32‰ at **Unimak** Pass to a low of 28‰ near the Kvichak River. During all three cruises, a **local** salinity minimum occurred at Port

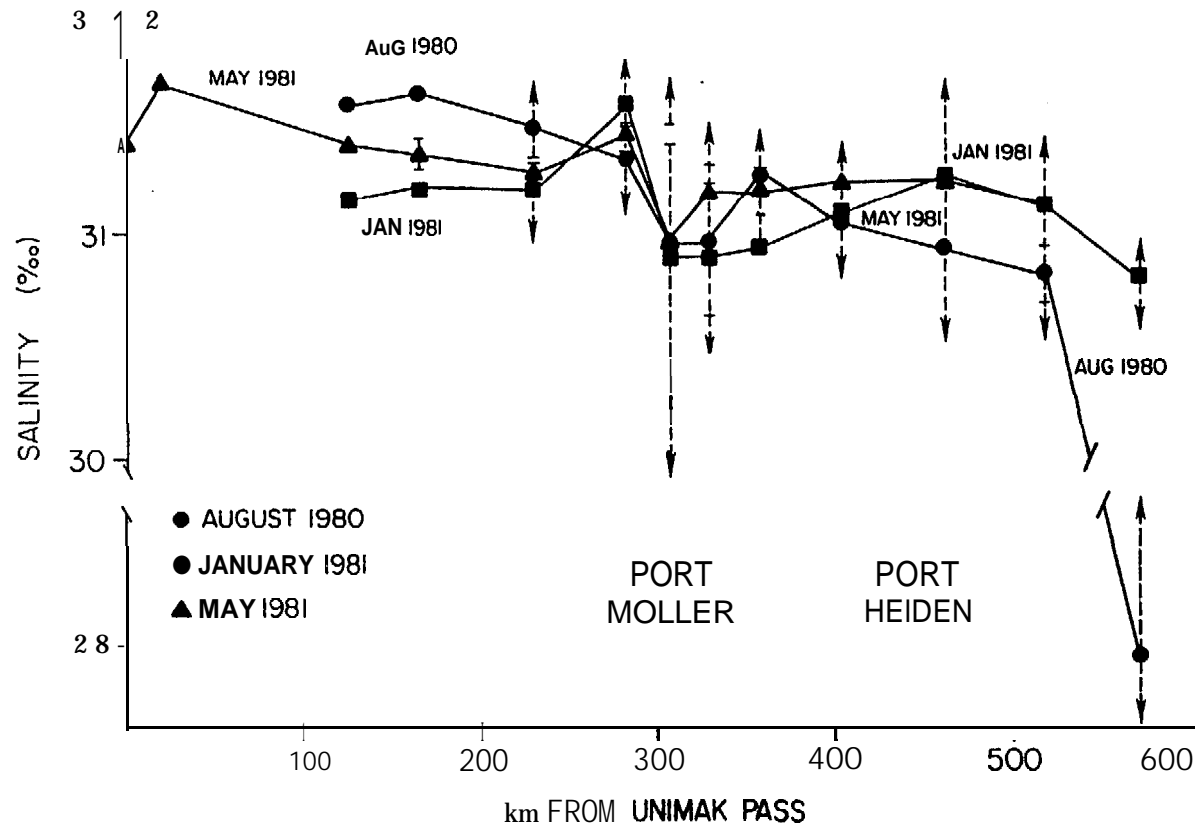


Figure 14. The average longitudinal distribution of salinity along the NAS coastal zone. Only stations at which the depth of water was less than 40 m were included in the analysis. The dashed arrows indicate the range of values about the mean. Note the large variations at the entrance to Port Moller.

Moller, indicating the significance of this source. The salinity profiles for February 1981 and May 1981 indicate that the mean drift of the coastal water is toward the east, in agreement with the **cyclonic** circulation through Bristol Bay. During February, the freshwater influence of Port **Moller** was evident to Port Heiden, a distance of about 150 km. To the east of Port Heiden, the effect of the **Kvichak** River is evident in the systematic decrease in salinities.

A decrease in the mean salinities along the NAS can be interpreted in two ways. The first is that **cyclonic** circulation through Bristol Bay results in a continual freshening of the high salinity water entering through Unimak Pass. This assumes that the flux of salt across the inner front is not totally sufficient to balance the freshwater input. The second case assumes that circulation is anticyclonic and that the salinity of the coastal water steadily increases due to cross-frontal salt flux and a decrease in the freshwater supply to the west along the shelf. Current meter measurements suggest that the circulation is indeed **cyclonic** (Kinder and Schumacher, 1981b), an interpretation that is supported by the distribution of methane as well.

The horizontal surface distribution of dissolved methane in the coastal zone and the adjacent middle shelf region is shown in Figures 15a,b,c. In August (Fig. 15a), the middle shelf region was characterized by surface concentrations of methane of 400 **nL/L** or nearly 8 times supersaturation. Concentrations of methane along the inner front were approximately 500 **nL/L**, decreasing toward the northeast. The highest concentration of methane observed was 22,000 **nL/L** inside the Port **Moller** estuary, decreasing to approximately 1200 **nL/L** at the entrance. The concentration of methane at the entrance to Port **Moller** depends on the stage of the tide, as one might expect.

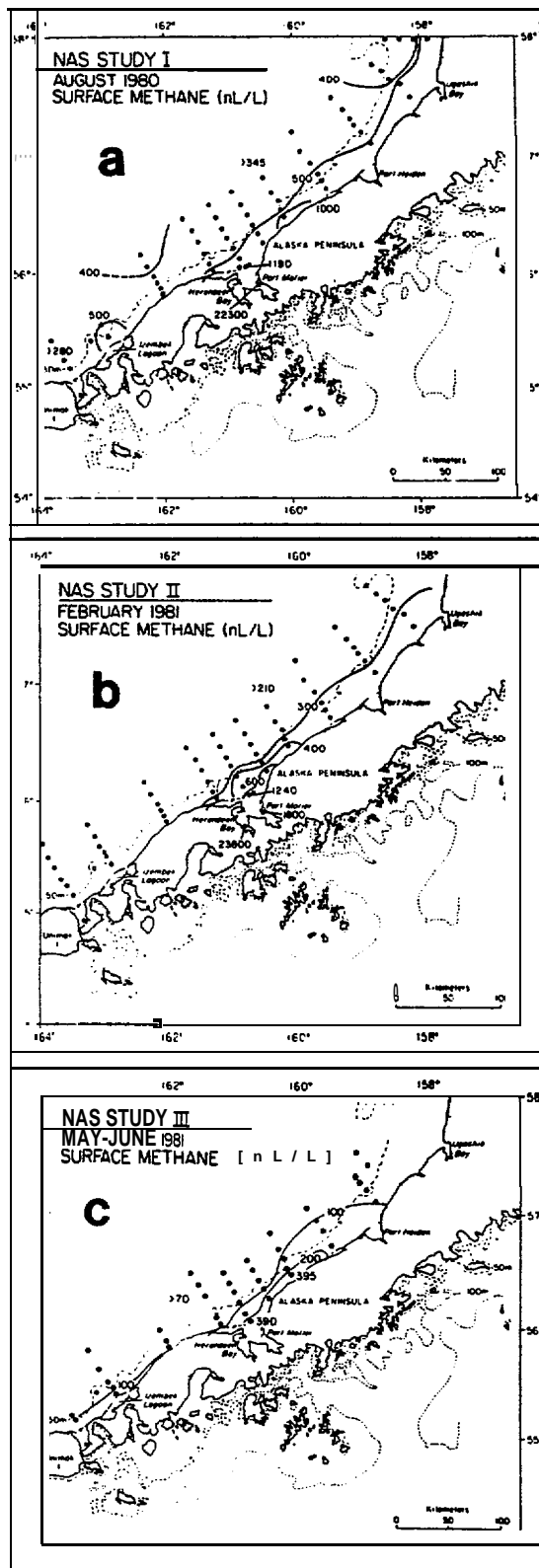


Figure 15. The distribution of methane at the surface along the NAS in (a) August 1980, (b) February 1981, and (c) May 1981. Concentrations are in nL/L (STP).

In February (Fig. 15b), the offshore concentrations had decreased to less than 300 nL/L, whereas the average value near the entrance was about the same as seen the previous August. The inner front was characterized by concentrations of methane of 300 nL/L. The observed systematic decrease in the ambient levels of methane between August and February is attributed to a decrease in biological activity and a seasonal drop in temperature.

The following May, concentrations of methane had decreased to the lowest levels observed (Fig. 15c). Offshore values were approaching saturation levels (~70 nL/L), while the coastal concentrations had fallen to 100-400 nL/L. This observation was unexpected because the spring bloom had commenced, but apparently the microbial production of methane lags the production of carbon by several months. This fact was also observed earlier during the initial baseline study (Cline, 1976).

For each of the observational periods, the trajectory of methane was toward the northeast in agreement with previous observations (see above). The dominant source of CH₄ to the coastal zone was from Port Moller, but other diffuse sources along the coast could not be totally evaluated. We will show below that the tidal flux of methane from Port Moller is sufficient to account for the along-shore distribution of methane without invoking additional sources. In particular, the bottom sediments are not believed to be a significant source of methane because of their coarse texture (coarse sand) and low organic carbon content (Sharma, 1974).

Once the dissolved methane from Port Moller enters the coastal zone, it is rapidly mixed vertically and laterally out to the inner front. This is shown in Figure 16 for two orthogonal sections near Port Moller during the August cruise (see Fig. 9 for ref.). Section IV, located east of Port Moller, shows the offshore decrease in dissolved methane, and the vertical homogeneity of the water column. Only station NA-33 reveals a surface

maximum. Near the front (NA-31), the concentration had fallen to about 450 nL/L and systematically decreased in the offshore direction. Section V, located farther to the east, shows the same vertical homogeneity as was seen in the previous section. Concentrations of methane near the front are approximately 400 nL/L. A vertically homogeneous water column with respect to methane indicates that mixing of the low salinity, high methane waters from Port Moller is essentially complete within 10-20 km of the entrance, or approximately 1-2 tidal excursions.

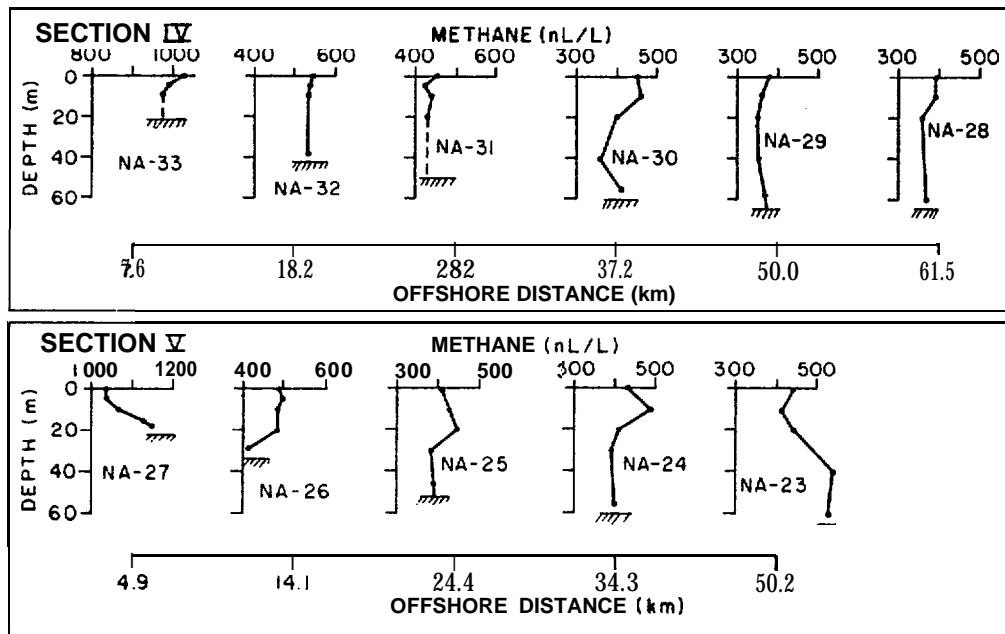


Figure 16. The vertical distributions of methane along sections IV and V east of Port Moller (see Fig. 9a). Measurements were made in August 1980.

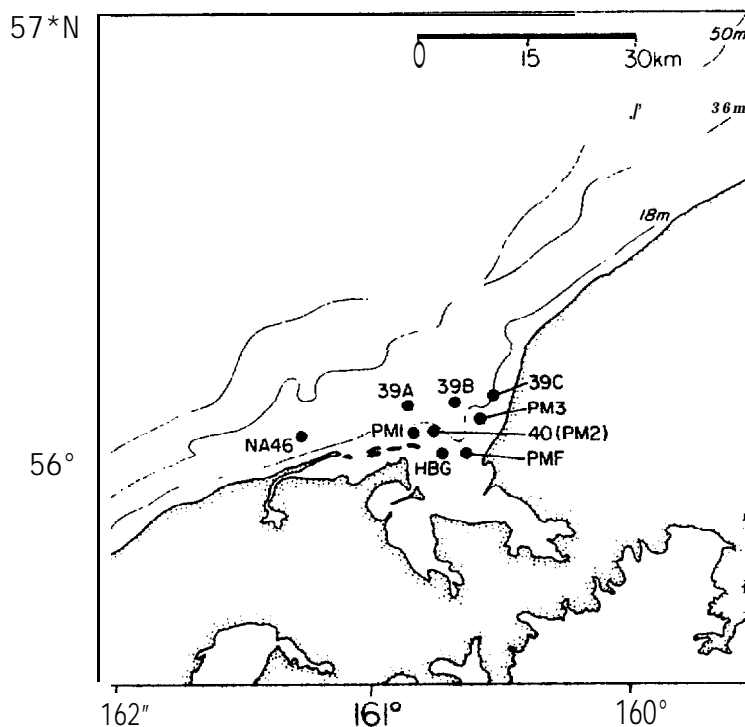


Figure 17. The location of 24-hour time series stations at the entrance to Port **Moller**. Stations PM1, PM2, PM3 were occupied in August 1980; Station PM3 in February 1981; and Stations 39A, 38B, and 39C in May 1981.

In order to quantify the flux of methane from Port **Moller**, which was required to satisfy the boundary conditions of the model (see page 362), a time series was conducted near the entrance during all three visits. The location of these stations is given in Figure (17). Stations PM1, **PM2 (NA40)**, and PM3 were occupied in a cyclic fashion over a period of 24 hours during the August and February cruises, while stations **NA-39A**, B, C were occupied during the May cruise. These stations were used to establish the tidal flux conditions for the model.

The methane enriched water was always found along the eastern shore of the estuary as depicted in Figures (18a,b,c). In August, the largest concentrations (3-4 $\mu\text{L/L}$) of methane were observed at PM-3, decreasing abruptly to $1\mu\text{L/L}$ at PM-2. Stations **NA-38** (Figure 9), located at the inner front,

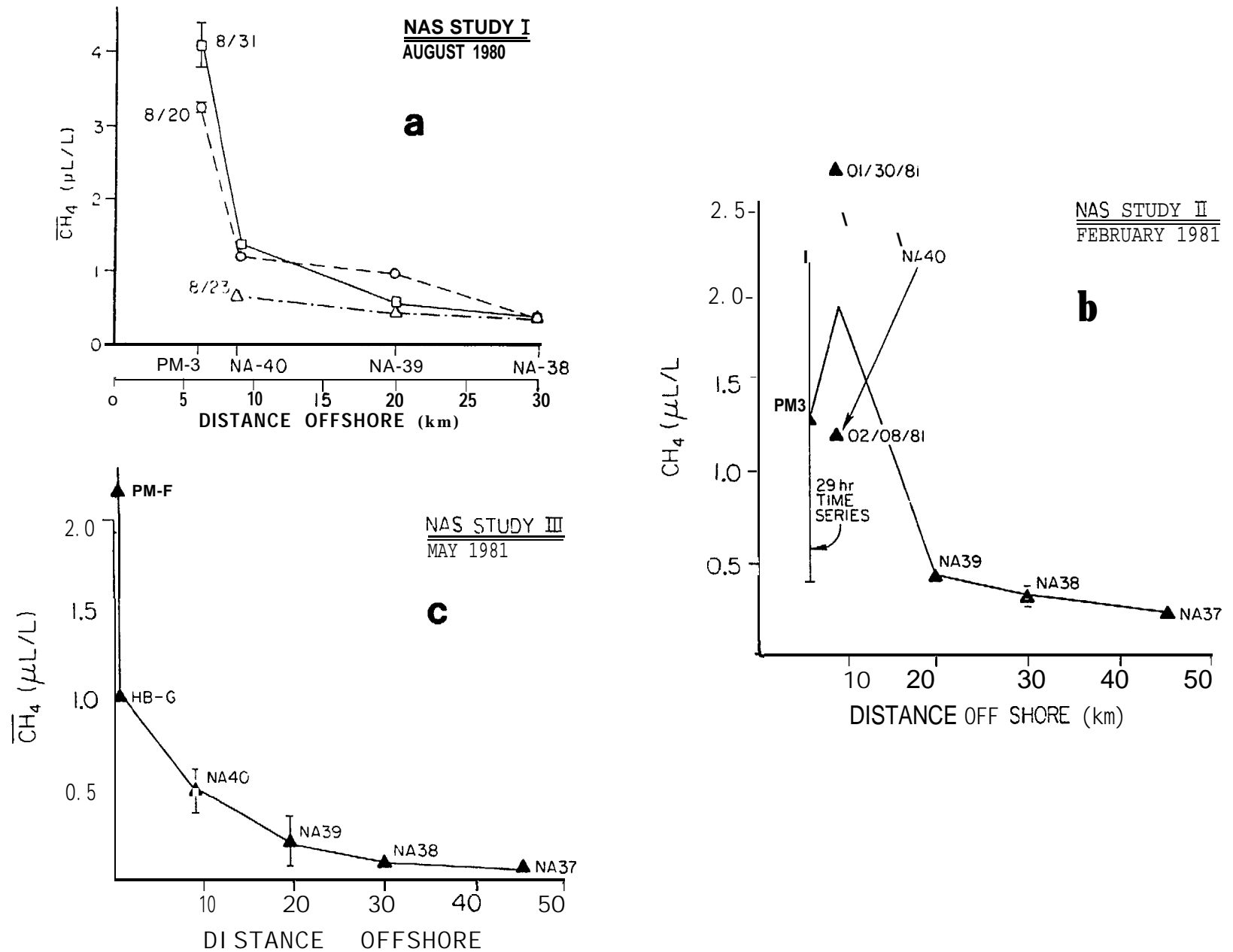


Figure 18. The time-averaged distribution of methane across the entrance to Port Moller in (a) August 1980, (b) February 1981, and (c) May 1981. In those cases where more than one measurement was made, the vertical lines indicate the range of values about the mean.

showed a relatively constant concentration of methane of $0.5\mu\text{L/L}$, the background level observed for that time of year. As we will show later, the concentration of methane (i.e., depth averaged) at the entrance shows large variations due to tidal influences; however, the highest concentrations of methane are always found along the eastern shore, regardless of the stage of the tide.

In February (Fig. 18b), the highest concentrations were observed at PM-3 and NA-40 (PM-2). The mean at each of these stations was $1.3\mu\text{L/L}$ and $1.9\mu\text{L/L}$ respectively as compared to a background level of $0.2\mu\text{L/L}$. The large ranges (e.g., extrema) observed at PM-3 and NA-40 are due to the stage of the tide.

As noted earlier, the concentration of methane over the entire NAS in May was lower than had previously been observed. This was the case for Port Moller as well (Figure 18c). As before, the highest concentrations of methane were observed at PM-F and H'B-G, stations located at the entrance to Port Moller. Ambient levels offshore fell to approximately $0.1\mu\text{L/L}$ or 100nL/L as noted earlier.

The influence of tides on the fluxes of salt and methane is shown in Figure 19, which describes the observations taken at PM-3 over a 24-hr period. Temperature showed little variation over the period, whereas salinity varied from 30 to 31‰ , depending on the stage of the tide. The concentration of methane varied from $0.3\mu\text{L/L}$ to over $2.5\mu\text{L/L}$ in concert with the flood and ebb of water from Port Moller. It is this tidal flux that sustains the plume of methane observed along the coast.

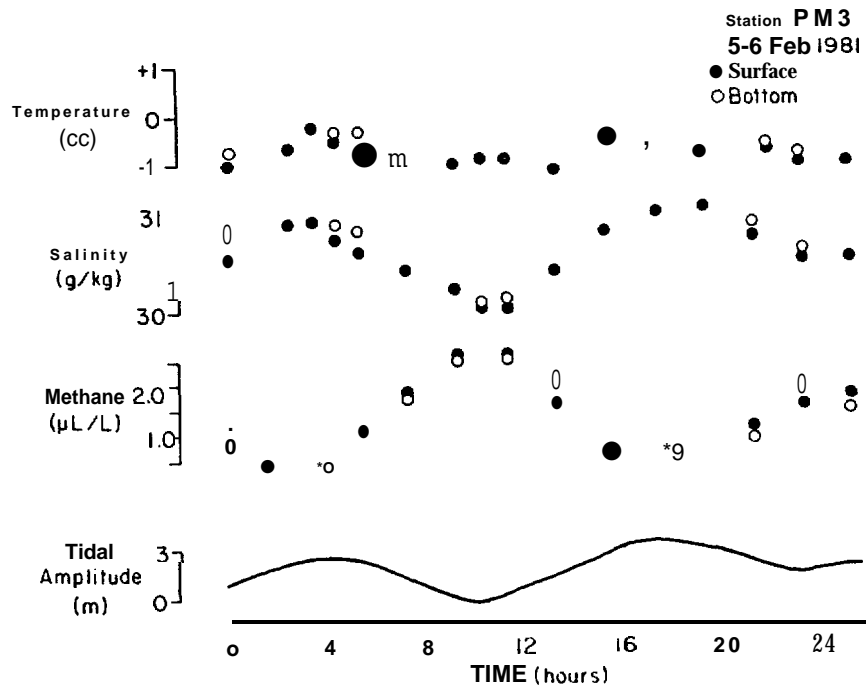


Figure 19. The diel variation in temperature, salinity, and methane at Station PM3. Measurements were made on 5-6 February 1981. Note that low salinity, methane-enriched water is found at the entrance to Port Moller during ebb tide.

5. TRANSPORT MODELS

5.1 Horizontal Trajectory Model

The distribution of dissolved methane in the two survey regions was modeled to provide limits on the horizontal and vertical scales of mixing. The model also provides a comparative check on the magnitude of the mean current speeds, which under most conditions will govern the transport of both surface and 'dissolved' oil.

The usefulness of dissolved methane as a chemical tracer depends critically on the characteristics and strength of the source. For a point source of **uniform** strength, the spatial distribution of methane can be used to define limits on mixing and transport processes. The most straightforward use of this tracer was found along the North Aleutian Shelf (**NAS**), where the biological production of methane within Port **Moller** (see Figure 18) resulted in a significant tidal flux to the coastal zone. This region is **hydrographically** complex (**Csanady**, 1981), seasonally and spatially variable, and strongly under the influence of coastal winds. Moreover, subtidal frequencies are strongly dependent on the frequency and duration of storms (Schumacher, 1981). Our purpose here was not to attempt to resolve short-term spatial variations, but rather to clarify the mean condition that exists along the shelf for time periods **>30 d**.

To examine the salient spatial features of dissolved methane along the NAS, we adopted a stationary, two-dimensional model described by **Csanady** (1973). This particular model has been used to predict the dispersion characteristics of wastewater injected along a pipe (line source) into a coastal zone environment. The particular model chosen assumes steady state, balances lateral diffusion against horizontal advection, and includes a first order decay *term*, which incorporates both biological consumption and the air-sea exchange of methane. The assumption of steady state is not valid

for transient events, but should be valid for time scales in excess of one month ($u \geq 3$ cm/s), given a **Lagrangian** tracer scale of 75 km or more. The model is

$$\frac{\partial}{\partial y} \left\{ K_y \frac{\partial C}{\partial y} \right\} - u \frac{\partial C}{\partial x} - kC = 0, \quad (1)$$

where the space dependency of the horizontal eddy diffusivity is retained.

The solution to (1) for a line source of length b is

$$C = (C_0/2) \exp\{-kx/u\} [\text{erf}(y_1) + \text{erf}(y_2)] \quad (2)$$

where

$$y_1 = \frac{b/2+y}{0.1039(x/u)^{1.17}}$$

$$y_2 = \frac{b/2-y}{0.1039(x/u)^{1.17}}$$

x = longshore direction
 y = cross-shelf direction
 u = longshore mean velocity
 k = first order decay constant
 C_0 = concentration of methane at the source

In this description, we ignore diffusion in the x -direction and scale the horizontal diffusivity (K_y) in the y -direction according the **Lagrangian** time **scale**. For simplicity, we assume that mixing is isotropic in the x - and y -directions. However, **Okubo** (1971) has shown that dispersion is enhanced in the direction of mean flow. The magnitude of the difference is approximately a factor of three for those coastal situations that have been studied (**Okubo**, 1971). Along the **NAS**, tidal currents are strongly rectilinear, which presumably results in an enhanced mixing alongshore. In the presence

of a mean flow, u , it can be shown that:

$$\sigma_{rc}^2 = 2\sigma_x \sigma_y \quad (3a)$$

where σ_{rc} is the mean square radius of diffusing substance, σ_x and σ_y are the respective standard deviations of the plume in the x- and y-directions (Okubo, 1971). If we assume uniform horizontal mixing ($\sigma_{rc}^2 = 2\sigma_y^2$) the apparent diffusivity defined by Okubo is:

$$K_Y = \sigma_y^2 / 4t \quad (3b)$$

or

$$K_Y = \sigma_y^2 / 2t, \quad (3c)$$

where $\sigma_{rc}^2 = 2\sigma_y^2$ and t is the diffusion time. The characteristic time (or length) scale can be computed from $t = x/u$. Substituting into (3c), we obtain:

$$K_Y = \sigma_y^2 u / 2x \quad (3d)$$

Based on dye patch studies, Okubo (1971) has given estimates of K_y in terms of the characteristic length scale ℓ . He found that the 4/3 law overestimated the magnitude of K_y and presented a log regression diagram that shows:

$$K_Y \propto \ell^{1.1} \quad (3e)$$

or that

$$\sigma_{rc}^2 = 0.0108 \ell^{2.34} \quad (3f)$$

In equation (2), the horizontal eddy diffusivity is formulated in terms of the variance of the plume in the y-direction $\sqrt{2} S_Y$. After substitution of $t = x/u$ into (3f) we find:

$$\sqrt{2}s_y = 0.1039 t^{1.17} \quad (3g)$$

Based on the diffusion diagram given by Okubo (1971), we expect

$10^5 \text{cm}^2/\text{s} \leq K_Y \leq 10^7 \text{cm}^2/\text{s}$ for length scales between 10 and 100 km. If we assume that K_Y is proportional to the tidal excursion, which is approximately 10 km, then $K_Y \cong 10^5 \text{cm}^2/\text{s}$.

Dissolved methane may be lost from the water column via air-sea exchange and biological oxidation. Since both processes can be formulated in terms of first order kinetics, they are included in the model as a single term:

$$k = k_{a/s} + k_{\text{biol}} \quad (4)$$

Computation of $k_{a/s}$ requires knowledge of sea-surface roughness (a function of wind speed), the molecular diffusion and Bunsen volatility coefficients as a function of salinity and temperature. All of these parameters are known to within 30% (Broecker and Peng, 1974), thus $k_{a/s}$ can be estimated (see Cline, 1981 for details on the calculation of $k_{a/s}$).

Biological oxidation rates of methane, not previously known for these waters, have been determined by Griffiths et al., (1982). Water samples were inoculated with a known amount of $^{14}\text{CH}_4$ and incubated for 24 to 48 hours. The $^{14}\text{CO}_2$ given off after oxidation was counted and the rate constant computed. The kinetics generally obeyed a first order reaction when incubation time and substrate levels were varied.

The model is formulated in terms of a line source of length b . If the depth of the mixed layer (Δz) is known, then the mass transport of methane out of Port Moller is simply:

$$Q_{\text{CH}_4} = (b) \cdot (\Delta z) \cdot (u) \cdot (C_0), \quad (5)$$

where the mass transport Q has dimensions Mt^{-1} . Thus, the **diffusion-advection** model is sensitive to the boundary conditions: b , source length; Δz , mixed layer depth; u , mean alongshore velocity; C_0 , initial concentration at the boundary.

A schematic representation of the NAS and the major transport terms used in the model are shown in Figure (20). Because the water depth increases offshore, the methane distribution in the surface layer must be vertically averaged to provide a realistic representation of the actual distribution.

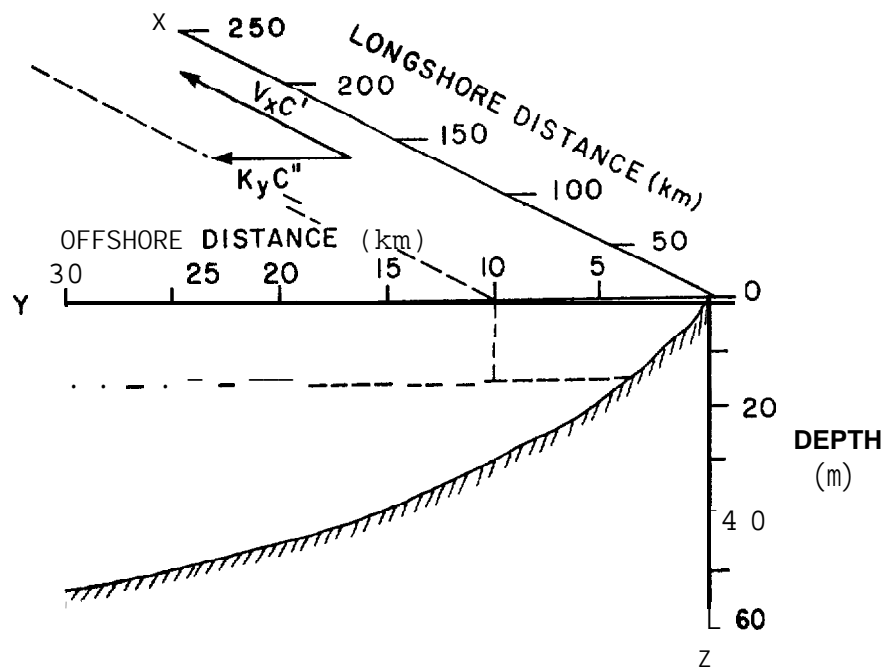


Figure 20. A schematic diagram of the NAS region. The significant transport terms include longshore advection $\bar{v}C'$, and the flux divergence $K_y C''$. The well mixed coastal zone is approximately 20 m deep and 32 km wide. Not shown in the diagram is the air-sea exchange of methane, which is proportional to the concentration of methane.

In the following discussions, we will use this model to estimate mean currents along the NAS and to compare these results with the current meter observations. Along any orthogonal section to the flow, the transport of methane must be balanced by the tidal source at the entrance to Port Moller. Time series measurements made at the entrance allow us to estimate C_0 , b , and Q ; thus the model is constrained by both a concentration at the boundary and the flux. Because the air-sea exchange and biological oxidation of methane are seasonally dependent, appropriate values will be used in the individual modeling comparisons.

5.2 Vertical Flux Model

In a stratified water column, a portion of the methane produced at the bottom diffuses vertically through the pycnocline. In the absence of biological consumption, the curvature in the methane profile provides an independent estimate of the magnitude of K_V within the pycnocline. In the situation where oil may be released at the bottom, vertical transport is limited by strength of the pycnocline. In St. George Basin, the water column is seasonally stratified, thus if oil (dissolved and emulsified) is released into the bottom waters, it will largely remain in the lower boundary layer. To estimate the rate at which dissolved material might be transported vertically in stratified waters of St. George Basin, we used methane as a dissolved tracer.

To quantify the magnitude of the vertical transport parameter K_V within the pycnocline, we adopted a one-dimensional flux model describing the vertical distribution of dissolved methane. The one-dimensional flux model assumes that the curvature in the methane profile is the result of variable shear within the pycnocline and not due to in situ consumption. This assumption is not totally valid in all instances, but it does place a lower

limit on the magnitude of K_v . The essence of the model is that \square ethane is produced at the bottom and is removed by horizontal and vertical transport processes. Most of the biologically produced methane is removed by horizontal **advection**, but a small portion diffuses vertically through the **pycnocline** and is removed by air-sea exchange. In the absence of biological processes, the model describing the distribution of methane within the **pycnocline** is

$$K_v \{dC/dz\} = \text{constant}, \quad (6)$$

where K_v is the depth dependent vertical eddy diffusivity. Since the flux across any horizontal plane is a constant, that constant must be equal to the air-sea evasion flux.

$$F_{a/s} = \frac{D}{h} \{c - c^*\}, \quad (7)$$

where D is the molecular diffusivity of dissolved methane, h is the thickness of the **laminar** boundary layer, and C^* is the equilibrium volatility of methane at the sea surface. The equilibrium concentration of methane is a function of its atmospheric mixing ratios, salinity, and temperature (Yamamoto et al., 1976). The constants D and h are known parameters, the latter being largely a function of wind velocity (Emerson, 1975). By combining equations 6 and 7, the vertical eddy diffusivity can be calculated from the methane gradient. To compute the gradient, the vertical distribution of methane was smoothed by eye, fit with a cubic **spline** function, and differentiated to provide a smooth distribution of K_v as a function of depth.

The magnitude of K_v is not actually depth dependent, but rather depends in a complicated way on the **local** velocity shear and stability of the water column (Welander, 1967). In the discussion to follow, K_v will be plotted as

a function of the Brunt- Vaaisala frequency, which is equal to

$$N^2 = (\rho/\rho_0) \frac{d\rho/dz}{\rho} \quad (8)$$

The stability of the water column is proportional to the density gradient, $d\rho/dz$. The factor g is the acceleration due to gravity.

6. DISCUSSION

6.1 North Aleutian Shelf

The distributions of methane observed along the North Aleutian Shelf were modeled to estimate the mean trajectory of the water mass, its mean velocity, and mixing characteristics. The model is simplistic and does not include such variables as velocity shear, complex bathymetry, and short term variability in the source of methane or the currents. All of these variables as well as complex frontal interactions will result in significant deviations between the observed data and the model predictions. However, the model does reproduce general features and is useful in corroborating the mean velocity and diffusion fields.

The model is two dimensional and stationary (see section 6.1). This does not imply that the distribution of methane is temporarily invariant--only that the model is not responsive to time intervals less than about a month. This estimate was made on the assumption that the mean velocity is about 3 cm/s and that the tracer scale is ≥ 75 km.

The only adjustable parameters in the model are the mean velocity, u , and the air-sea exchange rate parameter, k . The constant k also includes the biological oxidation rate (Griffiths, et al., 1982), which was a factor of about 3 less than the air-sea exchange rate. Also included explicitly in k is the depth of water. Because the depth changes systematically from zero at the shore to about 50m at the inner front, we selected a mean depth of 20m. By doing this, the significance of the air sea exchange term is minimized in shallow water ($z < 20\text{m}$) and maximized in deeper water ($z > 20\text{m}$). Similarly, we assume no horizontal shear ($\partial u / \partial y = 0$), divergence or convergence within the coastal zone. Transport across the inner front is by diffusive mixing only.

The principal source of methane is Port **Moller** and all other sources including bottom sediments are considered insignificant. The modeling of such a distribution is relatively simple as the model need only include source flux at the entrance to the estuary. Dissolved methane is fluxed into the coastal zone by tidal pumping, hence the large diel excursions observed in the concentrations. The source term was tidally averaged to provide a stationary source flux, but was spatially digitized to more accurately describe the offshore dilution of the source. As **methane-**enriched water is transported out to the inner front, it mixes with water of lower methane concentration. The diluted water from Port **Moller** is then transported northeast along the coast in the coastal drift. To account for the variable source in the y-direction (see Fig. **18**), the time and depth averaged source function was subdivided into 8 individual line sources, each 4 km in length. The total dispersion field was obtained by summing the individual contributions, including that reflected from the coastline. To avoid other model complexities, the ambient background concentrations of methane were subtracted from both the source and the coastal waters to give the distribution of excess methane, or that portion contributed by the Port **Moller** estuary.

As an example, we show the average distribution of methane at the entrance to Port **Moller** in August 1980 (Fig. 21). This distribution was based on all measurements taken, including the 24-hour measurements taken at Stations PM3, PM2, and **PM1**. The mean and the range are shown by closed triangles and dashed lines, based on 'n' measurements. This source was subdivided into 4 km source increments, after removing the background concentration of 0.45 $\mu\text{L/L}$. **PM13**, sampled only twice, was approximately 5 km offshore. For modeling purposes, we assumed the concentration was constant between **PM13** and the shore. By making this assumption, no serious error is envisioned because the depth of water was less than 5 m.

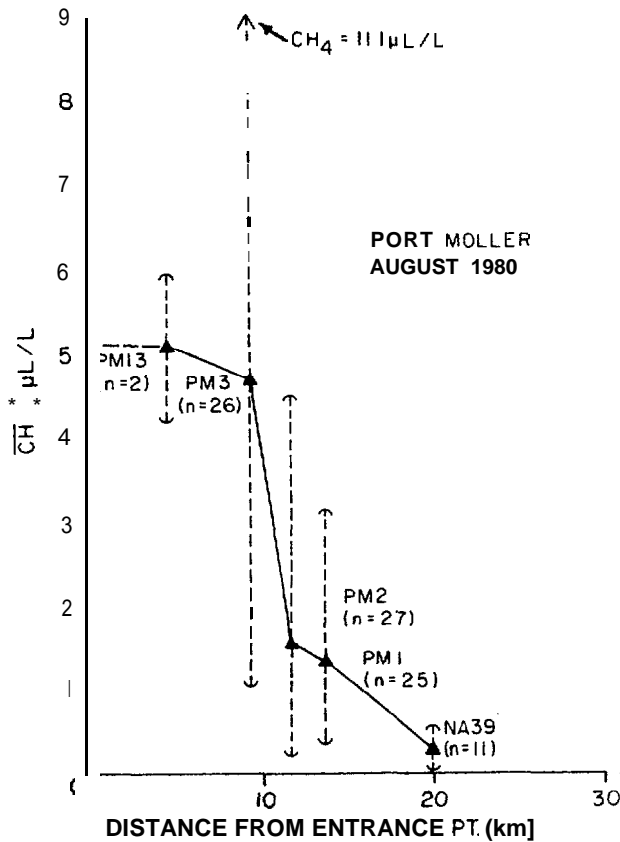


Figure 21. The average distribution of dissolved methane across the entrance to Port Moller. Observations were conducted in August 1980. The mean and range of values (n observations) are shown by the closed triangles and dashed arrows. The concentration of methane shoreward of Station PM13 was assumed constant. A background of 0.45 $\mu\text{L/L}$ was subtracted to give the concentration of excess methane from Port Moller.

One of the major deficiencies of the model is its inability to predict the effects of variable bottom bathymetry. To partially offset this problem, the model concentrations were depth averaged to sill depth (i.e. 20m). After summing all the plumes, the resultant concentration field was then depth averaged to the actual bottom depth. The reason for this was to see if the model simulation would improve the observed relationship between bathymetry and methane distribution. In reality, however, a mixing does not occur in this way. Mixing is essentially complete near the entrance of Port Moller and the distribution of methane is determined by spatial variations

in the mean velocity and by cross-frontal exchange processes. In the absence of any cross-frontal transport, varying the depth of water must result in a systematic change in the local velocity field.

6.1.1. August 1980

The depth-averaged, normalized distribution of excess methane is shown in Figure (22a). The background concentration of methane was 450 nL/L, which was removed from the concentration field. A residual mean concentration of 30 nL/L represents normal spatial variability. Near the source, the concentration of excess methane was approximately 5 $\mu\text{L/L}$ (5000 nL/L), decreasing to about 0.1 $\mu\text{L/L}$ at 180 km. The plume trajectory indicates a mean flow to the northeast, paralleling the shoreline.

The distributions of methane and salinity near Port Moller appear influenced by bottom bathymetry (Fig. 22a,b), and in particular the location of the inner front (see 45 m isobath on Figs. 22a,b). Because both constituents are related to freshwater discharge from Port Moller, the observed correlation between water depth and distributions may reflect two processes. The first is that offshore dilution of the freshwater (i.e. vertical mixing) results in the apparent distribution. This must be accompanied by a compression of the streamlines to preserve the apparent offshore intrusion of high salinity water (see $x = 60$ km). Density is closely related to salinity in these waters, which is why the isopycnal surface shows strong correlation with salinity and provides additional evidence that the coastal flow is controlled by bathymetry. The remaining explanation is that the inner front forms a hydrographic barrier to the onshore transport of salt. This might be envisioned as a surface convergence along the front accompanied by a near bottom divergence. Within the front, the onshore transport of salt would be inhibited by a diffusive barrier. However, there appears to be little

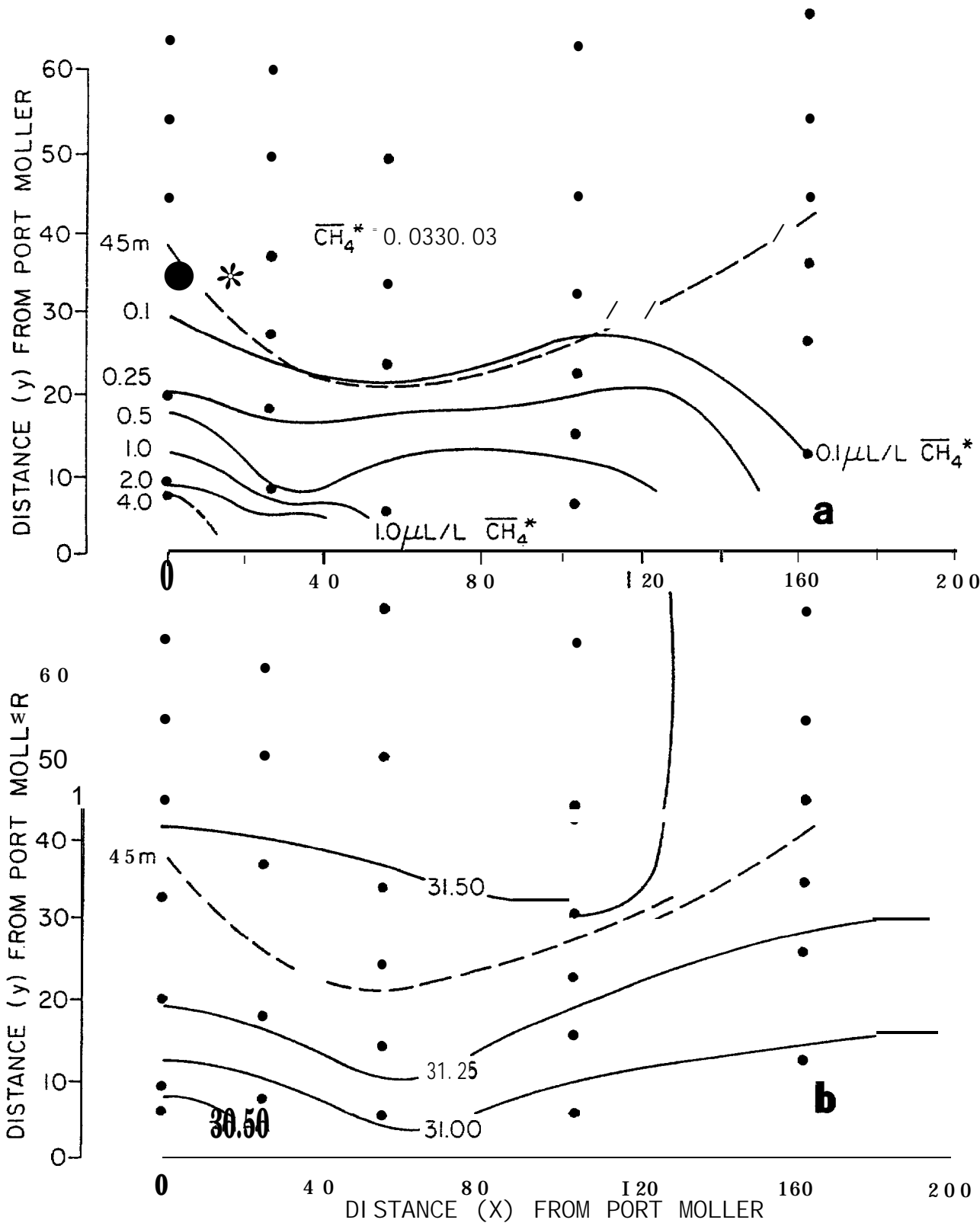


Figure 22. The depth-averaged distribution of (a) dissolved methane and (b) salinity and Port Moller in August 1980. A background concentration of $0.45 \mu\text{L/L}$ was subtracted from the observed field, leaving a residual concentration of $0.03 \mu\text{L/L}$ north of the inner front. The inner front is located near the dashed line (approximately 45 m).

evidence that the front is little more than a demarcation between the strong mixing of the coast zone and the seasonally stratified offshore waters (Jim Schumacher, personal communication). At this point, and because our analyses do not disprove it, we provisionally favor the latter explanation.

The constant k is the sum of the air-sea exchange rate and the biological oxidation term. The air-sea exchange term was computed from the mean wind velocity and the sea surface temperature. For a mean wind speed of 6 m/s and a sea surface temperature of 11°C, the computed air-sea exchange coefficient was 4.0×10^{-7} /s (Table 1). Adding to that the biological oxidation rate of 1×10^{-7} /s (Griffiths et al., 1982), the value of k is 5.0×10^{-7} /s. An uncertainty in the mean wind results in an uncertainty in k of about 50%. Using a mean k of 5.0×10^{-7} /s and an uncertainty of 50% ($\pm 2.5 \times 10^{-7}$ /s), mean velocities were arbitrarily chosen until the best visual fit was obtained.

Table 1. A summary of parameters used to estimate the air-sea exchange rate (R) of methane along the NAS coastal zone. The model is

$$R = - \frac{D}{h \cdot \Delta z} (C) = -k_{a/s} (C)$$

Date month/yr	Wind Speed m/s	Temp. °C	D cm ² /s	Δz m	h μm	k _{a/s} s ⁻¹
Aug. 1980	6	10.7	1.12X10 ⁻⁵	40	70	4.0X10 ⁻⁷
Feb. 1981	9.5	0.0	0.68X10 ⁻⁵	40	20	8.5 x 10 ⁻⁷
May 1981	7.5	6.5	0.96x10 ⁻⁵	40	50	4.8 x 10 ⁻⁷

The best fit was obtained for $u = 3.8$ cm/s and a $k = 5.0 \times 10^{-7}$ /s (Fig. 23). The model fit overestimates the transport in the near field ($x \leq 120$ km), but is in good agreement beyond that point. Increasing k or decreasing u would improve the fit in the near field, but only at the expense of the far field. The fit is quite sensitive to the magnitude of u and to a less extent k . Increasing k to a maximum acceptable level of 7.5×10^{-7} /s did not change the coastline intercepts appreciably, but did reduce the offshore penetration of dissolved methane.

Allowing k to vary between the limits 2.5×10^{-7} /s and 7.5×10^{-7} /s, u was arbitrarily chosen to provide the best fit. These results are shown in Figures (24a,b). Because the model contains the ratio, k/u , in the die-off term (see eq. 2), it is not surprising that minor adjustments in k require similar adjustments in u to maintain goodness of fit. For example, if $u = 2.5$ cm/s and $k = 2.5 \times 10^{-7}$ /s, the plume geometry is largely determined by lateral diffusion (Fig. 24a). If the velocity were decreased even further to improve the coastline fit, offshore diffusive transport would increase markedly, resulting in a poorer fit. However, mean velocities less than 2.5 cm/s were not used because the model formulation does not include diffusive transport in the x -direction, which would be required as $u \rightarrow 0$. Increasing k to 7.5×10^{-7} /s requires that u be at least 5 cm/s to maintain goodness of fit (Fig. 24b).

To demonstrate the effect of increasing the mean velocity, the mean flow was increased to 7.5 cm/s while keeping $k = 5.0 \times 10^{-7}$ /s. These results are shown in Figure (25). Note the flat distribution, indicating the dominance of **advection**. Clearly, this distribution is not similar to the observations shown in **Figure** (22a), where the 2.0 $\mu\text{L/L}$ and 1.0 $\mu\text{L/L}$ isopleths intersect the coastline axes between 40-60 km.

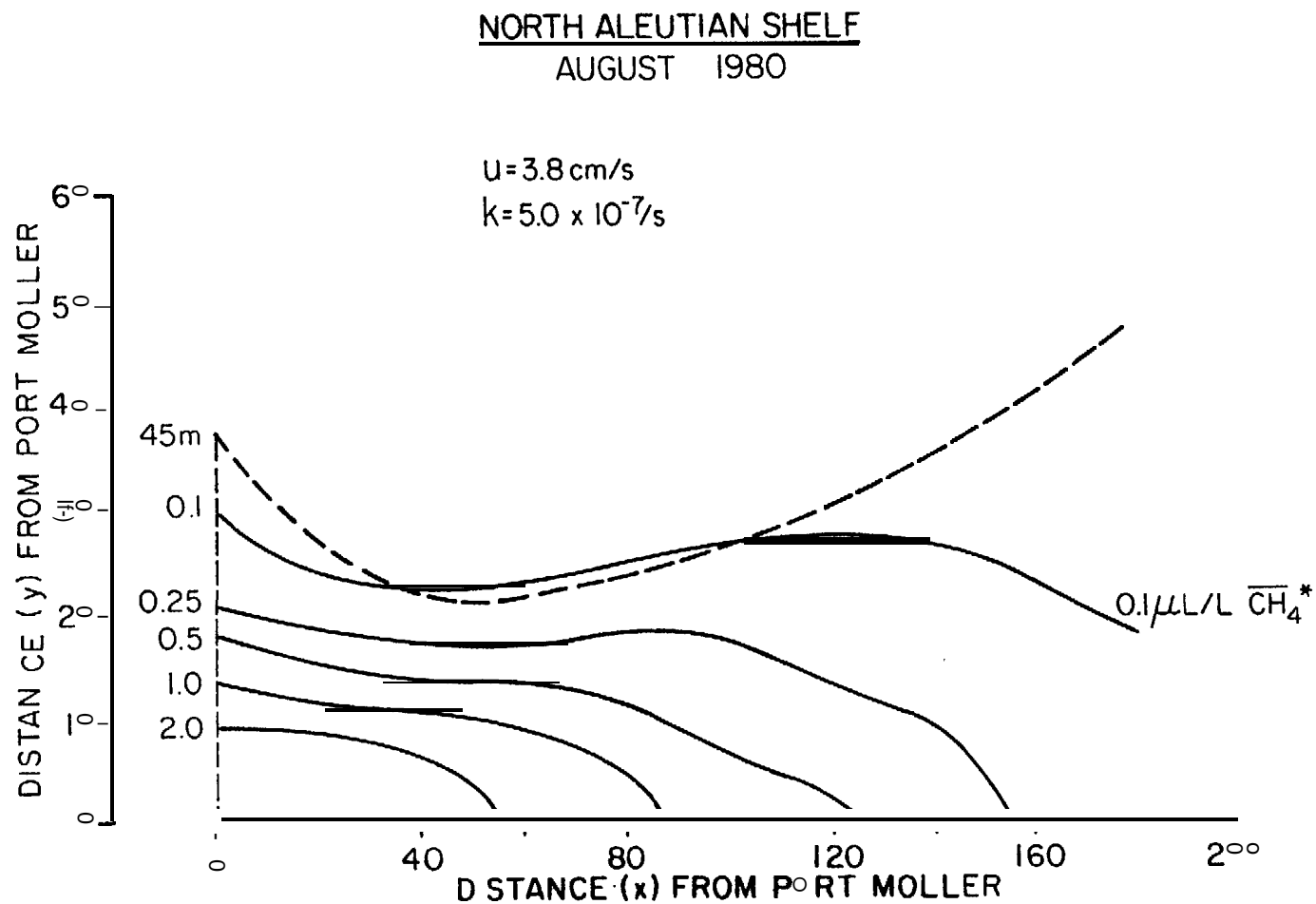


Figure 23. Model simulation of the distribution of methane for $u = 3.8 \text{ cm/s}$ and $k = 5.0 \times 10^{-7} / \text{s}$. This is the best fit to the observations shown in Fig. 22a. Concentrations are in $\mu\text{L/L}$. The position of the 45 m isobath is indicated by the dashed line.

NORTH ALEUTIAN SHELF
AUGUST 1980

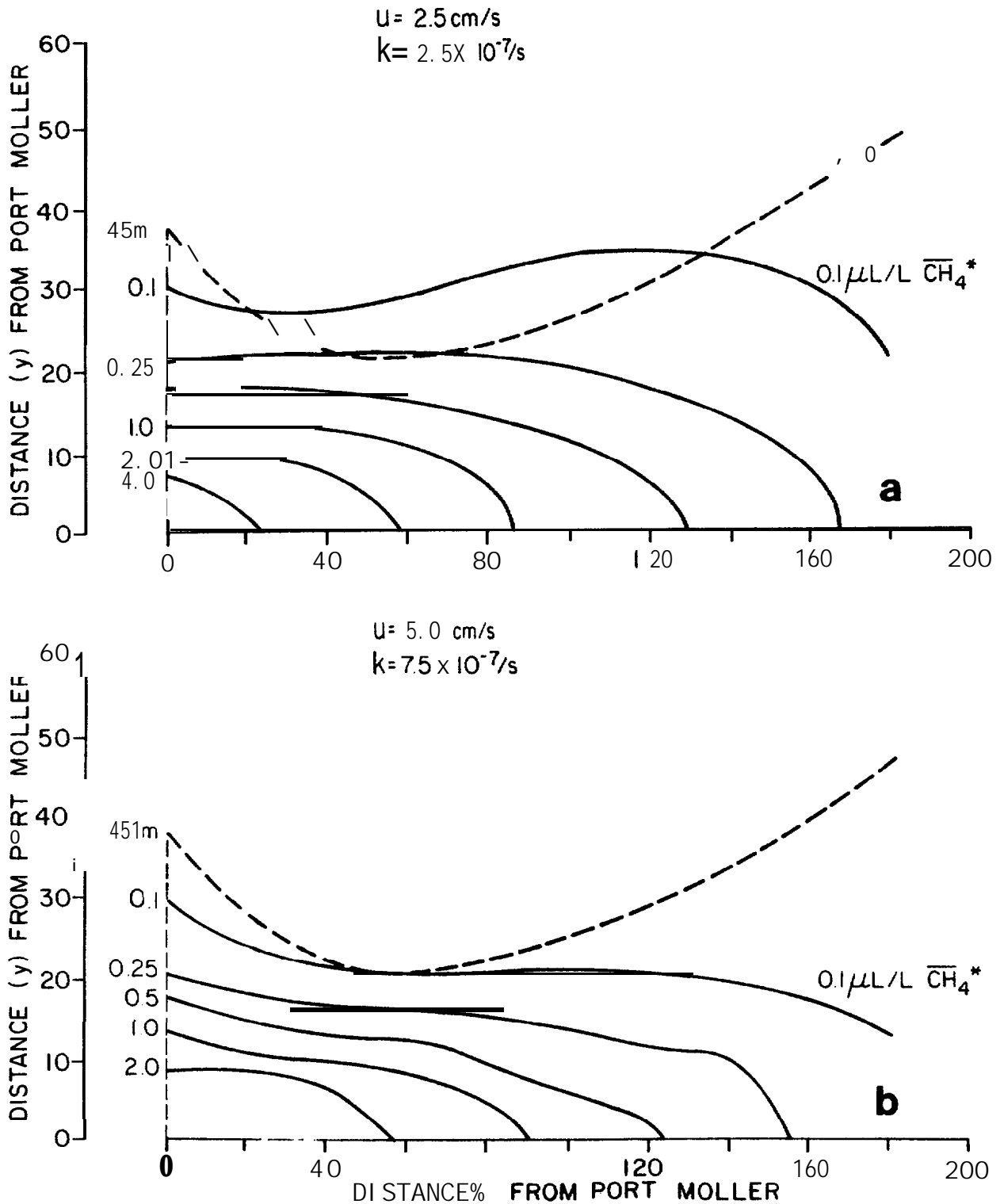


Figure 24. Model simulation of the distribution of methane for (a) $u = 2.5$ cm/s, $k = 2.5 \times 10^{-7} / \text{s}$ and (b) $u = 5.0$ cm/s and $k = 7.5 \times 10^{-7} / \text{s}$ in August 1980. Concentrations are expressed in $\mu\text{L/L}$. The position of the 45 m isobath is indicated by the dashed line.

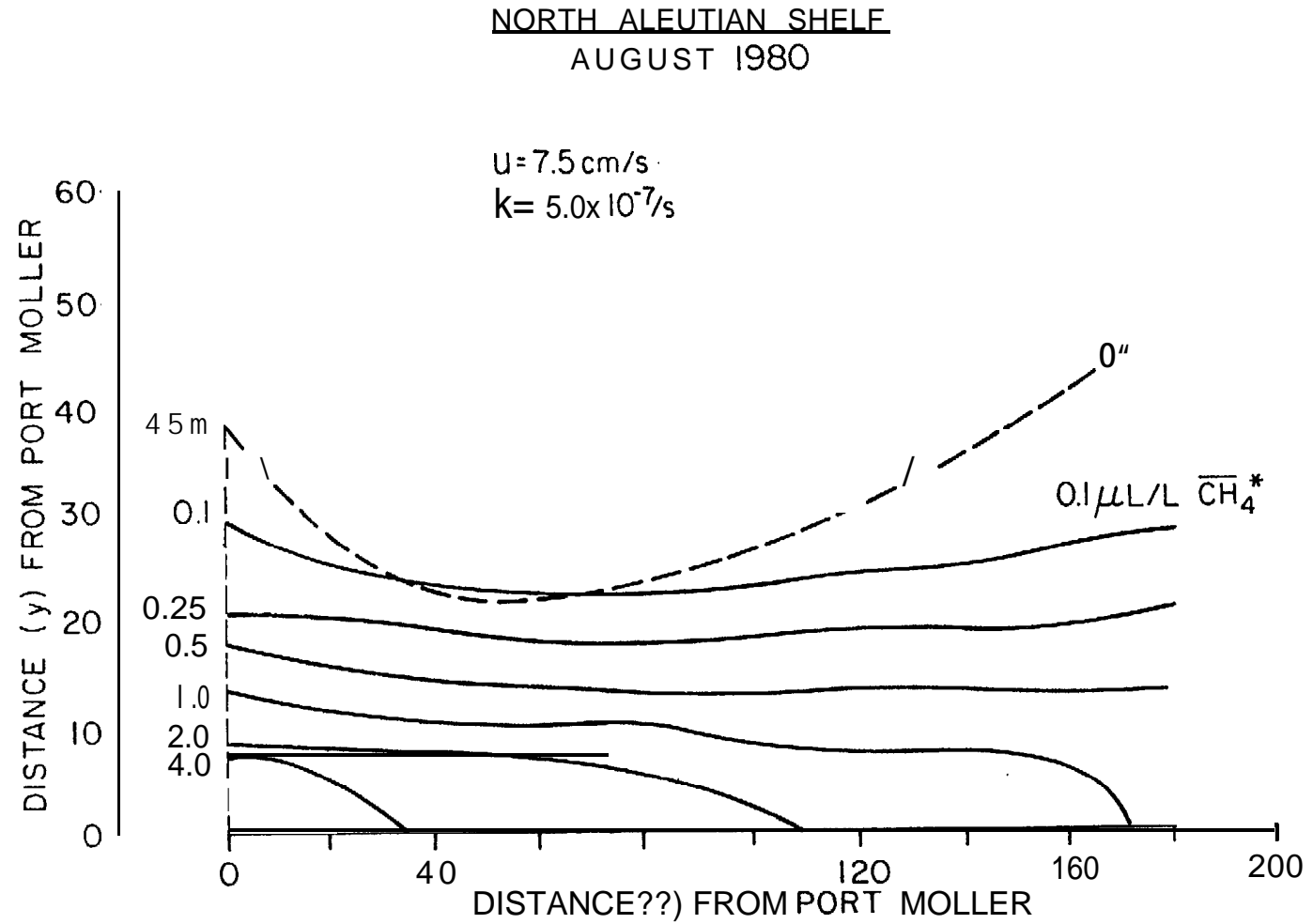


Figure 25. Model simulation of the distribution of methane for $u = 7.5 \text{ cm/s}$ and $k = 5.0 \times 10^{-7} / \text{s}$ in August 1980. Concentrations are in $\mu\text{L/L}$. The position of the 45 m isobath is indicated by the dashed line.

The diffusive scale (K_x) is functionally dependent on the Lagrangian scale, about 200 km in the present case. From the monograms presented by Okubo (1971), K_x varies from $2 \times 10^{-5} \text{ cm}^2/\text{s}$ to about $2 \times 10^6 \text{ cm}^2/\text{s}$, assuming a minimum and maximum scale of 20 km and 200 km respectively. The corresponding K_x would be about a factor of three greater than these estimates. Because our simplistic model does not take into account temporal variations in circulation, horizontal shear, or the effects of a complex bottom bathymetry, there is no reason to adopt other mixing parameters unless a more rigorous diagnostic model were to be developed.

In summary, our best estimate of the mean velocity in August 1980 was 3-5 cm/s, in good agreement with the estimate of 1-6 cm/s given by J. Schumacher (personal communication). Our estimate is, however, higher than the value of 1-2 cm/s given previously by Kinder and Schumacher (1980).

6.1.2. February 1981

The flux of methane from Port Moller in winter was significantly less than observed the previous August. Concentrations at the entrance were a factor of 5 less, which was presumably due to a seasonal drop in temperature (11° to 1°C) and the concomitant decrease in microbial activity. Although the concentration of methane was significantly reduced, so were the background concentrations, permitting the plume to be distinguishable for at least 200 km as before (Fig. 15b).

The distribution of methane observed in February 1981, after depth averaging and removing a background concentration of 110 nL/L, is shown in Figure (26a). Note that the plume is clearly developed for approximately 60 km and less so for distances beyond that point. As we noted earlier, bathymetric influences on the distribution of methane were clearly evident as it was with salinity (Fig. 26b).

NORTH ALEUTIAN SHELF
FEBRUARY 1981

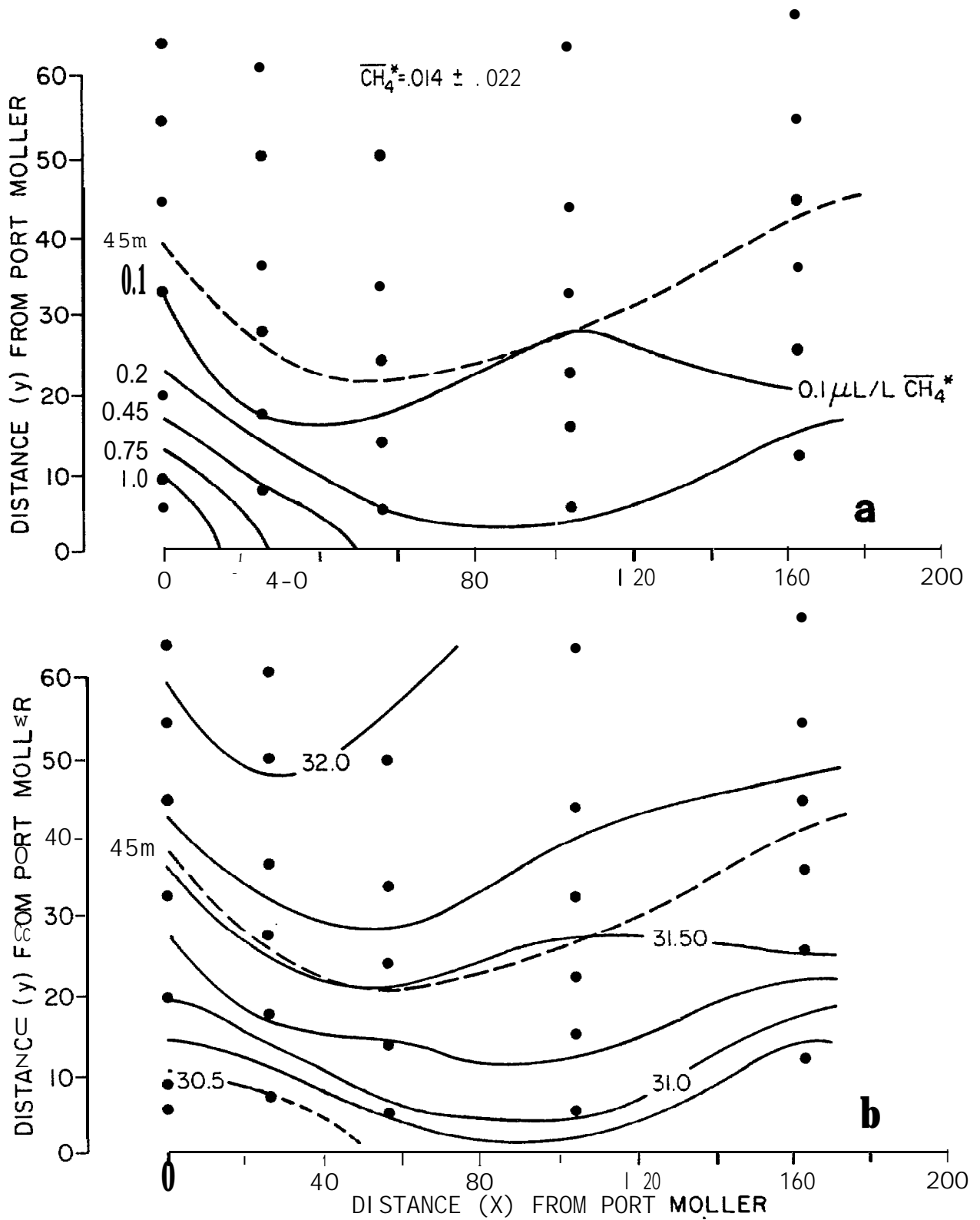


Figure 26. The depth-averaged distribution of (a) dissolved methane and (b) salinity in February 1981. A background concentration of 0.11 $\mu\text{L/L}$ has been subtracted from the concentration field, leaving a mean residual of 0.014 $\mu\text{L/L}$. The inner front is located near the 45 m isobath and is indicated by the dashed line.

The methane source distribution is shown in Figure (18b). Only PM3, located about 5 km from shore, was occupied for 24 hrs; all others were sampled twice. Because of paucity of data, average values for these stations are poorly known. For example, NA40(PM2) appeared to have the highest mean, but that may be due to the sampling frequency and the stage of the tide during which sampling occurred. The source function reflected in Figure (18b) was adjusted downward by 210 nL/L before being digitized into line sources, each 4 km in length.

The air-sea exchange rate constant in February was estimated to be 8.5×10^{-7} , based on a mean wind of 9.5 m/s and a mean sea surface temperature of 0°C (Table 1). The larger value of k is due to higher wind velocity and a concomitant decrease in the stagnant film boundary layer thickness. As described above, k was allowed to vary by 50% or $\pm 4.2 \times 10^{-7}/s$. Biological oxidation was not a significant factor during winter (Griffiths et al., 1982).

The best simulations of the observations are shown in Figures (27a,b). The predicted velocity range was 3-7 cm/s, given the uncertainties in k and other characteristics of shelf circulation. The wider range of predicted velocities for February was due to a diminished source and poor model resolution. The velocity estimate for February is not statistically different than that observed in August and falls within the estimate of 1-6 cm/s.

The estimates of lateral eddy diffusivities (K_y) are the same as observed in August because the Lagrangian scale is similar.

6.1.3 May 1981

The depth-averaged distribution of methane is shown in Figure (28). The pattern is similar to previous observations, but the concentrations are generally lower. Maximum concentrations at the entrance were about 2 $\mu\text{L/L}$, decreasing to 0.1 $\mu\text{L/L}$ at about 100 km.

NORTH ALEUTIAN SHELF
FEBRUARY 1981

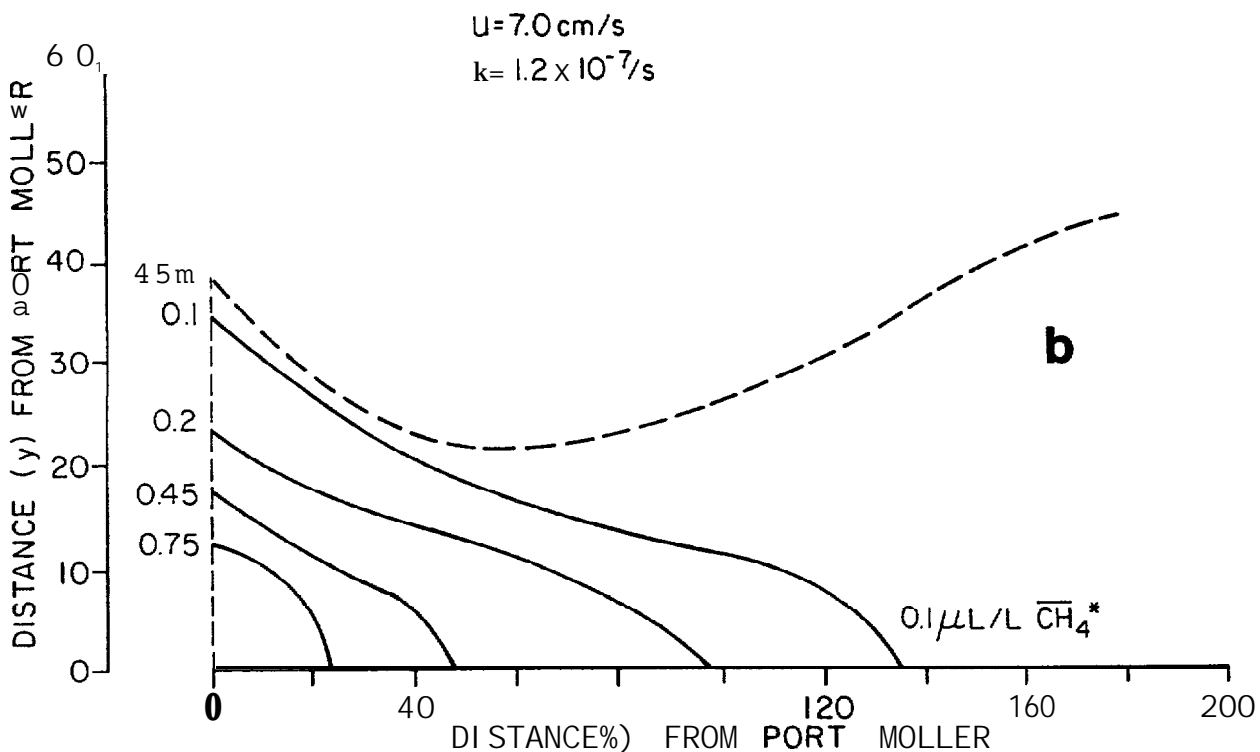
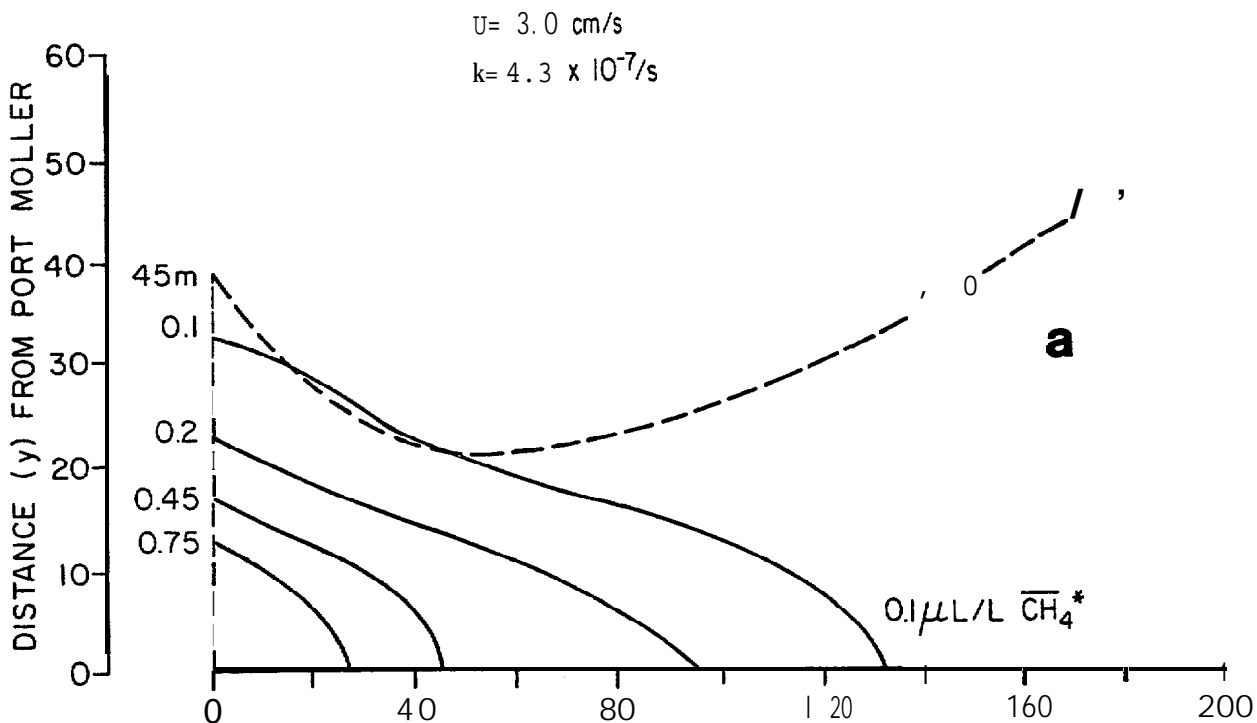


Figure 27. Model simulations of the distributions of methane for (a) $u = 3.0 \text{ cm/s}$ and $k = 4.3 \times 10^{-7}/s$ and (b) $u = 7.0 \text{ cm/s}$ and $k = 1.2 \times 10^{-7}/s$ in February 1981. Both distributions are reasonably good fits to the observed distributions. Concentrations are in $\mu\text{L/L}$. The position of the inner front is indicated by the dashed line.

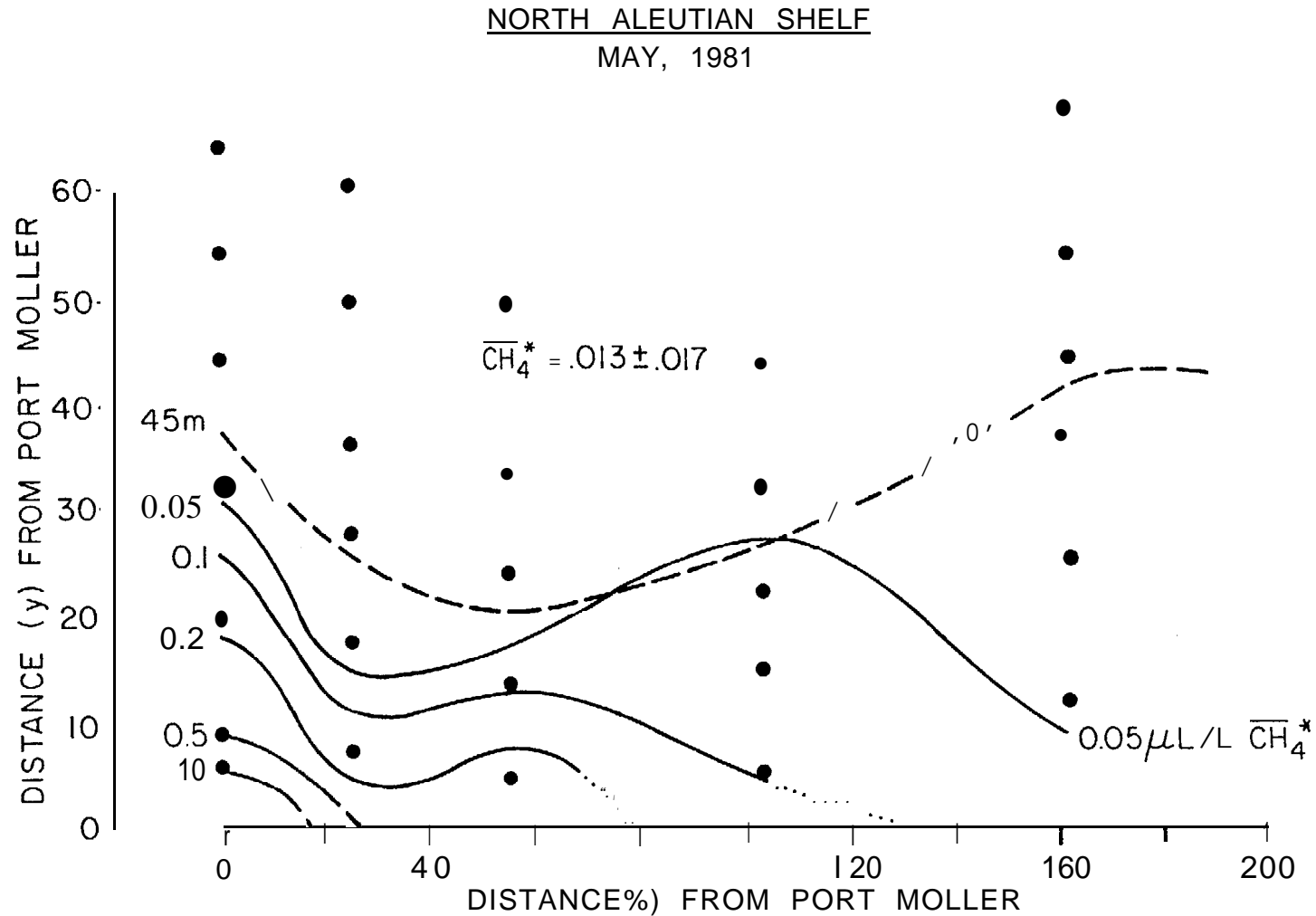


Figure 28. The depth-averaged distribution of dissolved methane in May 1981. A background concentration of $0.1 \mu\text{L/L}$ has been subtracted from the concentration field, leaving a mean residual of $0.013 \mu\text{L/L}$. The inner front is located near the 45 m isobath and is indicated by the dashed line.

In May, the surface concentration of \square ethane seaward of the front was 80-100 nL/L, indicating minimum production in the offshore waters. Equilibrium concentrations for this time of year were 60 nL/L; consequently, percent saturation levels ranged from 130 to 160%. In contrast, the saturation levels in August were 900%. The interannual variations in the surface concentrations are strongly a function of water temperature and degree of ice formation the previous winter (Cline et al., 1981).

The time average distribution of methane at the entrance to Port Moller is shown in Figure (18c). Maximum concentrations of 2 μ L/L were observed at PM-F, decreasing markedly to background concentrations of 100 nL/L at station NA38. As noted earlier, the source is hyperbolic and decays rapidly to background levels at about 30 km. This source was subdivided equally into 8 individual line sources, as before.

The air-sea exchange constant, k, was found to be $4.8 \times 10^{-7}/s$, based on mean wind of 7.5 m/s and a mean sea surface temperature of 6.5°C (Table 1). The calculated thickness of the diffusion layer was 50 μ m. Biological oxidation, proportional to water temperature and the concentration of methane, was at a minimum ($<1 \times 10^{-8}/s$) and was not included in the above rate constant (Griffiths et al., 1982).

The best model fits to the methane distribution are shown in Figures (29a, b). Assuming a mean k of $4.8 \times 10^{-7}/s$ and a variance of $\pm 2.4 \times 10^{-7}/s$, a range of velocities was fit to the observations. The best simulations were obtained for $u = 2-3$ cm/s. Larger velocities gave elongated plumes that were not in good agreement with the observations. We conclude that in May, the mean velocity along the coast was in the range of 2-3 cm/s and did not exceed 5 cm/s. Horizontal diffusivities are in the range of $1 \times 10^5 \text{ cm}^2/s$ to $5 \times 10^6 \text{ cm}^2/s$ for the plume dimensions described here.

NORTH ALEUTIAN SHELF
MAY 1981

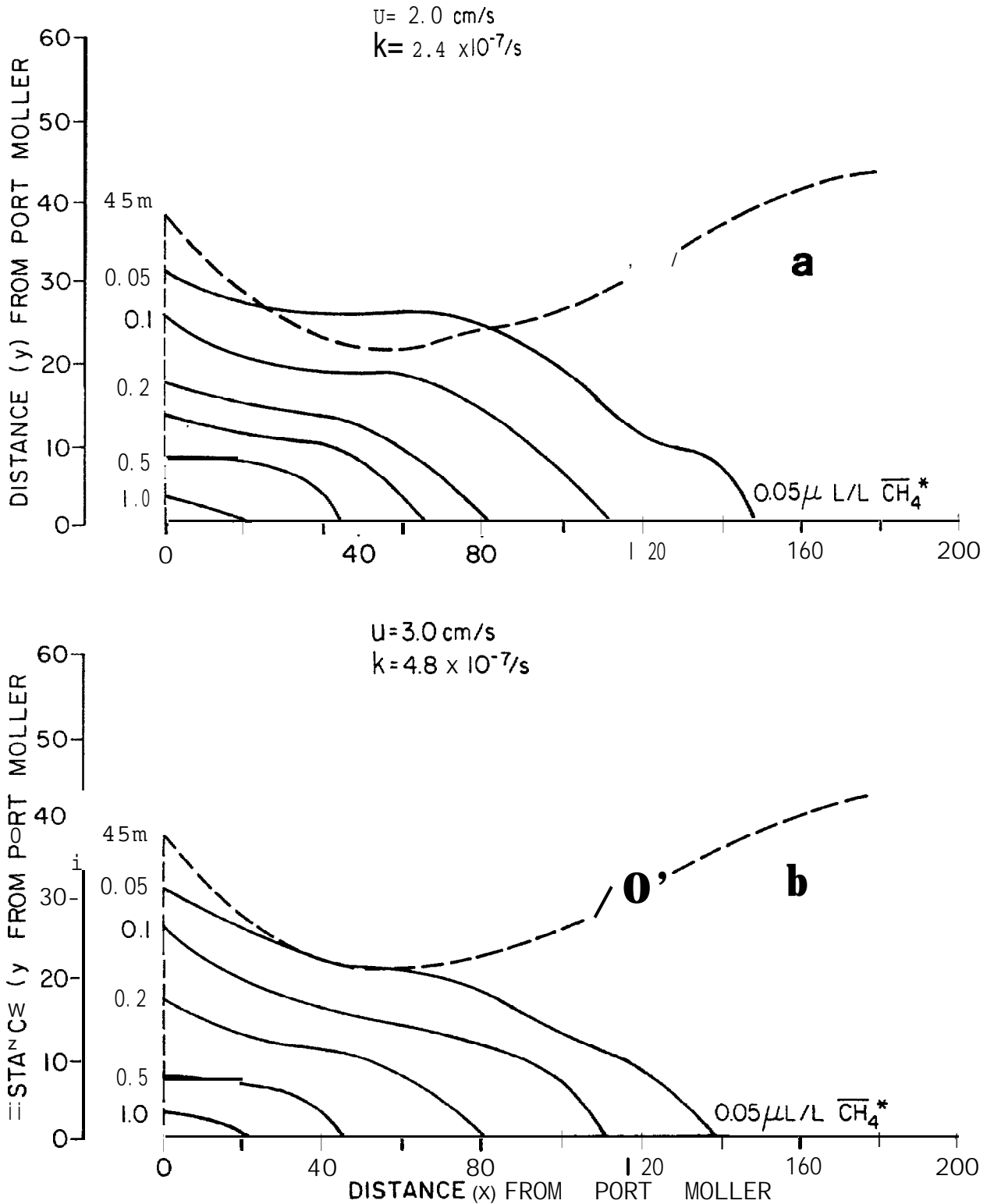


Figure 29. Model simulations of the distribution of dissolved methane for (a) $u = 2.0 \text{ cm/s}$ and $k = 2.4 \times 10^{-7} / \text{s}$ and (b) $u = 3.0 \text{ cm/s}$ and $k = 4.8 \times 10^{-7} / \text{s}$ in May 1981. Both distributions are reasonably good fits to the observed distribution. Concentrations are in $\mu\text{L/L}$. The position of the inner front is near the 45 m isobath and is indicated by the dashed line.

6.1.4. Port Moller Tidal Flux

In describing the horizontal distribution of methane along the NAS, we established concentrations along the shelf boundary perpendicular to the coast. Because the concentrations of methane are temporally variable near the entrance to Port Moller, we occupied a series of stations repetitively to estimate the average diel flux at the boundary. The boundary was placed near the entrance to Port Moller but was of sufficient distance to avoid the large tidal currents at the entrance. A check on our model can be made by comparing the estimated transport of methane through the entrance on each ebb tide with the time average distribution determined by the model. The implicit assumptions are that air-sea exchange and biological consumption are insignificant over the distance between the entrance and the model boundary (approximately 15 km).

The minimum distance across the entrance to Port Moller is between Entrance Point on the east and Fawn Point in the west. The main channel is approximately 5 km wide, 16 m deep and located toward the eastern shore. A large sand bar extends eastward from Fawn Point and is exposed during low water. At low water the effective channel width is about 9 km. Tidal currents are strong at the entrance, reaching average maximum velocities of 1.7 kts 3 miles west of Entrance Point and 1.2 kts at Entrance Point (Department of Commerce, 1979). For the purpose of calculations, we will assume an average maximum tidal current of 1.5 kts, or 0.8 m/s.

The principal assumption is that during any given tidal cycle, there is little or no recycling of water within the entrance of Port Moller. If this condition is met, then the tidal driven transport of methane to the coastal zone is proportional to the average concentration at the entrance, the width and depth, and the ebb velocity.

$$T_t = \sum C_i \ell \Delta z_i \bar{v} \quad (6)$$

For the sake of simplicity, we assume that C_i , the average excess methane concentration decreases linearly across the entrance from a maximum measured value on the east side to zero on the west. This is a crude approximation to the observations shown in Figure (18). The increment of length, ℓ , is set to 2 km, while the depth, Δz_i , is varied according to the bottom bathymetry. The mean velocity, \bar{v} , across the entrance was calculated from the average maximum velocity according to the formula $\bar{v} = v_{\max}/\pi/2$ (Sverdrup et al., 1942). The results of the tidal transport calculations for each of the three visits are shown in Table 2.

If the model assumptions are reasonably correct, then the tidal flux must equal the flux of methane across the model boundary. To calculate the latter, we used equation (6) and estimates of C_0 from Figure (18). The mean depth was set equal to 20 m and the velocity was estimated from the model fits. The length of the model boundary varied seasonally from 24 to 36 km, which was subdivided into 4 km increments for the purpose of calculation. The results of these calculations also are shown in Table 2.

Table 2. A comparison of the tidal transport of methane (T_t), from Port Moller with the transport of methane at the tidal boundary (T_m). The mean tidal velocity is \bar{v} and the mean coastal current is u .

Date	\bar{v} m/s	u	T_t ML CH ₄ (STP)/s	T_m
August 1980	0.5	0.038	5.7×10^4	4.9×10^4
February 1981	0.5	0.050	3.4×10^4	4.2×10^4
May 1981	0.5	0.025	2.3×10^4	0.8×10^4

In August the two transport figures are in good agreement; they only differ by 16%. The comparison in February is also reasonably good, although the coastal transport, T_m , exceeds the source strength by 23%. Uncertainty in the mean coastal velocity could easily account for this difference. The comparison in May is poor. There, the source strength exceeded the coastal transport by a factor of nearly three. The reason for the discrepancy may lie in our choice of the concentration distribution across the entrance. Apparently the concentration gradient across the entrance was more nearly hyperbolic (see Fig. 18) than linear as assumed above.

The near agreement between the two transport terms suggests that the model assumptions are nearly correct, conditions during May notwithstanding. This implies that the Port Moller estuary is the dominant source of methane to the coastal zone and that the model fits to the distributions and therefore gives reasonable estimates of the mean velocity field and the eddy diffusivities. Clearly more sophisticated models could be applied to the transport of methane from Port Moller, but non-linear perturbations to the mean velocity field coupled to an incomplete observational record precludes a detailed effort at this time.

6.1.5. North Aleutian Shelf Summary

A summary of the estimated velocities determined from the distributions of methane is presented in Table 3. While the model is crude and numerous approximations were made, the mean velocities range from 2-7 cm/s, depending on season. These estimates are in excellent agreement with current meter observations (J. Schumacher, personal communications). The small variances in the mean velocity field suggest that the flow is baroclinic and responds to the freshwater input. The small seasonal variation in the salinity field also indicates that seasonal variations in the baroclinic field should be small.

Table 3. A summary of the mean velocities along the coastal zone of the North Aleutian Shelf as determined from the distributions of dissolved methane. The air-sea exchange and biological rate constant (combined) was varied by $\pm 50\%$.

Month/year	k S ⁻¹	ℓ km	u cm/s
Aug. 1980	$4.0 \pm 2.0 \times 10^{-7}$	>200	3.8 ± 1.3
Feb. 1981	$8.5 \pm 4.2 \times 10^{-7}$	>200	5.0 ± 2.0
May 1981	$4.8 \pm 2.4 \times 10^{-7}$	200	2.5 ± 0.5

Model simulations of the methane distributions explicitly contain a cross-stream horizontal eddy diffusivity (K_y). This parameter was scaled to the mean velocity through equations (3a-3g), which allow the turbulent scale to grow as the plume increases in size. In the model simulations, the value of K_y ranged from $10^4 \text{ cm}^2/\text{s}$ at $x=0$ (4 km wide) to $10^6 \text{ cm}^2/\text{s}$ at $x=200$ km. Given the transient behavior in the current field and the complex bottom bathymetry, the model simulations do not permit a close examination of the magnitude of the turbulent field as a function of the Lagrangian scale. However, suffice it to say, that the cross-stream diffusion of methane is not inconsistent with the empirical formulations given by Okubo (1971). For a point source release, the variance of the plume grows at a rate

$$\sigma_{rc}^2 = 0.0108t^{2.34}, \quad (3f)$$

which also can be used to predict the behavior of point source releases of **souluble** or dispersed materials.

The simulations showed markedly the influence of the mean velocity field on the observed distributions. At velocities below 5 cm/s, eddy diffusion on the x- and y-directions should be included to improve the model fits. However, at velocities in excess of 5 cm/s and over limited space scales ($Q \leq 200$ km), the diffusive terms are relatively insignificant in determining the observed distributions.

6.2. St. George Basin

Enhanced production of methane occurs whenever elevated concentrations of organic carbon are present. This is the case in St. George Basin where relatively high concentrations of organic carbon are found in the surface sediments. The distribution of carbon (Gardner, et al., 1978) is nearly circular and occupies an area of about 8000 km² near the center of St. George Basin (56°N; 167°W) (Fig. 30). In cross section, the surface distribution of organic carbon is nearly Gaussian in form, which implies that the production rate of methane is also Gaussian in form. We will return to this point later in the discussion concerning the methane source term.

The concentration of methane, which depends on the strength of the local source and the intensity of mixing over the basin, is elevated in the fall when microbial production and water column stability are at maximums. Minimum concentrations were observed in the spring and are related to minimum microbial production. Both water temperature and the lack of a suitable organic substrate precluded a significant release of methane in the spring.

The model adopted for the simulation of the near-bottom distribution of methane in St. George Basin is the same model used along the North Aleutian Shelf (see Sec. 5.1). The description is two-dimensional, steady state, and balances lateral diffusion against horizontal advection and biological

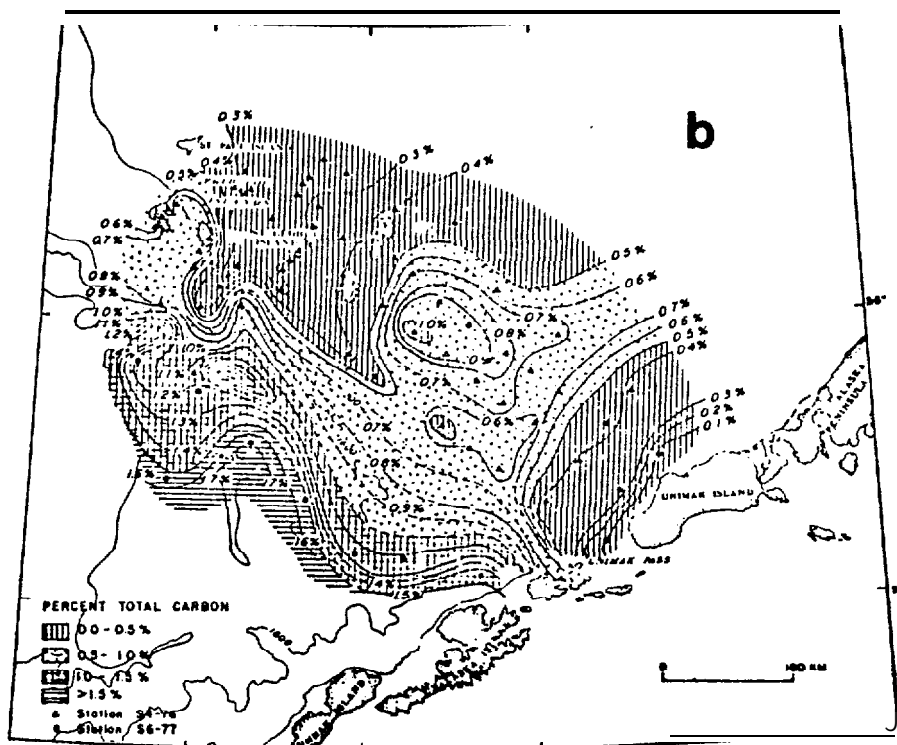
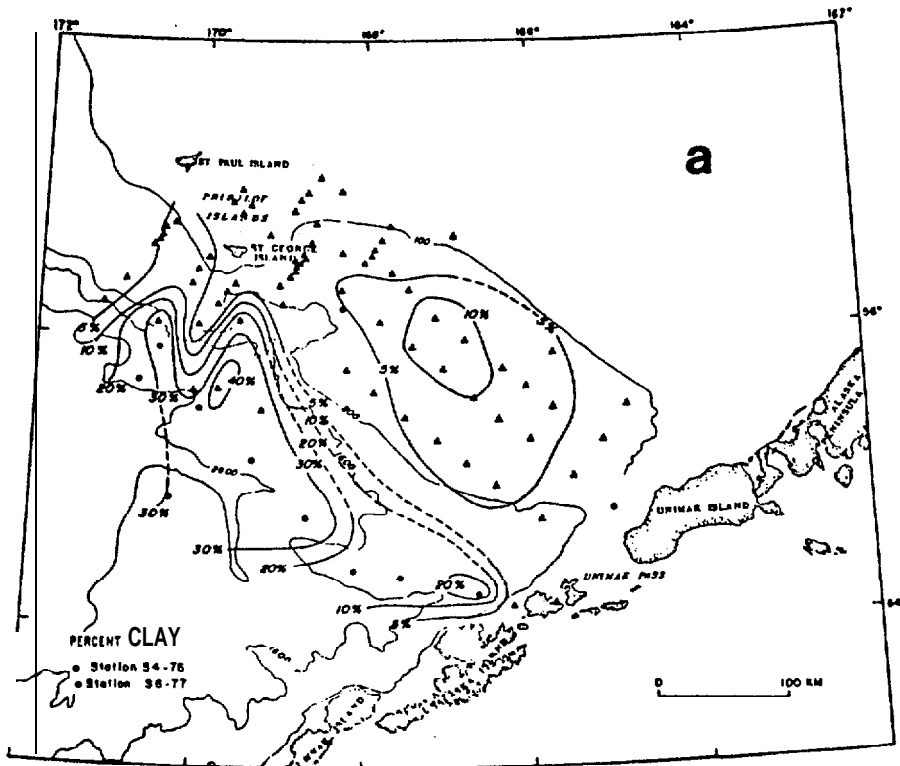


Figure 30. Distributions of (a) clay content and (b) total carbon in the surface sediments of St. George Basin. The locus of the high carbon concentrations is approximately $56^{\circ}\text{N } 167^{\circ}\text{W}$, which is the location of Stations SG5, SG29, SG24, and SG70 (see Fig. 2). This figure was taken from the report by Gardiner et al., 1978.

consumption. The oxidation of methane is considered first order as determined by Griffiths, et al., (1982).

The most serious deficiencies of the model include the source function and the vertical flux of methane across the **pycnocline**. For modeling purposes, we **assume** that the source of methane is a plane whose width is the y-dimension of the plume and whose height is the distance from the sea bottom to the base of the **benthic** boundary layer. This line source is subdivided into individual plane sources, each of which is 4 km in length and approximately 40 m in depth. Because the concentration varies across the source, each planar segment is assigned an initial concentration, C_0 . The source functions used for each of the three simulations are shown in Figure (31). Note that the initial concentration at the source is nearly normal as hypothesized earlier. Each planar section is treated as a separate plume; the total distribution results from the **sum** of all of the individual plumes.

An examination of the distribution of methane suggests that the source is circular or perhaps elliptical as indicated by the distribution of organic carbon (Fig. 30). By assuming a line source, the source of methane is confined to plane rather than an area. This simplifies the arithmetic at the expense of physical reality. However, the simulation does result in physical bounds on the diffusive and **advective** transports.

Another serious drawback to the simulation is the lack of a vertical flux term (see eq. 1). We "have assumed that this term is **small** because of the stability above the bottom boundary **layer**, which inhibits the vertical exchange of materials. Our estimate is that the vertical eddy diffusivity is $< 0.5 \text{ cm}^2/\text{s}$, which minimizes the vertical transport of CH_4 . In section 6.3, a scaling argument is presented to show that the vertical processes are indeed **small compared to** the horizontal transport terms and thus the former can be ignored to the first approximation.

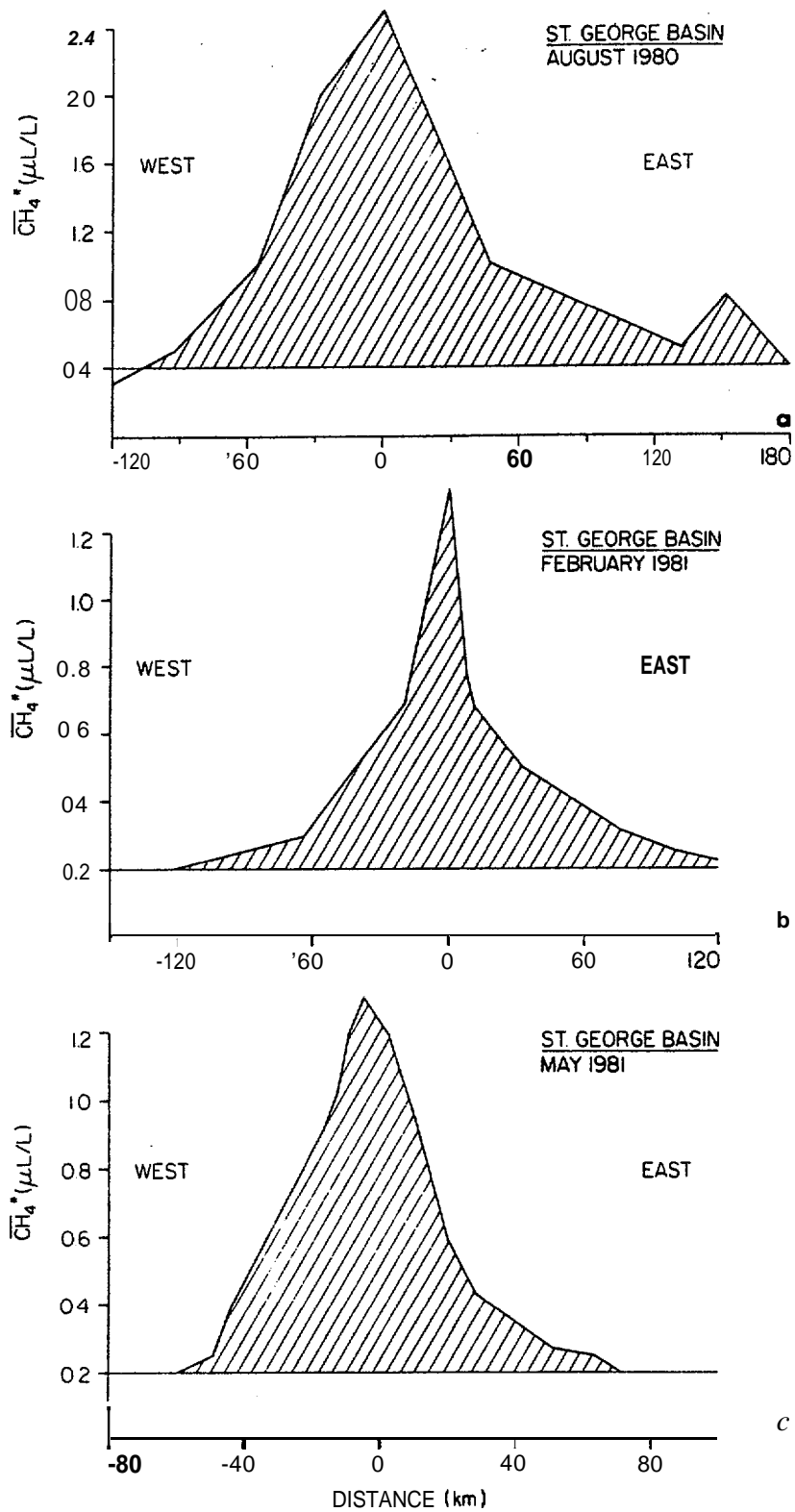


Figure 31. The average excess concentration of methane in the **benthic** boundary layer across the center of the plume. Data are collected in (a) August 1980, (b) February 1981, and (c) May 1981. Concentrations are expressed $\mu\text{L/L}$.

The **areal** distributions of methane in the near bottom waters appear as ellipses, elongated in the direction of the axis of the basin (see Figs. 6a,b,c). For modeling purposes, we chose the bottom boundary layer thickness to be 20-30 m, depending on the season, and a planar source of sufficient width to mimic the concentration field at the source. Initial concentrations along the source are interpolated from depth-averaged observations. The mean velocity, u , is the only adjustable parameter, because the biological rate constant that governs the consumption rate of \square ethane was measured. The value of the K_y is scale dependent and is calculated as a function of the **Lagrangian** distance (see Sec. 5.1).

6.2.1. August 1980

The depth-averaged distribution of methane in August 1980 is shown in Figure (6a) and is redrawn onto rectangular coordinates shown in Figure (32a). The best model fit to the observations is shown in Figure 32b for $u = 2$ cm/s and $k = 8.6 \times 10^{-8}$ /s. Because the source ($x=0$) bisects the **plume**, the model fit shown in Figure (32b) is only representative of the downstream portion of the plume. A velocity of 3 cm/s also was assumed, but resulted in unrealistically large concentrations along the axis of the plume. Thus, we conclude that the mean velocity in August 1980 was ≤ 2 cm/s. Because of the scale of the plume, K_y ranges from $1 \times 10^6 \text{ cm}^2/\text{s}$ to $2 \times 10^6 \text{ cm}^2/\text{s}$ (Okubo, 1971).

The elongation of the **plume** in the northwest direction suggests a weak current **along** the shelf in general agreement with the observations (Kinder and Schumacher, 1981). However, an onshore component is also evident in Figure (32a). This is **also** in agreement with refinements in the current trajectories that recently have been made (J. Schumacher, personal communication). Current meter deployments made between March and December 1976

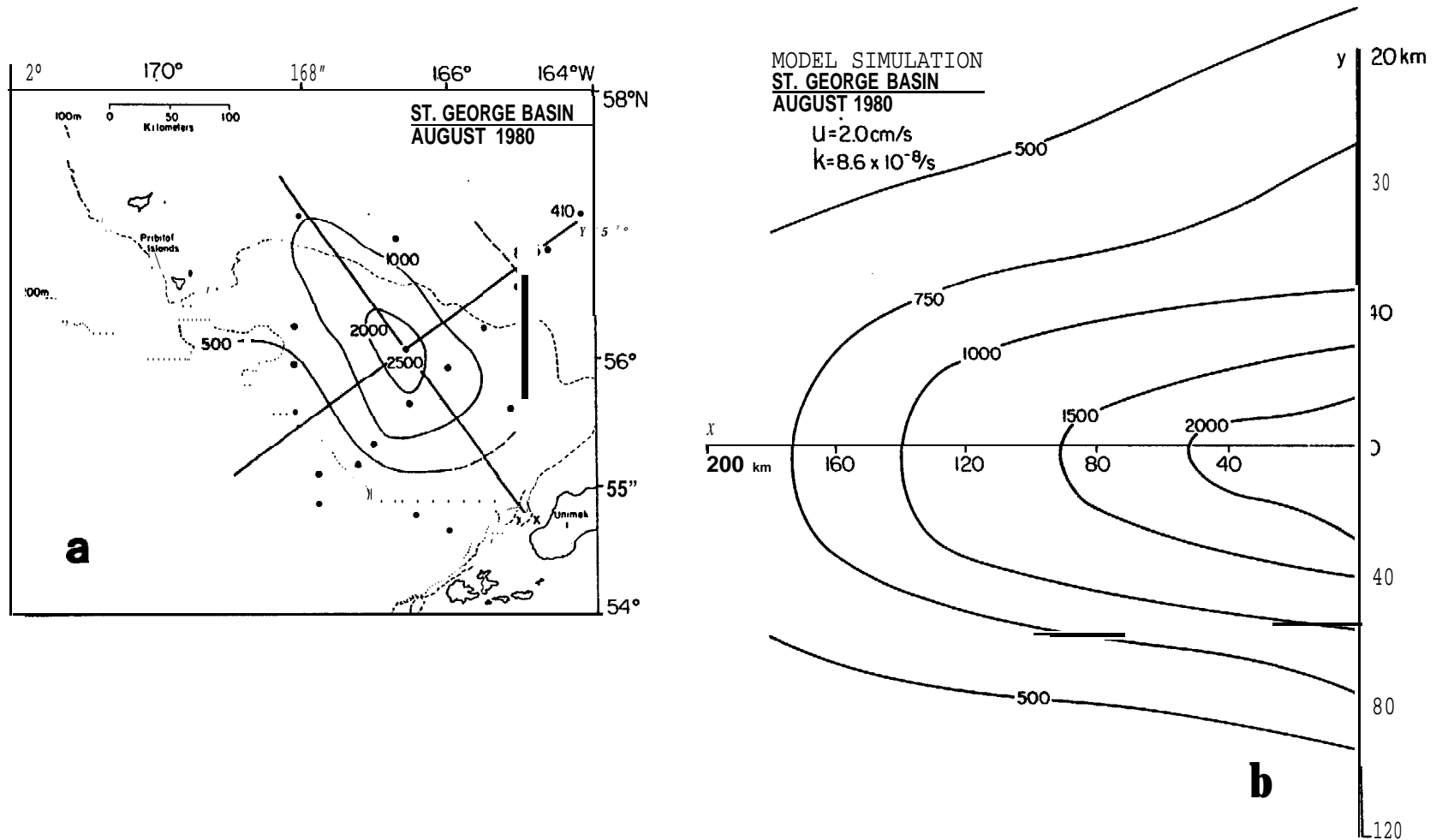


Figure 32. (a) The average near-bottom concentration of dissolved methane in St. George Basin in August 1980. The axes show the position of the model grid. (b) The model simulation of the methane distribution using the source function shown in Fig. (31a). The best fit was obtained for $u = 2.0 \text{ cm/s}$ and $k = 8.6 \times 10^{-8} \text{ /s}$.

indicate vector mean speeds of 2-4 cm/s in the lower 15 to 20 m of the water column (Kinder and Schumacher, 1981). Our model simulation suggests that the mean current speed will fall in the lower range when the effects of diffusion in the x-direction are taken into account.

The presence of significant concentrations upstream of the source demonstrates the broad extent of the source and the importance of alongshelf diffusion. The model used here did not explicitly include alongshelf diffusion; consequently, this effect is accounted for in the velocity term.

6.2.2. February 1981

The depth-averaged distribution of methane during February 1981 is shown in Figure (6b) and has been remapped onto a rectangular grid for model simulation (Fig. 33a).

The average concentration in February 1980 was lower than that measured in August. The plume trajectory is the same as August, and extends about 200 km downstream of the source (e.g. 300 nL/L contour). The width was reduced to about 120 km as compared to 280 km in August.

The best fit to the observed distribution was again obtained with $u = 2$ cm/s and $k = 5.6 \times 10^{-8}$ /s (Figure 33b). The biological rate term was smaller in February, presumably due to the reduced water temperature. As before, the mean velocity, u , was arbitrarily increased to 3 cm/s to test model sensitivity. The fit to the distribution was not improved. Therefore, we conclude that the mean velocity in February was less than 2 cm/s in agreement with the model predictions for August 1980.

6.2.3. May 1981

The depth averaged distribution of methane observed in May 1981 is shown in Figure (6c) and is remapped into the model grid shown in Figure (34a). The maximum concentration of methane (near SG70) was 1200 nL/L and was lower

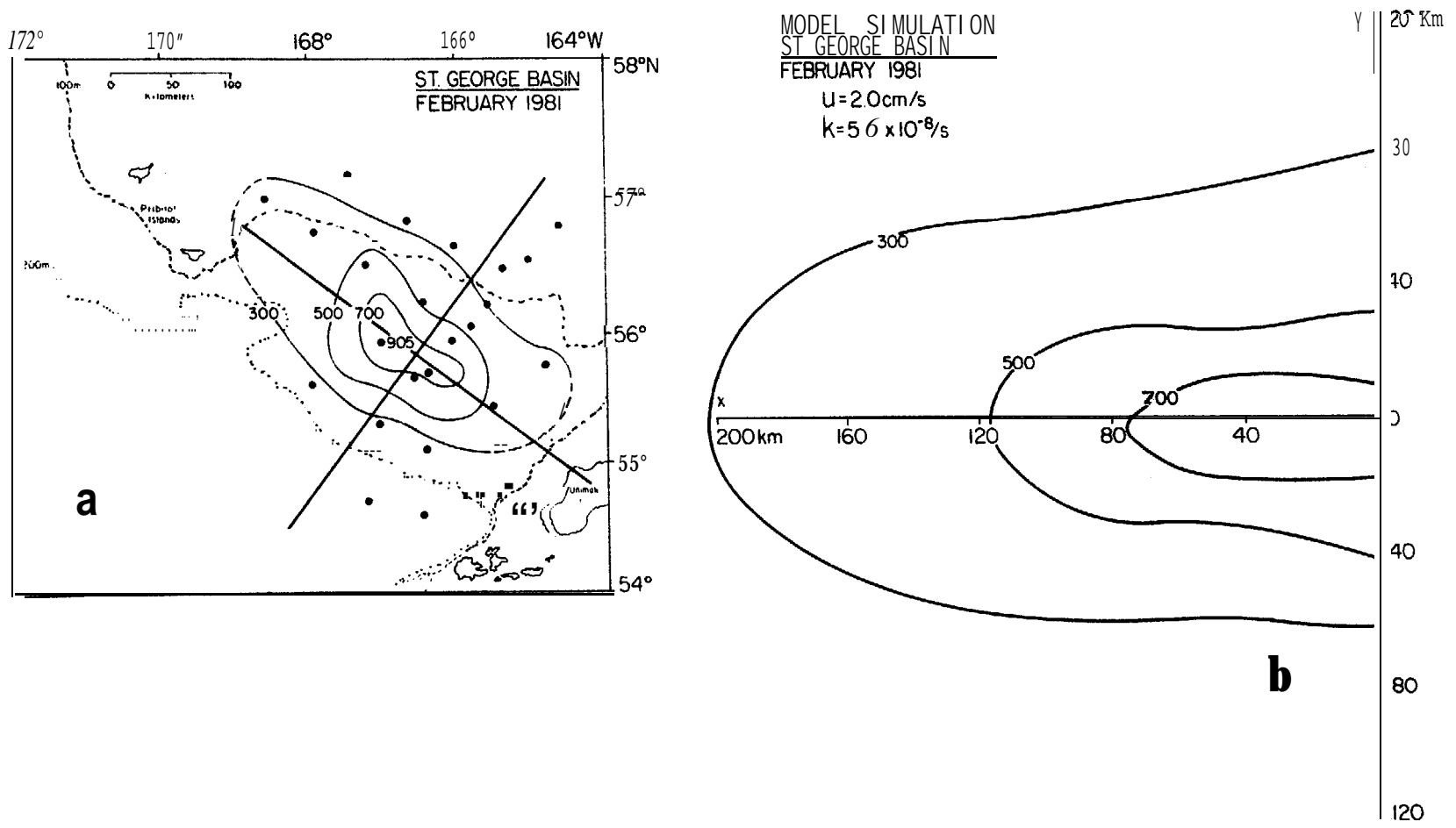


Figure 33. (a) The average near-bottom concentration of dissolved methane in St. **George** Basin in February 1981. The axes show the position of the model grid. (b) The model simulation of the methane distribution using the source function shown in Fig. (31b). The best fit was obtained for $u = 2.0 \text{ cm/s}$ and $k = 5.6 \times 10^{-8} \text{ /s}$.

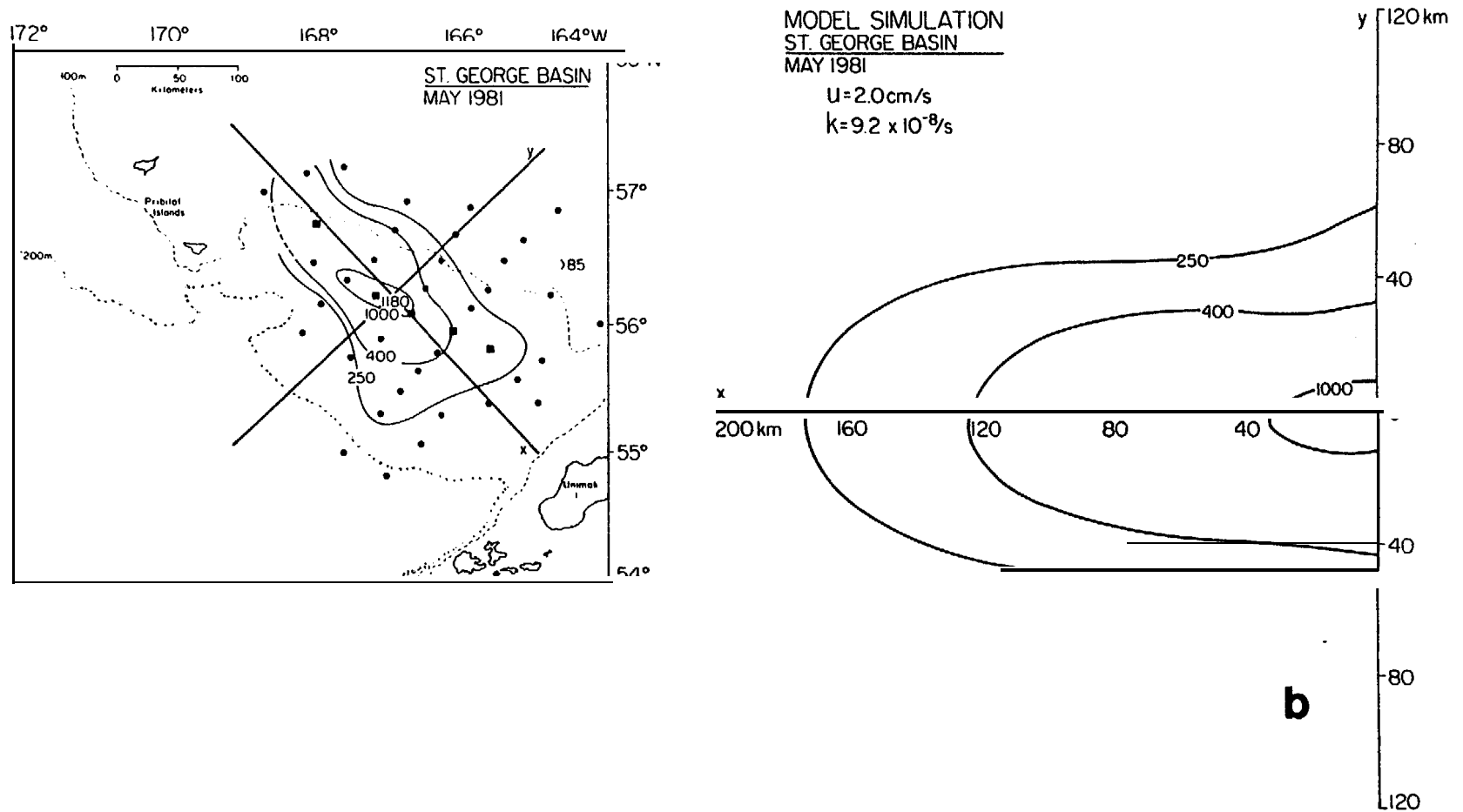


Figure 34. (a) The average near-bottom concentration of dissolved methane in St. George Basin in May 1981. The axes show the position of the model grid. (b) The model simulation of the methane distribution using the source function shown in Fig. (31c). The best fit was obtained for $u = 2.0 \text{ cm/s}$ and $k = 9.2 \times 10^{-8} \text{ /s}$.

than was observed during the two previous visits. The relatively low abundance of methane in May is believed to be related to the vertical carbon flux and possibly the bottom temperatures, as described earlier. The orientation of the plume is as before, except that its cross-shelf extent is much smaller than was observed in August 1980. Asymmetry of the plume suggests short term variations (< 1 month) in the speed and trajectory of the flow, which is not unexpected in the dynamic outer shelf region of the Bering Sea (Kinder and Schumacher, 1981a). As noted before the plume is elongated toward the northeast, suggesting a weak flow in that direction.

The best fit to data was achieved with the source function shown in Figure (31b), $u = 2$ cm/s, and $k = 9.2 \times 10^{-8}$ /s. The biological rate constant, which was determined by in vitro experiments aboard ship, is larger than was observed during the two previous visits. The goodness of fit was not improved by increasing the velocity, indicating as before, that the mean velocity was **probably** ≤ 2 cm/s.

6.2.4. Summary of St. George Basin Studies

The distributions of methane in the **benthic** boundary layer were modeled to determine the mean current trajectory, **mesoscale** mean current velocities, and the characteristic of diffusive mixing. Model simulations were made on three distributions observed in August 1980, February 1981, and May 1981.

The source of the methane is believed to be organic-rich sediments deposited on the basin floor of St. George Basin. The organic carbon content varied from about **0.5%** at the edges of the basin to slightly more than **1%** at the center of the distribution. The distribution of carbon is nearly circular and appears to be related to circulation processes over the outer shelf. A cursory examination of the dynamic height field suggests a divergent flow near the location of high carbon concentration, which might result in the

accumulation of fine **detrital** and organic materials. On the basis of sedimentary size analysis, we would expect the accumulation of organic carbon to correlate with weak circulation.

The distribution of methane was modeled by establishing a variable concentration at the boundary and summing the individual plumes. We also assumed that lateral mixing was isentropic, which may not be valid for these waters. Vertical flux calculations demonstrated that insignificant amounts of methane were lost through the **pycnocline**, which reduced the model to two dimensions. Biological oxidation of methane was included in the model in the basis of in vitro experiments performed on the ship.

The results of the modeling analyses indicated that the mean velocity was no greater than 2 cm/s, and probably less. This is in complete agreement with **mean** flow measurements of 1-2 cm/s. Plume trajectories **also** showed an onshore component, which was **also** in agreement with current meter measurements.

The plumes observed in August 1980, February 1981 and May 1981 all showed trajectories to the north-northwest, but significant amounts of methane were found to the southwest as well. This is indicative of the low mean velocities and the significance of horizontal diffusion in the x-direction, which **was** not accounted for in the model. We conclude that a more sophisticated model that includes flux divergence in the **x-direction** as well as the y-direction would predict a lower mean velocity than the 2 cm/s cited above. There is also reason to believe that the mixing is anisentropic, namely that diffusive transport in the x-direction is larger than in the y-direction. The reason for this belief lies in the distribution of the mass field. Flow **parallel** to the **isobaths** is along **isopycnal** surfaces, while cross-shelf flow is across **isopycnals**. On this basis we would expect that $K_x > K_y$ and that the plume asymmetry is strongly influenced by the imbalance in the horizontal flux divergence terms, particularly at these low mean velocities.

The impact of these findings is particularly relevant to offshore exploration and production activities. These analyses as well as the current meter measurements show the St. George Basin region to be characterized by weak currents and relatively long residence times. Oil spilled or retained in the near-bottom waters will not be removed rapidly by circulation processes; therefore the risk to marine habitats is elevated. However, the actual impact depends on the nature of the spill and the quantity of oil spilled. This point will be treated in the next section.

6.2.5 Oil Spill Scenario, St. George Basin

In the preceding discussion, we have considered the circulation characteristics of two subregions of the southeastern Bering Sea. Specifically the studies centered on the near-bottom circulation of St. George Basin and the coastal zone along the North Aleutian Shelf. In each case, we used a **localized** source of dissolved methane to describe advective and diffusive scales applicable to each region. This information is directly applicable to estimating or predicting how spilled oil might behave in these areas. We now proceed to develop and test a simple model that will be useful in describing the concentration field resulting from a spill event. These models are only applicable to the dissolved or emulsified fractions and do not describe the behavior of a surface slick.

The situation we wish to simulate here is an instantaneous release of oil at a fixed location, such as might occur in the collision or grounding of a tanker. The three dimensional model that describes the subsequent dispersion of oil under these conditions is given by the following equation (**Brubaker** and Rote, 1978):

$$C(x,y,z,t) = \left[\frac{Q}{(2\pi)^{3/2} \sigma_x \sigma_y \sigma_z} \right] \exp \left\{ -\frac{(x-ut)^2}{2\sigma_x^2} - \frac{y^2}{2\sigma_y^2} - \frac{z^2}{2\sigma_z^2} \right\}, \quad (7)$$

where Q is the mass of material released, $\sigma_x, \sigma_y, \sigma_z$, are the standard deviations of the plume as a function of time (t), and u is the mean velocity in the x -direction. To simplify equation (7), we will only consider the centerline distribution ($y=0$) for a constant depth interval, z . Setting $y=z=0$, equation (7) becomes

$$C(x,t) = \left[\frac{Q}{(2\pi)^{3/2} \sigma_x \sigma_y \sigma_z} \right] \exp \left\{ -\frac{(x-ut)^2}{2\sigma_x^2} \right\} \quad (8)$$

This model describes the time dependent behavior of spilled oil contained within a well-mixed lens of water (e.g., surface-mixed layer above the pycnocline). This model also predicts the maximum concentration of oil that will occur along the centerline of the plume. By inspection of equation (8) it is readily apparent that the concentration decreased exponentially in the x -direction. To solve equation (8), we need estimates of Q , u , σ_x , σ_y , and σ_z .

The model represented by equation (8) was solved for a given spill scenario stipulated for St. George Basin (April 1981). The amount of oil spilled was 50,000 bbl or 6.7×10^8 kg. To solve equation (8), a few assumptions were made concerning the duration of the spill as well as the size of the initial plume. In this particular prediction, we will assume that 'worst-case scenario,' which will lead to the largest volumetric impact.

The assumptions imposed on the spill scenario are the following. The spill occurs in the surface waters of St. George Basin in summer. The oil is instantaneously released and all of it is rapidly mixed downward to

the top of the **thermocline**, or about 40 m. The oil is considered conservative (i.e., does not evaporate nor is it biologically degraded). Also, no flux through the **thermocline** is permitted. This computation will maximize the concentration of dissolved and emulsified oil and its impact area.

The concentration of oil at any point in time and space depends critically on the rate of mixing. The mixing parameters are implicitly embodied in σ_x , σ_y , and σ_z , the standard deviation of the plume as a function of time or distance. The parameters are linked through the mean velocity $u = x/t$. For the purpose of the model, we assume σ_z is a constant, whereas σ_x, σ_y are allowed to vary with t according to the empirical relationships given by Okubo (1971). The relevant relationships are:

$$\sigma_{rc}^2 = 2\sigma_x\sigma_y \quad (3a)$$

$$\sigma_x\sigma_y = 0.0054 t^{2.34} \quad (9)$$

$$\sigma_y = 0.074 ax \quad (10)$$

$$\sigma_x = 0.0197t^{2.34} \quad (11)$$

The initial size of the spill is somewhat arbitrary, but for our purpose here we assume a radial spill of 200 m and a mean depth of 40 m. Consequently, the average concentration of oil is $C_0 = (6.7 \times 10^8 \text{ kg}) / (200 \text{ m})^2 (40 \text{ m}) = 425 \text{ kg/m}^3$ or 425 g/L. This amount of oil could not be dissolved in one liter of seawater. For the sake of simplicity, we will retain these initial conditions, recognizing that more realistic scenarios can be easily scaled from these results. By analogy with equation (8), the initial plume disper-

sion parameters are easily calculated, $\sqrt{2\pi} \sigma_x^0 = \sqrt{2\pi} \sigma_y^0 = 200$ m; $\sqrt{2\pi} \sigma_z^0 = 40$ m. Hence $\sigma_x^0 = \sigma_y^0 = 80$ m and $\sigma_z^0 = 16$ m. The initial concentration of oil in the spill, C^0 , is equal to $C_0 = Q / (2\pi)^{3/2} \sigma_x \sigma_y \sigma_z = 425$ g/L.

To examine the temporal development of the spill scenario described above, we assume mean velocities of 2.5, 5.0, and 10 cm/s, which are in the range of observed velocities for St. George Basin (Kinder and Schumacher, 1981a). The results of the modeling are described in Figures (35), (36), and (37), for periods of 2d, 5d, 10d, and 30 d. To express the results generically, we have chosen a relative concentration scale, where C_0 is the initial concentration of oil at the spill. For reference purposes, the 1 ppm and 0.1 ppm concentration lines are also included for comparison. Organisms are stressed or killed at oil concentrations (water soluble fraction) in the range 0.1 to 1 ppm.

Figure (35) depicts the plume development for a period of 30 d at a mean velocity of 2 cm/s. The maximum concentration of oil at 2 d is 1% of the original concentration and occurs at about 4 km downstream. At the fifth day, the center of mass has moved to 10 km, but lateral diffusion has decreased the relative concentration to 0.1%. Similar exponential decreases are noted for the subsequent time periods.

The impact of oil on organisms depends on both duration of exposure and concentration. The spill being considered here was instantaneous and decays according to the mathematical representation of the mixing. If we arbitrarily choose the 0.1 ppm reference level, the concentration of oil is everywhere less than this value after 16 or 17 d.

In Figure (36) is shown the same spill event except the mean velocity was increased to 5 cm/s. The immediate effect of the increased velocity is to elongate the plume in the downstream direction. At comparable distances, the maximum concentration of oil is greater at the higher velocities because

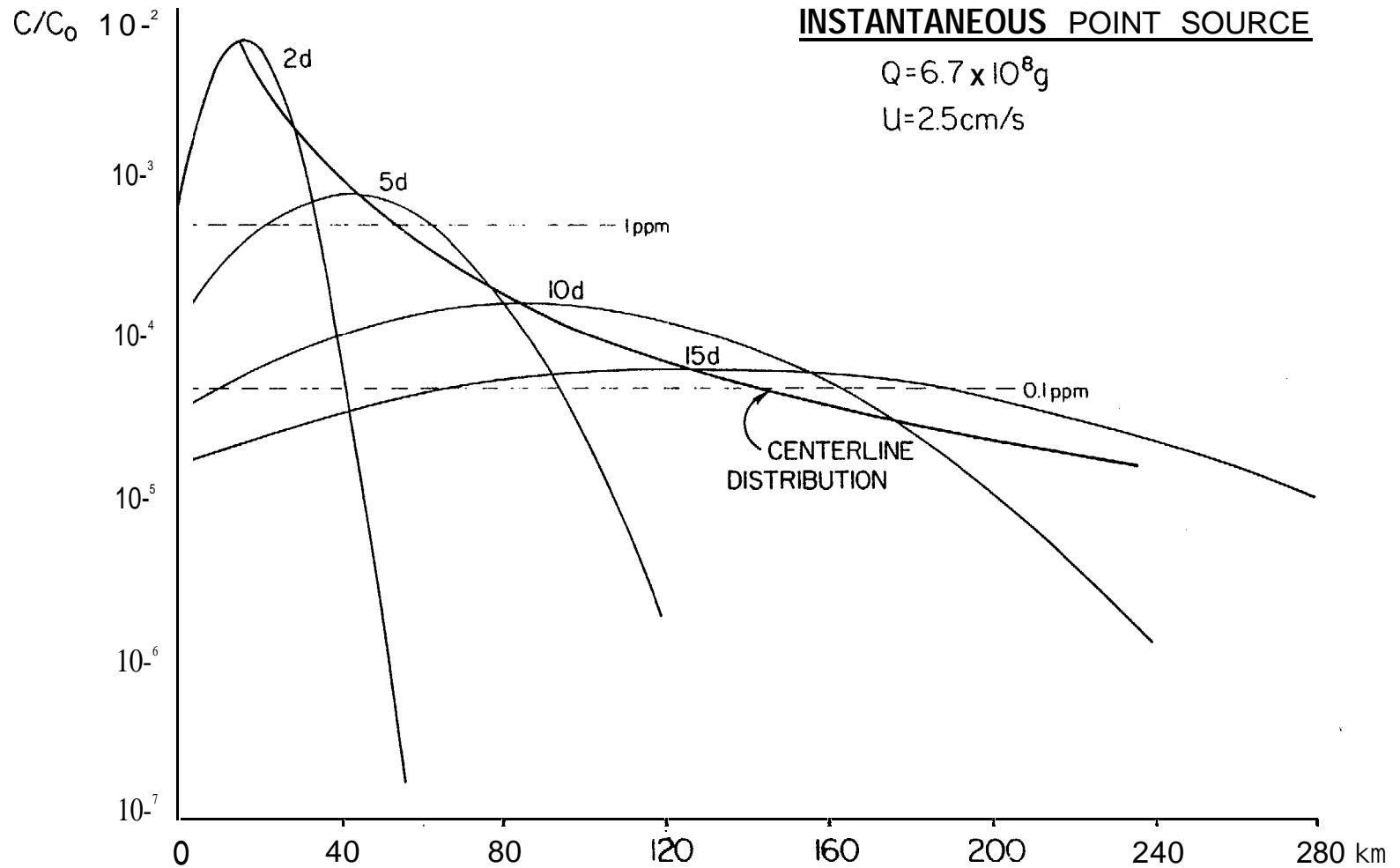


Figure 35. The **development** of a plume of 'dissolved' oil resulting from an instantaneous release of $6.7 \times 10^8 \text{g}$ (50,000 bbls) confined to a 40 m, vertical-lens of water. The centerline distribution shows the temporal history of the spill locus for a mean current speed of 2.5 cm/s. Reference concentrations of 0.1 and 1.0 ppm 'dissolved' oil also are indicated.

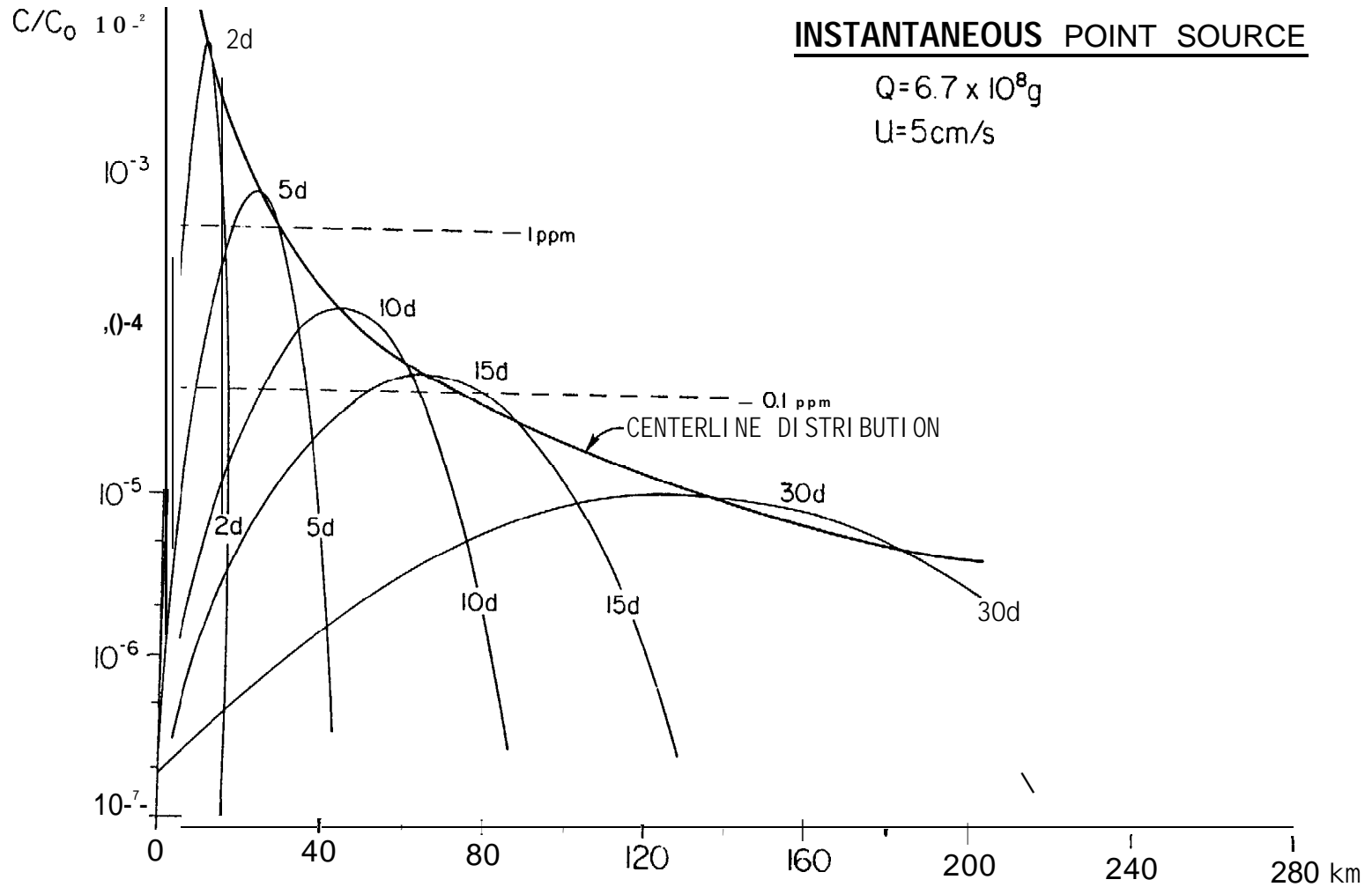


Figure 36. The development of a plume of 'dissolved' oil resulting from an instantaneous release of $6.7 \times 10^8 \text{ g}$ (50,000 bbls) confined to a 40 m, vertical-lens of water. The centerline distribution shows the temporal history of the spill locus for a mean current speed of 5.0 cm/s. Reference concentrations of 0.1 and 1.0 ppm 'dissolved' oil also are indicated.

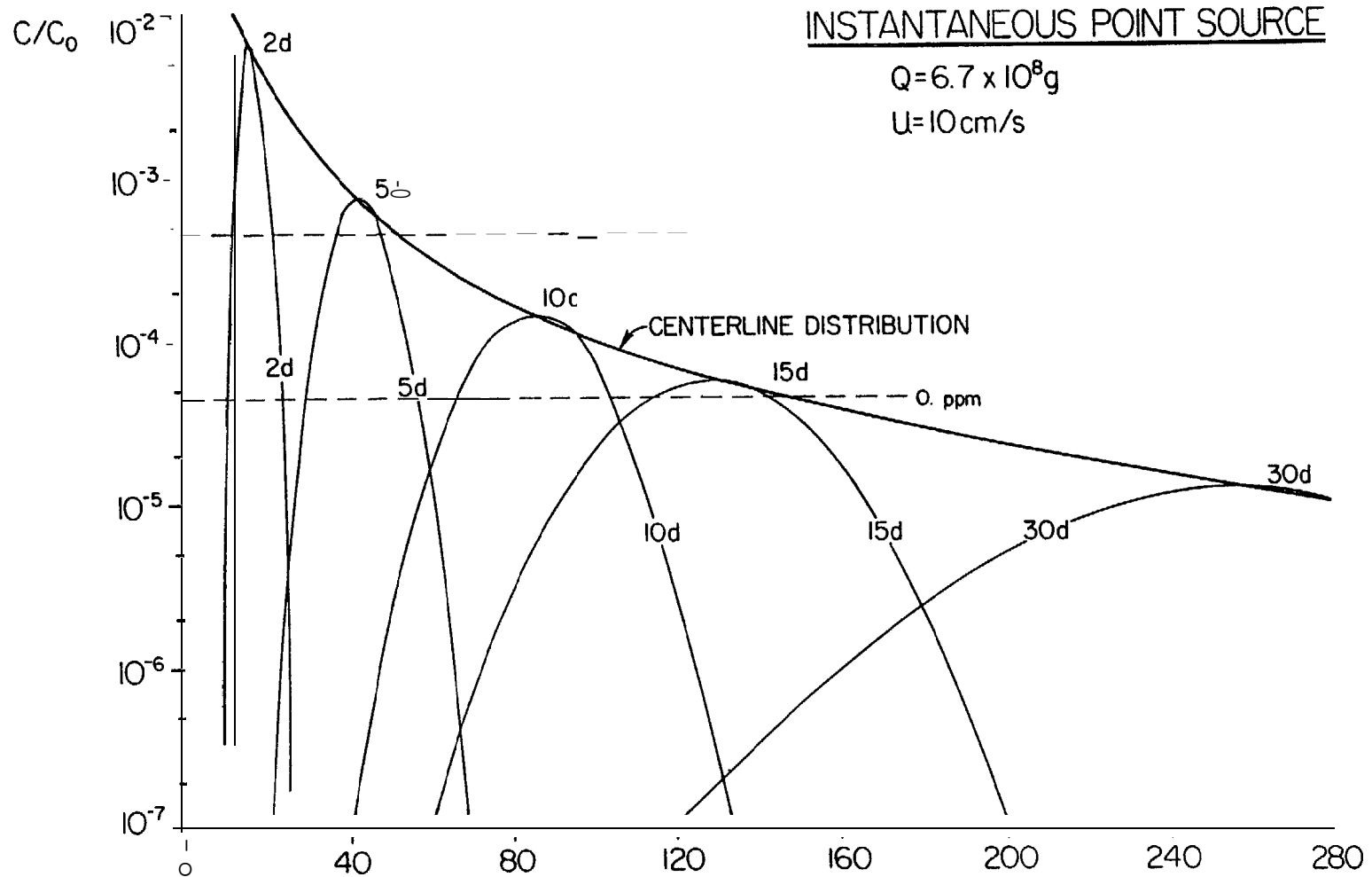


Figure 37. The development of a plume of 'dissolved' oil resulting from an instantaneous release of $6.7 \times 10^8 \text{ g}$ (50,000 bbls) confined to a 40 m, vertical-lens of water. The centerline distribution shows the temporal history of the spill locus for a mean current speed of 10 cm/s. Reference concentrations of 0.1 and 1.0 ppm 'dissolved' oil also are indicated.

the flux of oil across any orthogonal plane must be conserved (i.e. oil is conservative). At 15 d, the maximum concentration of oil has **fallen** to **0.01%** of the original concentration at a distance of 64 km. In the present case, the concentration of oil would be about 0.3 ppm. After 30 d, the concentration of oil is everywhere less than **0.001%** or 50 ppb.

The situation for 10 cm/s is shown in Figure (37). The plume is elongated in the x-direction, as noted above. The maximum concentration after 15 d is about 0.1 ppm and occurs 130 km downstream of the spill site.

In the foregoing, the effect of increasing the velocity was to increase the longitudinal transport at the expense of lateral diffusion. However, the amount of oil spilled was constant; therefore, we expect the environmental impact volume to be the same regardless of the velocity. The geometry of the plume will, however, be different. To estimate the impact volume of the hypothetical spill given above, we need only consider the temporal development of the plume and the concentration of oil above any given threshold level, say 0.1 ppm. Considering the 5 cm/s case (Fig. 36), the plume length to width was estimated for each period of time in which the concentration exceeded 0.1 ppm. For example, at 10 d (5 cm/s), the length (x) of the plume was 38 km and its width (y) was about 10 km. As the center of mass of oil is transported, it diffuses laterally and becomes more dilute. Because the diffusion coefficient is increasing as the size of the plume grows, these two effects combine to form a maximum extent in the y-direction to which we might expect biological effects. That downstream distance is about 40 km in the case where $u = 5$ cm/s. Beyond 40 km, the plume continues to grow, but its biological impact is diminishing due to dilution with surrounding water. According to our calculations, the maximum areal extent of the plume is 450 km^2 and would persist for about 15 d. It should be noted that the calculated area represents an accumulated effect area, not an instantaneous

effect area. The maximum instantaneous area affected would occur at about 40 km downstream and would be about 38 km x 10 km = 380 km². Since we assumed initially a homogeneous lens of water 40 m deep, the volume impact area would be about 18 km³.

The scenario discussed above is not totally realistic in that only a small fraction of spilled oil is actually going to be accommodated in the water column as dissolved or emulsified oil. If we assume that only 10% of the total oil is accommodated, then the potential impact area is reduced to about 40-50 km², an area very much smaller than the surface area of St. George Basin.

These elementary calculations suggest that a point source injection of oil (i.e., well blowout or tanker spill) of the magnitude of 50,000 bbl's will result in relatively small amounts of dissolved and/or emulsified oil in the water column and that a reasonable impact area from such an injection is no larger than 450 km² (given a 0.1 ppm threshold). More than likely it is a factor of ten less. These results **only** apply to the open reaches of St. George Basin and do not apply to the coastal zone of the NAS, where the hydrography and the proximity of the beach result in a much different set of conditions.

6.2.6 Horizontal Transport of Methane

In fitting the model to the observed distributions, a source function was hypothesized in terms of the concentration along a line bisecting the source region (e.g. see Figure 32a). It was assumed that the source of the methane was diffusive flux from the underlying sediments, or perhaps from methane production arising from microbial activity **at** the sediment-water interface. In either event, the near-bottom transport of methane must equal the integrated **benthic** production rate corrected for biological loss.

To evaluate the bottom flux of methane, we collected five vertical methane profiles to 50 cm in May 1981. Two such profiles taken in May 1981 are shown in Figure (38), where the vertical distributions of methane in the water column and in the sediments are shown. In each case, the maximum concentration in the sediment is approximately a factor of 10 above the bottom boundary layer concentration. The gradient across the **sediment-water** interface in part explains the accumulation of methane in the bottom waters of St. George Basin. The average flux to the water column, based on a molecular diffusivity of CH_4 of $8.5 \times 10^{-5} \text{ cm}^2/\text{s}$ (Witherspoon and Bonoli, 1968), was $1 \times 10^{-14} \text{ g/cm}^2/\text{s}$ (Katz et al., 1982). Assuming an area of $2.0 \times 10^{14} \text{ cm}^2$ ($r=80 \text{ km}$), the integrated methane production rate is 2 g/s. Integrating the production curve shown in Figure (31c) and assuming a mean velocity of 2 cm/s, we obtain a horizontal transport of 23 g/s, a factor of 10 higher than the **benthic** flux would suggest. The explanation for the difference may lie in the assumptions. By assuming a slightly larger molecular diffusivity (e.g. **bioturbation** in the upper 10 cm of the sediment column, Berner, 1980) or decreasing the mean velocity, a match could be achieved. Both of these parameters could be adjusted by appropriate factors to achieve the end result without perturbing seriously the known variances. Also, the interstitial water measurements do not measure production that might occur at the sediment water interface. Consequently, we conclude that methane production rate in the region of elevated carbon concentrations is in agreement with **the** horizontal transport derived from the model, if we assume a larger molecular diffusivity and/or a lower mean velocity. Our intuition is that the mean velocity is no larger than 2 cm/s and **could** very well be much lower if anisotropic mixing were invoked.

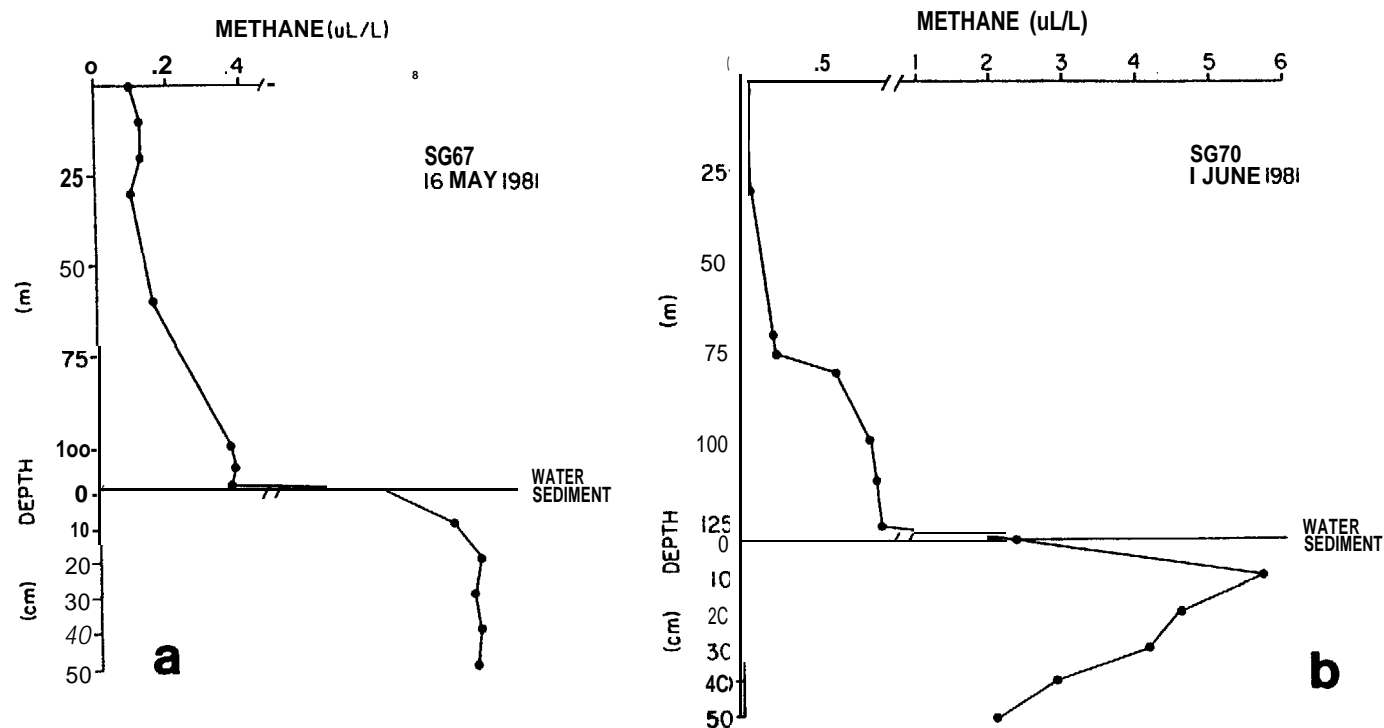


Figure 38. The vertical distribution of methane in the water column and surficial sediments at (a) Station SG67 and (b) SG70. These data were collected in May-June 1981. Note the scale change in concentrations between the water and the pore fluids.

6.2.7. Vertical Transport of Methane

St. George Basin is normally stratified due to seasonal changes in solar insolation and freshwater input. The strength of the **pycnocline** varies seasonally depending on buoyancy input and the depth of the mixed layer, but appears to be a maximum in late summer or early fall, and a minimum in late winter. Regardless of season, the density difference between the surface layers and the bottom is about one sigma-t unit (e.g., 25 to 26), but the gradient changes significantly over the year. This change in the gradient results in a variable vertical flux of dissolved constituents because the apparent vertical eddy diffusivity is a function of stability (Welander, 1975). In this section we test a simple model that estimates the magnitude of K_v .

On previous visits to St. George Basin it was observed that the vertical distributions of salt and methane were similar, suggesting that methane was quasi-conservative. A plot of methane versus salinity was usually **linear** (Fig. 39), implying that the vertical flux of methane from bottom sediments was impeded by the **pycnocline**. In an **analogous** fashion, the vertical transport of dissolved components of petroleum or micro-droplets of oil would be similarly inhibited.

In order to quantify the magnitude of K_v within the **pycnocline**, Station PL6 was occupied on two occasions in August 1980. Detailed measurements of salinity, temperature, and methane were made. The results of these measurements are shown in Figure (7). Note that the concentration of methane decreases approximately a factor of five between the bottom and the surface (100 m to 60 m), while σ_t decreases abruptly over the same depth range.

Assuming for the moment that methane is conservative, the vertical flux of methane across **any** horizontal plane is equal to the bottom flux or to the

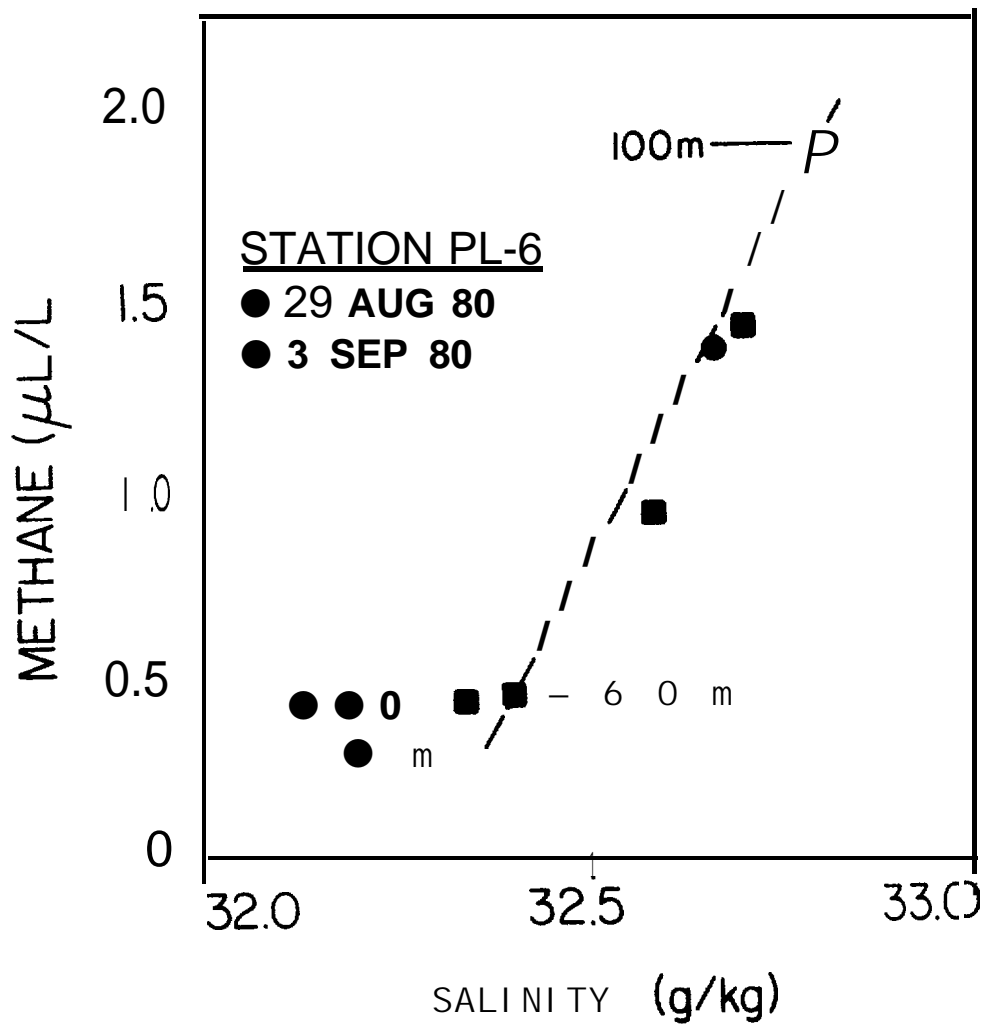


Figure 39. The relationship between salinity and methane at Station PL-6 in August 1980. The linear relationship suggests conservative mixing between the surface and bottom waters.

air-sea evasion rate (see Section 5.2). Since the latter is more easily estimated, a monthly mean air-sea flux was calculated from a knowledge of mean winds and sea surface temperatures. This value is equal to the product of the methane gradient and the apparent vertical eddy diffusivity (eq. 6).

The estimated K_z within the **pycnocline** was plotted against stability (Brunt-Vaaisaala Frequency) and is shown in Figure (40). In the near surface layers, K_z ranged from 20-50 cm^2/s in agreement with the high shear stresses below the mixed layer. Below 50 m, K_z decreased dramatically to a minimum of 0.2 cm^2/s near 65 m, then again increased to values in excess of 1 cm^2/s as the bottom boundary layer was approached. The slope of the line was -0.5, which indicates that vertical mixing is the result of vertical shear rather than the cascade of energy from large scale turbulence (Welander, 1975) .

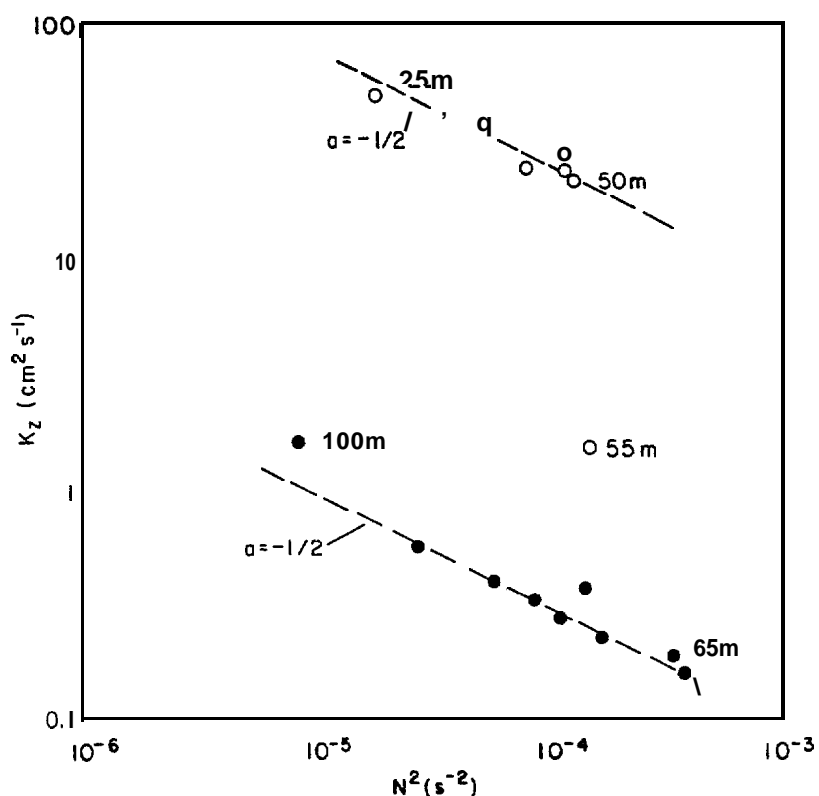


Figure 40. The relationship between the apparent vertical eddy diffusivity, K_z , and the Brunt-Vaaisaala Frequency, N^2 , at Station PL6 in August 1980. The theoretical relationship for shear-induced turbulence is -0.5, which is shown by the dashed Lines.

The conditions modeled were typical for late summer and fall and indicate that vertical exchange is strongly retarded by the density gradient. However, what is of interest is the relative magnitude of the vertical flux of methane across the **pycnocline** compared to the horizontal flux. For this scaling exercise, we assume the following conditions, which existed in August 1980:

$$K_z = 0.2 \text{ cm}^2/\text{s}, d(\text{CH}_4)/dz = 5.0 \times 10^{-4} \text{ nL/cm}^4$$

$$K_h = 1.0 \times 10^6 \text{ cm}^2/\text{s}, d(\text{CH}_4)/dx = 1.1 \times 10^{-7} \text{ nL/cm}^4$$

It is readily apparent that $F_h \gg F_z$, thus to a first approximation, the horizontal flux terms dominate the distribution of methane in the bottom boundary layer and our original assumption that the vertical flux divergence term could be ignored appears valid (see section 6.2). Even if one increases K_v to $1 \text{ cm}^2/\text{s}$ and reduces K_h to $1 \times 10^5 \text{ cm}^2/\text{s}$, the horizontal terms remain dominant for a plume of the observed dimension.

This argument holds true for the velocity terms as well. The advective flux is the product of the mean velocity and the concentration at a specified point. Assuming a mean velocity of 2 cm/s and a methane concentration of 1000 nL/L (1.0 nL/cm^3), the advective flux is $3 \text{ nL/cm}^2/\text{s}$ compared to the horizontal flux divergence of $0.1 \text{ nL/cm}^2/\text{s}$. Clearly, the distributions of methane in the bottom waters of St. George Basin are strongly influenced by the weakest mean flows, even those that are at or below the threshold of conventional current meters.

7. CONCLUSIONS

7.1. North Aleutian Shelf Studies

Dissolved methane, tidally-fluxed from Port Moller, was used as a quasi-conservative tracer of circulation along the North Aleutian Shelf. Three separate observational periods were covered, August 1980, February 1981, and May, 1981. The distribution of dissolved methane along the coast was described using a two dimensional diffusion-advection model, which included a term for biological oxidation and sea-to-air exchange.

The results of the modeling effort predicted mean velocities along the shelf ($z < 50$ m) of 3-6 cm/s. These estimates represent mean velocities over the scale length of the tracer, or about two months. Short term variations in the velocity field (i.e. storm surges) were not detected by the tracer as the characteristic time scale is much shorter than one month.

The seasonal distributions of methane clearly showed the importance of bottom bathymetry and horizontal shear. The model was modified to partially account for bathymetry, but not for a variable u and k . The inner front, located at about 50 m, separates the well mixed shelf water from the seasonally stratified offshore water. Both salinity and methane distributions showed clearly the location of the front, but because the cross frontal gradients were weak, it was impossible to quantify the significance of the front relative to offshore transport. Because of these factors the model fits were not good, but parametric analysis demonstrated that the mean velocity is certainly within the above-stated range.

The model included a variable horizontal eddy diffusivity, K_y , which was scaled to the Lagrangian distance, ut . From our analysis, it appears that the empirical relationships presented by Okubo, 1971, are valid for K_y . K_y varied from about $2 \times 10^5 \text{ cm}^2/\text{s}$ to $2 \times 10^6 \text{ cm}^2/\text{s}$, depending on the size of

tile plume. For smaller sources, such as an oil spill, the horizontal eddy diffusivities would be correspondingly smaller.

7.2. St. George Basin Studies

St. George Basin is a fault graben located on the outer continental shelf of the southeastern Bering Sea and is a potential lease area for gas and oil development. First observed in 1975 and again in 1976, the organic-rich sediments of the basin represent a significant source of biogenic methane, which could be used as a Lagrangian tracer of mean circulation. To accomplish this, however, a much tighter observational grid was implemented and a series of seasonal observations was conducted in August 1980, February 1981, and May 1981.

The distribution of dissolved methane in the lower boundary layer was simulated using a two-dimensional diffusion-advection model like the one used for the North Aleutian Shelf. It differed, however, in that no air-sea evasion term was included. The results of the modeling indicated that the mean velocity was 1-2 cm/s and independent of season. These velocities are quite low and are in complete agreement with the measured currents. The above velocities may be an over estimate, because diffusion in the x-direction was not explicitly included in the model. Consequently, the inclusion of anisotropic mixing could result in the same distribution as was modeled with a variable K_y and constant u . There is some basis for this belief as mixing along shelf is isopycnal in contrast to mixing across shelf which is not. In either event, the mean velocities are low, which is supported by current meter measurements and the accumulation of fine-grained sediments.

8. REFERENCES

- Berner, R.A. 1980. Early Diagenesis, A Theoretical Approach. Princeton University Press, Princeton, N.J., 241 pp.
- Broecker, W.S. and T.H. Peng. 1974. Gas exchange rates between air and sea. Tellus 26: 21-35.
- Brubaker, K.L. and P.M. Rote. 1978. Dispersal models for sulfur oxides in urban environments. In: Sulfur in the Environment, Part I, 172-241, J.O. Nriagu (cd.), John Wiley and Sons, New York, 463 pp.
- Claypool, G.E. 1974. Anoxic diagenesis and bacterial methane production in deep-sea sediments. Ph.D. Thesis, University of California at Los Angeles, 277 pp.
- Claypool, G.E. and I.R. Kaplan. 1974. The origin and distribution of methane in marine sediments, In: Natural Bases in Marine Sediments, 99-140, I.R. Kaplan (cd.), Plenum Press, New York, 324 pp.
- Cline, J.D. and R. Feely. 1976. Distribution of light hydrocarbons, C_1-C_4 , in the Gulf of Alaska and southeastern Bering Shelf. In: Environmental Assessment of the Alaskan Continental Shelf, 9: 443-547, DOC/NOAA, Boulder, Colo.
- Cline, J.D. 1977. Distribution of light hydrocarbons, C_1-C_4 in the north-east Gulf of Alaska, Lower Cook Inlet, southeastern Chukchi Sea. In: Environmental Assessment of the Alaskan Continental Shelf, 8: 180-268, DOC/NOAA, Boulder, Colo.
- Cline, J.D., C. Katz, and H. Curl, Jr. 1981a. Circulation processes in Bristol Bay, Alaska using dissolved methane as a tracer. OCSEAP/OMPA Annual Report, August 1981, 53 pp.
- Cline, J.D., C.N. Katz, and H.C. Curl, Jr. 1981b. Dynamics of dissolved methane in Bristol Bay, Alaska. IAMAP Third Scientific Assembly, Hamburg, ACGP-1, ROAC, August 17-28, (Abstr.).
- Cline, J.D. 1981. Distribution of dissolved LMLO hydrocarbons in Bristol Bay, Alaska: Implications for future gas and oil development. In: The Eastern Bering Sea Shelf: Oceanography and Resources, 425-444, D.W. Hood and J.A. Calder (eds.), Vol. I, DOC/NOAA/OMPA, University of Washington Press, Seattle, Wash., 625 pp.
- Coachman, L.K. and R.L. Charnell. 1979. On lateral water mass interaction- A case study, Bristol Bay, Alaska, J. Phys. Oceanogr., 9: 278-297.
- Csanady, G.T. 1973. Turbulent Diffusion in the Environment. D. Reidel Publishing, Boston.
- Csanady, G.T. 1981. Circulation in the coastal ocean. EOS 62: 9-11.

- Department of Commerce. 1980. Tidal Current Tables, Pacific Coast of North America and Asia, DOC/NOAA/NOS, Rockville, Md., 260 pp.
- Emerson, S. 1975. Gas exchange rates in small Canadian shield lakes. Limnol. Oceanogr. 20: 754-761.
- Gardner, J.U., T.L. Vallier, W.E. Dean, K.A. Kvenvolden, and G.D. Redden. 1978. Distributions of grain size, total carbon, heavy and light minerals, clay mineralogy, and inorganic geochemistry of the outer continental shelf, southern Bering Sea. In: Annual Report, Environmental Assessment of the Alaskan Continental Shelf, Vol. XI, 300-353, DOC/DOI, OCSEAP, Boulder, Colo., 688 pp.
- Griffiths, R.P., B.A. Caldwell, J.D. Cline, W.A. Broich and R.Y. Morita. 1982. Field observations of methane concentrations and oxidation rates in the southeastern Bering Sea. Appl. and Environ. Microbiol., 44: 435-446.
- Katz, C.N. 1980. Processes affecting the distribution of low molecular weight aliphatic hydrocarbons in Cook Inlet, Alaska. M.S. Thesis, University of Washington, 131 pp.
- Katz, C.N., J.D. Cline, and R.P. Griffiths. 1982. The seasonal distribution of methane in the Bering Sea; a relationship between source and dispersion. EOS 63: 83.
- Kinder, T.H. and J.D. Schumacher. 1981a. Hydrographic structure over the continental shelf of the southeastern Bering Sea. In: The Eastern Bering Sea Shelf: Oceanography and Resources, 31-52, D.W. Hood and J.A. Calder (eds.), Vol. I, DOC/NOAA/OMPA, University of Washington Press, Seattle, Wash., 625 pp.
- Kinder, T.H. and J.D. Schumacher. 1981b. Circulation over the continental shelf of the southeastern Bering Sea. In: The Eastern Bering Sea Shelf: Oceanography and Resources, 53-76, D.W. Hood and J.A. Calder (eds.), Vol. I, DOC/NOAA/OMPA, University of Washington Press, Seattle, Wash., 625 pp.
- Niebauer, H.J. 1981. Recent short-period winter time climate fluctuations and their effect on sea-surface temperatures in the eastern Bering Sea. In: The Eastern Bering Sea Shelf: Oceanography and Resources, 23-30, D.W. Hood and J.A. Calder (eds.), Vol. I, DOC/NOAA/OMPA, University of Washington Press, Seattle, Wash., 625 pp.
- Okubo, A. 1971. Oceanic diffusion diagrams. Deep-Sea Res. 18: 789-802.
- Overland, J.E. 1981. Marine climatology of the Bering Sea. In: The Eastern Bering Sea Shelf: Oceanography and Resources, 15-22, D.W. Hood and J.A. Calder (eds.), Vol. I, DOC/NOAA/OMPA, University of Washington Press, Seattle, Wash., 625 pp.
- Reeburgh, W.S. and D.T. Heggie. 1977. Microbial methane consumption reactions and their effect on methane distributions in freshwater and marine environments. Limnol. Oceanogr. 22: 1-9.

- Schumacher, J. D., T.H. Kinder, D.H. Pashinski, and R.L. Charnell. 1979. A structural front over the continental shelf of the eastern Bering Sea. J. Phys. Oceanogr. **9**: 79-87.
- Scranton, M.I. and P.G. Brewer. 1977. Occurrence of methane in near-surface waters of the western subtropical North Atlantic. Deep-Sea Res. **24**: 127-138.
- Sverdrup, H.U., M.W. Johnson, and R.H. Fleming. 1942. The Oceans. Prentice-Hall, Inc. Englewood Cliffs, N.J., 1087 pp.
- Swinnerton, J.W. and V.J. Linnenbom. 1967. Determination of the C₁ to C₄ hydrocarbons in seawater by gas chromatography. J. Chromatogr. Sci. **5**: 570-573.
- Welander, P. 1967. Theoretical forms for the vertical exchange coefficients in a stratified fluid with application to lakes and seas. Acts Geophysics **1**: 1-27.
- Witherspoon, P.A. and L. Bonoli. 1969. Correlation of diffusion coefficients for paraffin, aromatic, and cycloparaffin hydrocarbons in water. Indust. Eng. Chem. Funds **8**: 589-591.
- Yamamoto, S., J.B. Aleuskas, and T.E. Grozier. 1976. Volubility of methane in distilled water and seawater. J. Chem. Eng. Data **21**: 78-80.